12-4-2006

The X-ray Variability of Seyfert Galaxies

Kevin Marshall

The X-ray Variability of Seyfert Galaxies

by

Kevin Marshall

Under the Direction of H. Richard Miller

Abstract

Strong and variable X-ray emission has long been known to be a universal property of active galaxies. However, despite years of study, the exact nature of the variability remains relatively unknown. We present here results of a multi-year monitoring campaign of a sample of Seyfert galaxies (3C 120, Mkn 509, 3C 390.3, and Akn 120), carried out using the *Rossi X-ray Timing Explorer (RXTE)*. For Mkn 509, we also present results of optical monitoring. Mkn 509 shows a strong correlation between X-ray and optical variations, with the optical leading the X-ray by 25 days. We also investigate the rms-flux relationship in our sample. The two radio loud objects in our sample (3C 120, 3C 390.3) show a clear correlation between flux and rms variability, while the two radio quiet objects (Mkn 509, Akn 120) show no such relationship. Monte Carlo simulations were used to estimate the shape of the underlying power spectrum, and we find that all of our objects have a break frequency below which the power spectrum flattens. The relationship between optical and X-ray variability

is discussed, with lags occurring most likely as a result of instabilities or changes in accretion flow propagating inwards through the disk. We also discuss possible physical timescales that could be related to the break frequency, along with connections to galactic X-ray binaries.

Index Words: Active galaxies, X-rays, astronomy

The X-ray Variability of Seyfert Galaxies

by

Kevin Marshall

A Dissertation Presented in Partial Fulfillment of Requirements for the Degree of

Doctor of Philosophy

in the College of Arts and Sciences

Georgia State University

2006

The X-ray Variability of Seyfert Galaxies

by

Kevin Marshall

Major Professor:	H. Richard Miller
Committee:	D. Michael Crenshaw
	Todd J. Henry
	William H. Nelson
	Paul J. Wiita

Electronic Version Approved:

Office of Graduate Studies
College of Arts & Sciences
Georgia State University
December 2006

Acknowledgments

No man is an island, and without the assistance and support of many people this work would not have been possible.

Firstly I would like to thank my adviser, Dick Miller, whose unique style of advising minimalism has proven challenging yet effective. As not only an adviser but also a graduate director and department chairman, your support for not only myself but all of the graduate students has not gone unappreciated. I would also like to thank all of the members of my committee, who have invested their own valuable time to help improve this document.

Speaking of which, I would also like to thank Lewis Roberts for developing the LaTeX dissertation template, and Alvin Das for bringing it up to spec and providing a truly excellent guide for use. I would also like to thank Doug Gies, whose vast knowledge of IDL helped me significantly.

All of the optical data in this dissertation were taken by the SMARTS consortium, of which GSU is a member. Alan Marscher provided me with preliminary X-ray observations of 3C 120, and I am very grateful for those data. Lowell Observatory has hosted me now a total of 14 times, and I would like to thank them for their hospitality, and not being too upset when I broke the dome.

Many of the foundations for optical data reduction were laid by members of the

PEGA group here: John McFarland, who automated nearly every step of the reduction with useful scripts; Angela Osterman, who always helped me fill in the details on what I was doing wrong; and Wes Ryle, who did an excellent job of downloading and organizing all of our SMARTS optical data.

Finally, I would like to thank my family for their continued and unconditional support. Without them, none of this would have been possible.

Table of Contents

Acknowledgments . . . . . **iv**

List of Tables . . . . . **x**

List of Figures . . . . . **xi**

Abbreviations and Acronyms . . . . . **xiv**

1 Introduction **1**

1.1 Historical Background 2

1.2 Types of AGN 4

1.2.1 Classification 4

1.2.2 Unification 5

1.3 Variability of AGN 6

1.3.1 X-ray Emission 7

1.3.2 Optical 11

1.4 Object Selection 12

1.4.1 3C 120 12

1.4.2 3C 390.3 13

1.4.3 Akn 120 13

1.4.4 Mkn 509 14

1.5 Outline of Dissertation 14

2 Data Reduction and Processing **16**

2.1 X-ray 16

2.1.1 X-ray Detectors 16

2.1.2 RXTE 19
2.1.3 Chandra 22
2.2 Optical 23

3 Data 25

3.1 Akn 120 26
3.2 3C 120 27
3.3 3C 390.3 32
3.4 Mkn 509 35
3.4.1 X-ray Data 35
3.4.2 Optical Data 35
3.4.3 Cross Correlation 36

4 Analysis 42

4.1 Fundamentals of Time Series Analysis 42
4.2 Stationarity 47
4.3 The rms-flux Relationship 50
4.4 Computing the Power Density Spectrum 54
4.4.1 Windowing 54
4.4.2 Aliasing 55
4.4.3 Red Noise Leakage 56
4.4.4 Normalization 57
4.4.5 Variance of the PDS 57
4.5 Monte Carlo Simulations 58
4.6 The PDS of Cygnus X-1 64
4.7 Results 65
4.7.1 Mkn 509 71
4.7.2 3C 390.3 75
4.7.3 3C 120 78

4.7.4 Akn 120 83

5 Conclusions 87

5.1 Optical/X-ray Lags in Mkn 509 87

5.2 Accretion Timescales 89

5.3 Variability States 91

5.4 The rms-flux Relationship 94

5.5 Mass-Break Frequency Relationship 95

5.6 Future Work 96

References 99

Appendices 105

A Source Code 106

A.1 pypeline.py 106

A.2 stationary.pro 114

A.3 simulate.pro 116

B Reducing RXTE Data 120

B.1 Intro to RXTE 121

B.1.1 Detectors and Modes 121

B.1.2 Retrieving Data 122

B.1.3 Data Files and Directory Structures 123

B.1.4 Background Issues 125

B.2 Extracting Light Curves and Spectra 126

B.2.1 REX - the Easy Way 126

B.2.2 Xselect - the Bad Way 129

B.2.3 Manually - the Ugly Way 136

B.3 Analysis of Light Curves and Spectra 141

B.3.1 xronos 141
B.3.2 `xspec` 146
B.4 Miscellaneous 153
B.4.1 FAQs 153
B.4.2 Resources 157

C X-ray Data 158

C.1 3C 390.3 158
C.2 Akn 120 168
C.3 3C 120 177
C.4 Mkn 509 207

D Optical Data 216

D.1 Mkn 509 216

List of Tables

1.1 AGN Unification Schemes 6

1.2 Objects Studied 12

3.1 Objects Studied 25

4.1 S Test Results 50

5.1 Break Timescales for Objects Studied 89

5.2 Masses and Luminosities for Objects Studied 93

5.3 Known Break Frequencies 95

C.1 3C 390.3 Long Term X-ray Data 158

C.2 3C 390.3 Intermediate Sampling X-ray Data 166

C.3 Akn 120 Long Term X-ray Data 168

C.4 Akn 120 Short Term X-ray Data 173

C.5 3C 120 Long Term X-ray Data 177

C.6 3C 120 Intermediate Sampling X-ray Data 181

C.7 3C 120 Short Term X-ray Data 186

C.8 Mkn 509 Long Term X-ray Data 207

D.1 Mkn 509 Optical Data 216

List of Figures

1.1 Mean Quasar Spectral Energy Distribution 6
1.2 NLS 1 X-ray Variability 8
1.3 Fe Kα Line in MCG–6-30-15 9
1.4 Typical X-ray Spectrum for an AGN 10

2.1 X-ray Mirror Design 17

3.1 Long Term X-ray Light Curve for Akn 120 28
3.2 Short Term X-ray Light Curve for Akn 120 28
3.3 Long Term X-ray Light Curve for 3C 120 29
3.4 Intermediate Sampling Light Curve for 3C 120 29
3.5 Short Term X-ray Light Curve for 3C 120 30
3.6 Chandra Observation of 3C 120 31
3.7 Chandra Observation of 3C 390.3 33
3.8 Long Term X-ray Light Curve for 3C 390.3 34
3.9 Intermediate Sampling Light Curve for 3C 390.3 34
3.10 3C 390.3 Light Curve and Sliding Variance 35
3.11 Long Term X-ray Light Curve for Mkn 509 36
3.12 Finder Chart for Mkn 509 37
3.13 Optical data for Mkn 509 38
3.14 Check Minus Comparison for Mkn 509 38

3.15 Mkn 509 X-ray and Optical Data 39
3.16 Cross Correlation Function for Mkn 509 40
3.17 Mkn 509 X-ray and Optical Data with Offset 41

4.1 White Noise Light Curves 45
4.2 Red Noise Light Curve 46
4.3 Flicker Noise Light Curve 47
4.4 Simulated Light Curve with Power Law Spectrum 48
4.5 $F_{\rm var}$-flux and rms-flux Relationship for 3C 390.3 52
4.6 $F_{\rm var}$-flux and rms-flux Relationship for 3C 120 52
4.7 $F_{\rm var}$-flux and rms-flux Relationship for Mkn 509 53
4.8 $F_{\rm var}$-flux and rms-flux Relationship for Akn 120 54
4.9 Comparison of Binned and Unbinned Power Spectra 59
4.10 PDS of Cygnus X-1 65
4.11 Power Law Fit Probabilities for Mkn 509 66
4.12 Power Law Fit Probabilities for 3C 390.3 67
4.13 Power Law Fit Probabilities for Akn 120 68
4.14 Knee Model Power Density Spectrum 69
4.15 Broken Power Law Power Density Spectrum 70
4.16 Knee Model Confidence Contours for Mkn 509 71
4.17 Best-fit Monte Carlo Knee Model for Mkn 509 72
4.18 Broken Power Law Confidence Contours for Mkn 509 73
4.19 Best-fit Monte Carlo Broken Power Law Model for Mkn 509 74
4.20 Knee Model Confidence Contours for 3C 390.3 75
4.21 Best-fit Monte Carlo Knee Model for 3C 390.3 76
4.22 Broken Power Law Confidence Contours for 3C 390.3 77

4.23 Best-fit Monte Carlo Broken Power Law Model for 3C 390.3 78

4.24 Best-fit Monte Carlo Broken Power Law Contours for 3C 120 79

4.25 Best-fit Monte Carlo Broken Power Law Model for 3C 120 79

4.26 Best-fit Monte Carlo Knee Model for 3C 120 81

4.27 Best-fit Monte Carlo Knee Model Contours for 3C 120 81

4.28 Doubly-broken Power Law Power Density Spectrum 82

4.29 Doubly-broken Power Law Power Contours for 3C 120 82

4.30 Best-fit Monte Carlo Knee Model Contours for Akn 120 83

4.31 Best-fit Monte Carlo Knee Model for Akn 120 84

4.32 Best-fit Monte Carlo Broken Power Law Model Contours for Akn 120 86

4.33 Best-fit Monte Carlo Broken Power Law Model for Akn 120 86

5.1 Count Rate Versus Spectral Slope for 3C 390.3 94

5.2 Break Timescale Versus Mass 97

Abbreviations and Acronyms

ACIS	AXAF CCD Imaging Spectrometer
AGN	Active Galactic Nuclei
ANDICAM	A Novel Double-Imaging Camera
ASCA	Advanced Satellite for Cosmology and Astrophysics
ASM	All Sky Monitor
BLRG	Broad Line Radio Galaxy
CCD	Charge Coupled Device
CCF	Cross Correlation Function
CIAO	Chandra Interactive Analysis of Observations
DCF	Discrete Correlation Function
HEASARC	High-Energy Astrophysics Science Archive Research Center
HEXTE	High Energy X-ray Timing Experiment
HRC	High Resolution Camera
HRI	High Resolution Imager
IDL	Interactive Data Language
IPC	Imaging Proportional Counter
IR	Infrared
IRAF	Image Reduction Analysis Facility

MJD	Modified Julian Date
NLRG	Narrow Line Radio Galaxy
OVV	Optically Violent Variable
PCA	Proportional Counter Array
PCU	Proportional Counter Unit
PDS	Power Density Spectrum
PI	Principal Investigator
PSF	Point Spread Function
QSO	Quasi-Stellar Object
QSRS	Quasi-Stellar Radio Source
ROSAT	Röntgen Satellite
RXTE	Rossi X-ray Timing Explorer
SAA	South Atlantic Anomaly
SED	Spectral Energy Distribution
SIS	Solid-State Imagine Spectrometer
SMARTS	Small and Moderate Aperture Research Telescope System
UV	Ultraviolet
VLBI	Very Long Baseline Interferometry
XMM	X-ray Multi Mirror
3C	Third Cambridge Catalog

– 1 –

Introduction

Astronomers have three fundamental methods for collecting data and learning about the structure and composition of the universe: imaging, spectroscopy, and photometry.

Image analysis consists of measuring the structure, orientation, and position of objects in the sky. From this, we can map out the orbits of stars in the sky, the location of dust and gas in a nebula, or the spiral arms of a galaxy. Although once the primary method of astronomers, imaging is limited by the practicality of constructing ever-larger telescopes, and the distorting effects of our own atmosphere. Space-based telescopes and interferometry have helped to push back these limits in recent years.

Late in the 19^{th} century, astronomers found they could use a simple prism to split light into its component colors, and thus the science of spectroscopy was born. By analyzing the intensity of light at different wavelengths, astronomers have been able to determine the composition and temperature of not only the Sun, but of nearly any star that we can see. New companions have been been found for stars once thought to be previously isolated, thanks to the effects of an otherwise unseen neighbor. Measurements have been made for gas escaping the centers of galaxies at thousands of kilometers per second, and the distribution of interstellar clouds has been mapped out. Spectroscopy, although over a century old, remains the best way to determine

the actual composition of the baryonic portion of the universe.

Finally, we have the science of photometry. Early astronomers realized that some stars in the night sky would change in brightness on a regular basis. In modern times, astronomers have used photometry to support the existence of black holes, both of stellar mass and at the centers of galaxies. Photometry at radio wavelengths has also been used to study pulsars, and provided the first evidence for the existence of planets outside our own Solar System. Although providing little direct knowledge, sophisticated photometric analysis techniques allow us to discern a great deal about the structure and underlying physics of many of the objects we see.

Amongst all of the objects in the sky, few are more massive, more variable, and more extreme than active galaxies.

1.1 Historical Background

Soon after astronomers began looking at galaxies with a telescope, they realized that some galaxies had cores that were much brighter than the surrounding galaxy. At the time, galaxies were not recognized as a separate class of object, and were thought to be 'nebulae' residing inside the Milky Way. E. A. Fath at Lick Observatory was the first person to take a spectrum of an active galaxy, in 1908. He noted the presence of strong emission lines in the 'nebula' NGC 1068. Not long afterwords, V. M. Slipher, at Lowell Observatory, obtained a higher resolution spectrum and noted that the emission lines seen are very similar to those observed in planetary nebulae. He also

noted that the lines have widths of several hundred km/s (Peterson 1997).

Active galaxies were first recognized as a separate class of objects by Seyfert (1943). Studying galaxies with high-excitation emission lines, Seyfert noted that the objects in his sample had very broad emission lines, and the hydrogen Balmer lines were sometimes, but not always, wider than the other lines.

After World War II, the science of radio astronomy exploded, and it was soon discovered that Seyfert's sample of galaxies had radio emission. Woltjer (1959) noted that the extraordinary width of the lines required a very high velocity. Such a velocity in such a compact region of space almost certainly required a very large concentration of mass.

Around the same time, astronomers were finding a number of unusually strong radio sources in the sky with no obvious optical counterparts. Using methods such as lunar occultations, astronomers were able to find the source of radio emission for objects like 3C 48 and 3C 273. Optically, these objects were all stellar like in appearance, with unusually blue spectra and strong emission lines at seemingly strange wavelengths. Known as Quasi-Stellar Radio Sources (QSRS, or now 'quasars'), these objects remained a mystery until 1963, when Schmidt recognized that the unusual emission lines seen in quasars were the same lines seen in Seyfert galaxies, but redshifted to (what were then) amazingly high redshifts of $z = 0.1$ and larger. Greenstein & Schmidt (1964) recognized these redshifts as cosmological in origin, and the extraordinary brightness of these objects ($\sim 10^{45}$ erg/s) were most easily explained if

there were a large amount of mass (10^8 $M_\odot$) in a small volume of space (1 pc^3).

1.2 Types of AGN

1.2.1 Classification

With many diverse types of emission line galaxies, some sort of classification scheme was necessary. Khachikian & Weedman (1974) proposed that Seyfert galaxies be divided into 2 groups: type 1 galaxies with broad permitted and narrow permitted and forbidden emission lines, and type 2 galaxies with narrow permitted and forbidden lines. Recent evidence has shown that quasars can be similarly classified (Sturm et al. 2006; Zakamska et al. 2006).

Weedman (1977) later proposed that radio-quiet quasars were simply more distant cousins of Seyfert galaxies, and radio-quiet quasars were found in large numbers, mainly through the use of color surveys, because the quasars were extremely blue.

Optically Violent Variable (OVV) quasars and BL Lac objects comprise another class of active galaxy. Both are extraordinarily variable in the optical. OVV quasars typically have an emission-line spectrum, while BL Lac objects have a featureless non-thermal continuum. Together, these objects are known as blazars.

A radio-loud counterpart to the Seyfert galaxy was also recognized, with broad-line and narrow-line radio galaxies (BLRGs and NLRGs, respectively) being analogous to type 1 and type 2 Seyferts.

1.2.2 Unification

Despite the seemingly diverse nature of active galaxies, each class draws from a list of similar characteristics:

- Bright, star-like nucleus
- Variable flux at all wavelengths
- Relatively broad, high-excitation emission lines
- Emission throughout the electromagnetic spectrum

Given the large amount of energy produced and the compact size required, the best candidate for the central engine is accretion onto a supermassive black hole. Surrounding the accretion disk is a dusty torus, which blocks our direct view when seen from sufficiently high inclination. Antonucci & Miller (1985) provided strong evidence for this theory, with spectropolarimetry of the Seyfert 2 galaxy NGC 1068. Observing in polarized light (i.e. photons scattered by electrons above the putative torus) they found broad emission lines identical to that seen in Seyfert 1 galaxies.

For radio-loud galaxies, if we are looking through the torus we see a NLRG or perhaps a type 2 quasar. Looking more directly into the black hole, we see a BLRG or a quasar. And finally, looking almost directly along the jet, observations are dominated by the Doppler-boosted emission from the jet, and so we see the highly-variable featureless continuum of a blazar. A summary of unification schemes is given in Table 1.1.

Table 1.1: Unification schemes for various types of AGN[a].

Radio Properties	Face-on	Edge-on
Radio Quiet	Seyfert 1	Seyfert 2
	QSO	Type 2 QSO
Radio Loud	BL Lac	FR I
	BLRG	NLRG
	Quasar/OVV	FR II

[a] Adapted from Peterson (1997)

1.3 Variability of AGN

Variability has long been recognized as one of the defining characteristics of AGN. Some objects, such as BL Lac, were identified as variable stars before their true nature was known.

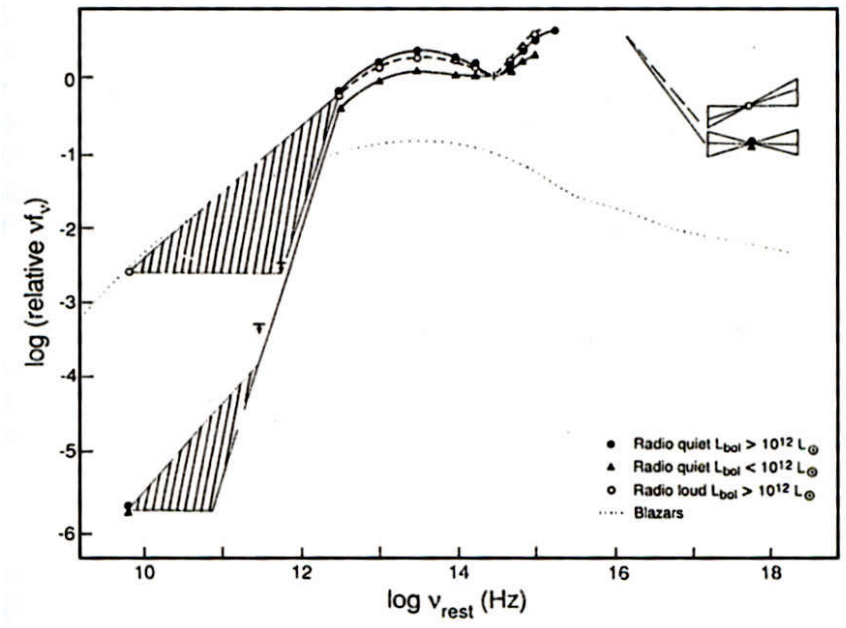

Figure 1.1: Mean QSO SED (Sanders et al. 1989)

Examining the continuum emission, we find different physical mechanisms responsible in different regimes of the electromagnetic spectrum. In the radio, we see a power law spectrum generated by synchrotron emission. Radio quiet objects generally show weaker radio flux by a factor of ~ 100 when compared to their radio loud counterparts, but the spectra are generally similar at other wavelengths. Typical spectral energy distributions (SEDs) for both a radio-loud and radio-quiet quasar are shown in Figure 1.1. In the infrared, the spectrum is probably dominated by thermal emission from the dusty torus. The bulk of both the radio and IR emission come from relatively large distances away from the central black hole, and will not be discussed further in this dissertation. Instead, we choose to focus on optical and X-ray emission, which we examine in more detail below.

1.3.1 X-ray Emission

X-ray emission is critical for understanding the nature of AGN, and offers us the best means for probing the innermost regions of the central engine. Using two simple arguments, we can deduce that X-rays originate from very close to the supermassive black hole:

- Temperature for an optically thick, geometrically thin accretion disk increases as $T \propto r^{-3/4}$ (Longair 1997, §16.3.4). For high-energy photons such as X-rays, temperatures on the order of $10^5 - 10^6$ K are required, so the thermal portion of the emission must come from the inner parts of the accretion disk where heating

occurs, and not further out.

- X-rays are the most variable of any wavelength, with some objects doubling their powers in less than 1000s (Boller et al. 1997). In general, the timescale for significant variations of an object must be less than the light crossing time for the emitting region, or $r < c\Delta t$, where r is the size of the emitting region, c is the speed of light, and Δt is the variability timescale. For X-rays, which can vary significantly in just a few hours, the emission must occur within a few Schwarzschild radii for a black hole of mass 10^6 $M_\odot$ or larger. The X-ray emission is produced far enough away from the black hole so that relativistic corrections are not needed. Such extreme variability is shown in Figure 1.2.

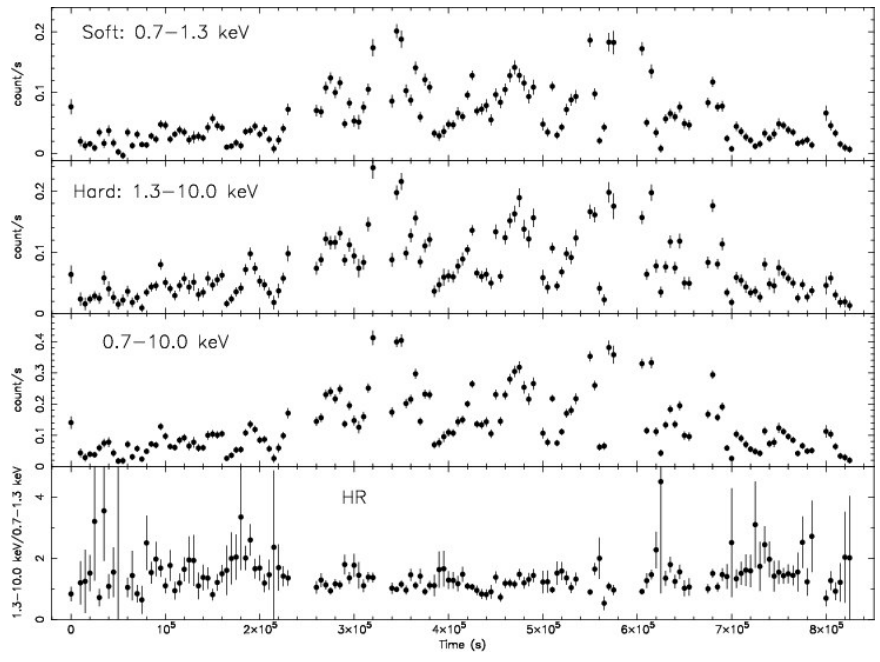

Figure 1.2: Data from a 10 day *ASCA* observation of the NLS1 IRAS 13224–3809. Bottom represents the hardness ratio. (Dewangan et al. 2002)

The X-ray spectra of AGN consist of several components. Not all components are detectable in all galaxies, usually because of sensitivity or spectral resolution issues with the detector.

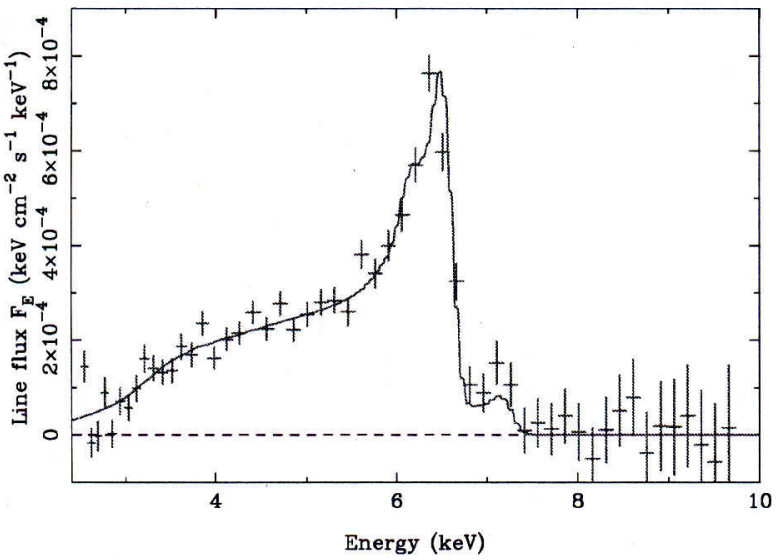

Figure 1.3: Fe Kα line in MCG–6-30-15, obtained from a 325 ks *XMM* observation by Fabian et al. (2002). The model is for an accretion disk surrounding a supermassive black hole, with an inner radius of 4.6 gravitational radii, and inclination of 38°.

The dominant spectral feature in the X-rays is a power law continuum, which decreases in flux as energy increases. At low energies ($E < 2$ keV), an excess is often seen above the power law component, along with photoelectric absorption. At higher energies ($E > 10$ keV), a similar excess is sometimes seen. An emission line is often seen at 6.4 keV, from Fe Kα. The width of this line corresponds to velocities of 10^4 km/s or more, and in at least one case very probably shows gravitational redshifting (Tanaka et al. 1995; Fabian et al. 2002). This redshifting is illustrated in Figure 1.3.

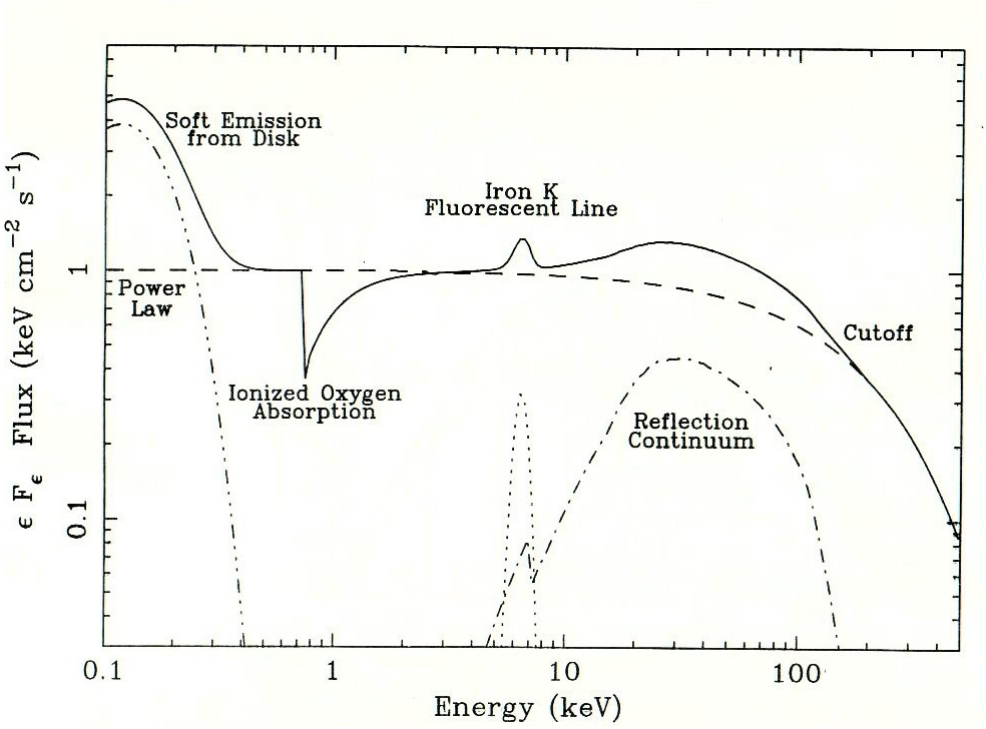

Figure 1.4: Typical X-ray spectrum for a Seyfert Galaxy. Solid line represents the observed spectrum, with dashed and dotted lines representing individual components.

A simple model which could explain many of the observed X-ray features involves a hot corona of electrons above the accretion disk (possibly as part of a jet), which inverse Compton scatters optical/UV photons up to X-ray energies. The tail end of the thermal spectrum from the accretion disk produces the soft X-ray excess, while illumination of a relatively cold slab of gas (such as the accretion disk) from above produces a Compton reflection component at higher energies, generating the Fe Kα emission as well (Peterson 1997, §4.2). This decomposition of the X-ray emission is shown in Figure 1.4.

Despite a modest understanding of the mechanisms underlying X-ray emission, little is known about the causes of variability. Turner et al. (1999) found that for

most Seyfert galaxies, objects with lower luminosities had higher amplitude X-ray variability. Markowitz et al. (2003a) monitored a sample of seven Seyfert galaxies for a period of years, and found little correlation between continuum flux and Fe Kα emission. The primary cause of X-ray variability remains unknown, whether it is changes in accretion rate, instabilities or hot spots in the accretion disk, or something else altogether.

1.3.2 Optical

The majority of the optical (and UV) emission from AGN is thought to be thermal emission from an accretion disk with a range of temperatures up to $\sim 10^6$ K. If we assume that the accretion disk is optically thick and geometrically thin, the emission in the optical regime will be a power law with form $L(\nu) \propto \nu^{1/3}$ (Longair 1997, §16.3.5).

One caveat of such a simplistic model is that optical and UV radiation will be produced in separate regions. However, monitoring has shown that optical and UV variations occur simultaneously. From the geometrically thin accretion disk model, the optical emission region would be expected to be ~ 7 times larger than the UV emitting region. One possible solution is that the optical emission is free-free, rather than thermal in nature (Kembhavi & Narlikar 1999, §8.5.2), however this model is highly controversial.

1.4 Object Selection

To explore the nature of X-ray variability in Seyfert galaxies, we have chosen four objects which represent a unique mix of characteristics. Each object has been previously well studied at other wavelengths, but does not have any long-term X-ray monitoring available. Additionally, 3 of our 4 objects have black hole masses $> 10^8$ $M_\odot$ (Peterson et al. 2004). A summary of each object's properties is given in Table 3.1. Below we describe each object in more detail.

Table 1.2: Basic properties of all objects studied.

Name	RA	Dec	Class	Redshift	L_X (2–10 keV erg/s)
3C 120	04 33 11.15	+05 21 15.7	BLRG	0.033	6×10^{43}
Akn 120	05 16 11.47	-00 08 59.3	Sy 1	0.033	2×10^{43}
3C 390.3	18 42 09.09	+79 46 17.2	BLRG	0.057	3×10^{44}
Mkn 509	20 44 09.84	-10 43 24.3	Sy 1	0.034	3×10^{44}

1.4.1 3C 120

The nearby ($z = 0.033$) BLRG 3C 120 presents itself as an interesting target for variability analysis. Originally classified as a type 1 Seyfert, 3C 120 was first discovered as an X-ray source by Forman et al. (1978) using the *Uhuru* observatory. A superluminal radio jet was later discovered by Zensus & Pearson (1988). 3C 120 has also exhibited extreme optical variability at times (Webb et al. 1988; French & Miller 1980), with variations of more than half a magnitude on timescales of a few days. Marscher et al. (2002) used coordinated *VLBI* and *RXTE* observations to show

that dips in the X-ray flux corresponded with the ejection of knots of radio material from the nucleus, similar to the behavior seen in micro-quasars. The unusual combination of these properties makes 3C 120 an excellent target for an analysis of X-ray variability.

1.4.2 3C 390.3

3C 390.3 is a broad-line radio galaxy with an X-ray luminosity of $L_{\rm X} = 3 \times 10^{44}$ erg/s, and redshift $z = 0.057$. In 1995, 3C 390.3 was intensively monitored at radio through X-ray wavelengths (Dietrich et al. 1998; O'Brien et al. 1998). Part of that monitoring included repeated observations with the *ROSAT* HRI by Leighly & O'Brien (1997), who reported possible non-linearity and non-stationarity in the light curve.

Gliozzi et al. (2003) observed 3C 390.3 with *RXTE* over a period of 60 days, and found a power law structure function with a turnover at $\sim$ 20 days. They did not search for non-linearity or non-stationarity in the data. Gliozzi et al. (2006) used 2 years of archival *RXTE* data to search for non-stationarity in the data set. They found only weak evidence of non-stationarity using traditional methods.

We set out to examine the long-term light curve in more detail, including analysis of the power spectrum.

1.4.3 Akn 120

Akn 120 is a Seyfert 1 galaxy which was first noticed in a survey of high surface brightness galaxies by Arakelian (1975). Not long after its discovery, variability was

noted in both the optical (Miller 1979) and X-ray (Mushotzky & Marshall 1980). Variability in the spectral lines was also noted by Foltz et al. (1981). Since then, the optical spectrum has been studied extensively (Peterson et al. 1989). Miller & Ferrara (1999) have obtained 2 years of optical and X-ray monitoring. They found evidence for a correlation between the optical and X-ray, with zero lag. Here we present a re-analysis of the X-ray data, using more sophisticated time series analysis methods.

1.4.4 Mkn 509

Mkn 509 is a nearby ($z = 0.034$) Seyfert 1 galaxy with an X-ray luminosity of $L_{\rm X} = 3 \times 10^{44}$ erg/s. First detected by *Ariel V* (Cooke et al. 1978), Mkn 509 was later found to have a soft X-ray excess at $kT = 70$ eV by Singh et al. (1989). Simultaneous observations with *GINGA* and *ROSAT* again showed a soft excess, with some flattening at higher energies due to reflection (Pounds et al. 1994). Later observations with *ASCA* showed the presence of an Fe Kα line at 6.4 keV, and the presence of a warm absorber rather than a soft excess (Reynolds et al. 1997). More recent observations with *XMM-Newton* show the origin of the soft X-ray excess lies mostly in thermal emission from the inner parts of the accretion disk (Pounds et al. 2001).

1.5 Outline of Dissertation

The goal of this dissertation is to probe the driving mechanism behind X-ray variability in Seyfert galaxies. To accomplish this task, we have monitored a sample of

four Seyfert galaxies with the *RXTE* observatory for periods of ~ 2 years each. We also have quasi-simultaneous optical data for one of our objects. In Chapter 2, we outline the data reduction methods used for both X-ray and optical observations. In Chapter 3, we present light curves and a basic analysis for each object. In Chapter 4, we use more sophisticated techniques, such as a Monte Carlo analysis of the power spectrum for each object. Finally, in Chapter 5 we present conclusions about the nature of variability in AGNs.

– 2 –

Data Reduction and Processing

This dissertation makes use of a large amount of data, covering a wide range of timescales. Although AGN vary at all wavelengths, we focus on the optical and X-ray variability.

2.1 X-ray

2.1.1 X-ray Detectors

The high-energy nature of X-ray photons presents unique challenges to designing and building an X-ray observatory. At wavelengths shortward of 1000 Å, photons will scatter off a normal mirror. Hans Woltjer discovered that if a photon struck the mirror at a low enough angle ($< 10°$), it would be reflected. Similar to optics for longer wavelengths, the surface irregularities in the shape of the mirror must be significantly less than the wavelength of the photons. For X-rays, this means surface accuracy on the order of 1 Å. Until recently, this type of accuracy was impossible to achieve.

Because of this, the earliest X-ray detectors (launched on sounding rockets) most closely resembled a Geiger counter. An X-ray photon enters the detector through a window, where it encounters a gas (typically Xenon). The photon strips one or

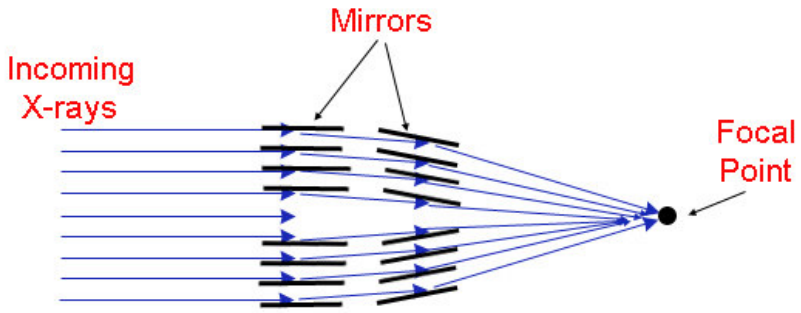

Figure 2.1: Typical design for an X-ray mirror. Photons are reflected at a shallow angle off one or more mirror surfaces, and focused to a single point

more electrons from the gas, which are drawn towards an anode at the center of the detector. As the electron moves towards the anode, it can ionize yet more atoms, causing an avalanche of electrons. The end result is a pulse of current detected on the central wire. The number of electrons collected by the anode is proportional to the energy of the incident X-ray photon, which gives this type of detector its name of proportional counter.

By the late 1970s, engineering technology had advanced to where the construction of accurate X-ray mirrors was possible. The mirrors consisted of concentric cylindrical shells, each one reflecting (by grazing incidence) X-ray photons onto an array of detectors (Figure 2.1).

One of the first such satellites to have imaging X-ray optics was the *Einstein* observatory. The Imaging Proportional Counter (IPC) on board *Einstein* consisted of a grid of wires kept at a high potential inside a gas. By measuring the x-y position

of every detection, along with the energy of the photon, proportional counters allow both imaging and spectroscopy to be performed at the same time, without the use of a grating or other dispersive element. Although proportional counters have good sensitivity and moderate spectral resolution (for an X-ray detector), the price to be paid is in image resolution. Typical PSFs for a proportional counter are on the order of several arcminutes. Thankfully, the X-ray sky is not very crowded!

Another type of X-ray detector is the microchannel plate. A microchannel plate consists of an array of small glass tubes fused together. The insides of the tubes are coated with a photosensitive material which releases electrons when struck with an X-ray photon. The avalanche of electrons is then recorded by a detector below the plate. The High-Resolution Imager (HRI) on *ROSAT* and the High-Resolution Camera (HRC) on *Chandra* are both examples of microchannel plates. Night vision binoculars also typically use microchannel plates, because they can have a very large gain (typically a factor of 10,000). Such a detector offers good sensitivity and very high spatial resolution ($\sim 0.5''$ for the HRC), although spectral resolution is typically so poor as to be unusable.

Finally, many modern X-ray observatories use Charge Coupled Devices (CCDs) as detectors. The Solid-State Imaging Spectrometer (SIS) on board the *Advanced Satellite for Cosmology and Astrophysics (ASCA)* and the Advanced CCD Imaging Spectrometer (ACIS) on board *Chandra* are both examples of X-ray CCD detectors. When an X-ray photon strikes the detector, it ejects a free photoelectron. As that

electron moves through the silicon lattice, it creates a trail of electron-hole pairs, each with an average energy of 3.65 eV. By measuring the number of electron-hole pairs, the energy of each incident photon can be determined.

2.1.2 RXTE

The Rossi X-ray Timing Explorer (*RXTE*) was launched on December 30, 1995, on board a Delta II rocket. Residing in a low-Earth orbit at an altitude of 580 km, *RXTE* was designed to measure the variability of X-ray sources on timescales from milliseconds to years, at energies from 2–250 keV.

RXTE carries three instruments: the All-Sky Monitor (ASM), the High Energy X-ray Timing Experiment (HEXTE), and the Proportional Counter Array (PCA). The ASM consists of three proportional cameras that scan 80% of the sky every 90 minutes (Levine et al. 1996). Although useful for monitoring X-ray binaries and detecting bright X-ray transients, the ASM is not sensitive enough to monitor AGNs, and will not be discussed further. HEXTE contains two clusters of four scintillation detectors each, and is designed to observe X-rays between 15–250 keV. Because of its small collecting area (800 cm^2), and because AGN X-ray spectra drop off steeply at higher energies, the HEXTE cluster is of limited usefulness and thus we do not include any HEXTE data in our results.

The PCA consists of 5 identical Proportional Counter Units (PCUs), each with an effective area of 1300 cm^2, for a total collecting area of 0.65 m^2 (**?**). The surface of each PCU consists of a beryllium copper collimator 8 inches deep. Under the collimator

are 2 sheets of mylar, with propane gas between them, forming the anti-coincidence layer. The interior of the detector is filled with a xenon/methane mixture. There are three separate layers of anodes in each PCU, stacked vertically.

The PCA does not contain any optics, and is thus a non-imaging detector. The field of view is set by the collimators, and is roughly 1° on the sky. Similar to optical astronomy, background subtraction involves analyzing an empty area of sky near the object. However, due to the non-imaging nature of the PCA, background subtraction must be estimated entirely from instrumental models and blank-sky pointings taken periodically. Although background count rates on the PCA can often be several times the amount of counts from the object, the PCA instrument team has done an excellent job of background estimation with their most recent models (Edelson & Nandra 1999, and references therein). Typical error bars on most recent data have been reduced to only a few percent for AGNs. The energy resolution of the PCA is $< 18\%$ at 6 keV.

Early in the *RXTE* mission, PCUs 3 and 4 began to suffer repeated breakdowns. In 1998, PCU 1 also began to experience intermittent failure. Because of this, we present data only from PCUs 0 and 2. Note that in early 2000, the propane veto layer on PCU 0 was lost. At present, only PCU 2 is fully functional. However, the loss of the veto layer affects mainly the observed spectrum. Due to the relatively faint nature of AGNs, the added signal from PCU 0 greatly increases the quality of our data, despite the small amount of uncertainty introduced.

All of our observations were reduced using FTOOLS v5.2 software, provided by

HEASARC. Data were excluded if the Earth elevation angle was $< 15°$, pointing offset $> 0.02°$, time since South Atlantic Anomaly (SAA) passage < 30 minutes, and electron noise < 0.1 units. Counts were extracted from the top PCU layer only to maximize the signal to noise. The PCA response matrix is not well defined above 10 keV, and the power law nature of AGN spectra makes them very faint at higher energies, so data were only extracted in the energy range of 2–10 keV.

Frequent monitoring of our objects means that large amounts of data are generated, all of which must be processed in a timely manner, with an output in the most convenient form possible. HEASARC provides the `rex` perl script to analyze data in bulk, however this script only analyzes a large amount of data at once, and produces a FITS format light curve, which is not binned by observation. The best format for simple analysis would be a text file containing basic parameters such as the date of observation and count rate observed.

In order to reduce our data in the most convenient and efficient way possible, the `pypeline` reduction script was created. Written in the Python scripting language (Lutz 2001), `pypeline` takes a list of objects and proposal numbers, retrieves the data via FTP, decrypts and un-tars the files, processes the data, and writes the date, exposure time, flux, spectral slope, spectral slope error, count rate, and count rate error to a text file. The main advantage of using `pypeline` is that it is aware of what data have already been downloaded and reduced, and only processes the data that it needs to. The source code for `pypeline` is included in Appendix A.1.

2.1.3 Chandra

For some of our objects, pointed observations were available with the *Chandra* X-ray Observatory. *Chandra* has 2 instruments: ACIS, and HRC (Nousek et al. 1998). The HRC consists of a microchannel plate with $0.5''$ resolution; however, all of our data were taken with ACIS and so the HRC will not be discussed further.

The ACIS consists of 10 separate CCD chips: four in a square pattern, and then six chips arranged linearly below it. The linear array of chips is designed to provide optimal viewing of spectra generated by two diffraction gratings that can be inserted into the light path. All of our data were taken without the gratings, and with the object on the central, four-chip part of the instrument. With a spatial resolution of $\sim 0.5''$ and energy resolution of $E/\Delta E = 10 - 60$ over the entire 2–10 keV bandpass, ACIS is one of the most sophisticated X-ray detectors ever launched.

Data from the Chandra Science Center come in the form of a level 2 event file, which contains position, timing, and energy information for each photon detected. Although the data can be re-reduced and a new event file generated, in our case this was not necessary. The only reduction necessary was to extract an image from the event file, and remove the ACIS readout streak that can occur when ACIS is still taking data while reading out the frame. All reduction was done using the Chandra Interactive Analysis of Observations (CIAO) software v3.3.

2.2 Optical

All optical data were obtained at Cerro Tololo Inter-American Observatory (CTIO) with the 1.3m reflector, which is operated by the SMARTS consortium. Observations were taken as part of a service observing program, and then reduced and analyzed by the SMARTS team.

The 1.3m reflector uses the ANDICAM instrument, which has a Fairchild 447 2048×2048 CCD chip with 15μm pixels. Using 2×2 binning, this yields a 6-arcminute field of view, with a plate scale of $0.369''$ per pixel. Observations were taken in standard Johnson BVR filters; however we present only the R filter data here, because the detector's response is greatest at this wavelength.

Along with object frames, bias and flat fields were taken each night. The camera is cooled with liquid nitrogen, which reduces thermal noise to near-zero levels. Therefore dark frames were not necessary. Image processing was done with the Image Reduction Analysis Facility (IRAF) code, using standard methods. A large number (typically 10) of bias and flat fields were taken each night, and then combined using a min/max rejection algorithm in IRAF.

Photometry was done using the CCDPHOT program, developed for IDL by Marc Buie. CCDPHOT was chosen over more standard IRAF routines like `apphot` for reasons of convenience. CCDPHOT allows the user to define templates of objects and check stars for each object, along with allowing automated photometry from one frame to the next. A $7''$ aperture was chosen to minimize any contributions

from the host galaxy. Photometric measurements were taken for the object and a number of check stars. All of the measurements presented here are differential, i.e. no photometric standard stars were used. This allows us to measure the relative changes in brightness of the object, without having to worry about photometric conditions in the sky. Airmass and sky conditions can be neglected due to the proximity of the check stars to the object (Noble 1995; Stalin et al. 2004).

– 3 –

Data

Active galaxies vary at all wavelengths and on all timescales. In order to properly study the nature of AGN variability, monitoring on timescales from hours to years is necessary. For our sample, we have observed all objects extensively in the X-ray, with additional optical observations for Mkn 509. Below are the X-ray observational parameters for each object.

Table 3.1: Basic properties of all objects studied.

Name	Start Date[a]	End Date[a]	Sampling Interval	N^b	μ^c	F_{var}^d
3C 120	50812.06	51563.18	7d	126	5.29	16.30
	52450.08	52756.28	2d	156	5.17	15.20
	52622.40	52631.22	1000s	786	5.70	6.10
Akn 120	50868.02	51662.07	3d	174	3.47	20.91
	51163.20	51165.93	2000s	141	7.24	5.65
3C 390.3	51186.03	51964.00	3d	257	3.67	30.95
	50220.63	50276.93	1d	58	2.58	27.77
Mkn 509	52726.35	53945.83	3d	330	5.23	19.42

[a] Modified Julian Date
[b] Number of data points
[c] Mean counts/sec
[d] Fractional variability (%)

Sampling on multiple timescales has been obtained for each object, with the exception of Mkn 509. With ~ 2 years of data for each object, we can begin to properly analyze the timing properties of our sample. Complete data for all of our objects are given in Appendix C.

To begin to quantify the intrinsic variability of each light curve, we have calculated the fractional variability, defined as

$$F_{\rm var} = \sqrt{\frac{S^2 - \langle \sigma_{\rm err}^2 \rangle}{\langle \mu \rangle^2}} \tag{3.1}$$

where S^2 is the variance of the light curve, $\langle \sigma_{\rm err}^2 \rangle$ is the mean error squared, and $\langle \mu \rangle$ is the mean count rate (Markowitz & Edelson 2004). All of our objects show $F_{\rm var}$ in the range of 15–30%, with smaller fractional variability on shorter timescales. As discussed in Vaughan et al. (2003a), for any red noise process, measurements of $F_{\rm var}$ can yield multiple values for different segments of time. Therefore $F_{\rm var}$ by itself does not tell us much about the underlying variability process, other than the variability seen in our objects is similar to that in other Seyfert galaxies (Markowitz & Edelson 2004).

3.1 Akn 120

Akn 120 was observed with *RXTE* once every 3 days from 1998 February 23 until 2000 April 27, a span of more than 2 years. The source was observed to be highly variable, with count rates from $\sim 2 - 5$ counts/sec/PCU. The most rapid change in flux occurred from MJD 51425–51500, with the flux dropping by a factor of 3 in only 75 days. The long term light curve is shown in Fig 3.1.

RXTE also observed Akn 120 nearly continuously from 1998 December 15–18, with gaps only for Earth occultation and scheduled observations of other objects.

The source showed high frequency variability of between 6.5–8.5 counts/sec/PCU. The light curve is shown in Fig 3.2. Gaps in the light curve were interpolated linearly between the end points of the gap.

During the entire observing campaign, optical data were obtained at Lowell Observatory and other facilities worldwide. Details of the X-ray/optical cross-correlation were discussed by Miller & Ferrara (1999), who found a strong correlation with zero lag at long timescales, and a somewhat weaker correlation with zero lag at short timescales.

3.2 3C 120

3C 120 has been monitored extensively in the X-ray as part of the ongoing program of Marscher et al. (2002). Observations with *RXTE* were taken once per week from 1997 December 29 until 2000 January 19. These data are shown in Figure 3.3. The source flux varies by a factor of 2, with high-frequency variability that is not resolved.

Marscher et al. (2002) later increased their sampling frequency to once every 2 days, from 2002 June 24 until 2003 April 26. These additional data give us a chance to explore the variability on intermediate timescales, and are shown in Figure 3.4.

Finally, 3C 120 was observed continuously with *RXTE* from 2002 December 13–22, with gaps only due to Earth occultation and other scheduled observing programs. The light curve from this intensive stare is shown in Figure 3.5. The high-frequency variability is now clearly resolved. Similar to Akn 120, gaps in the data set were

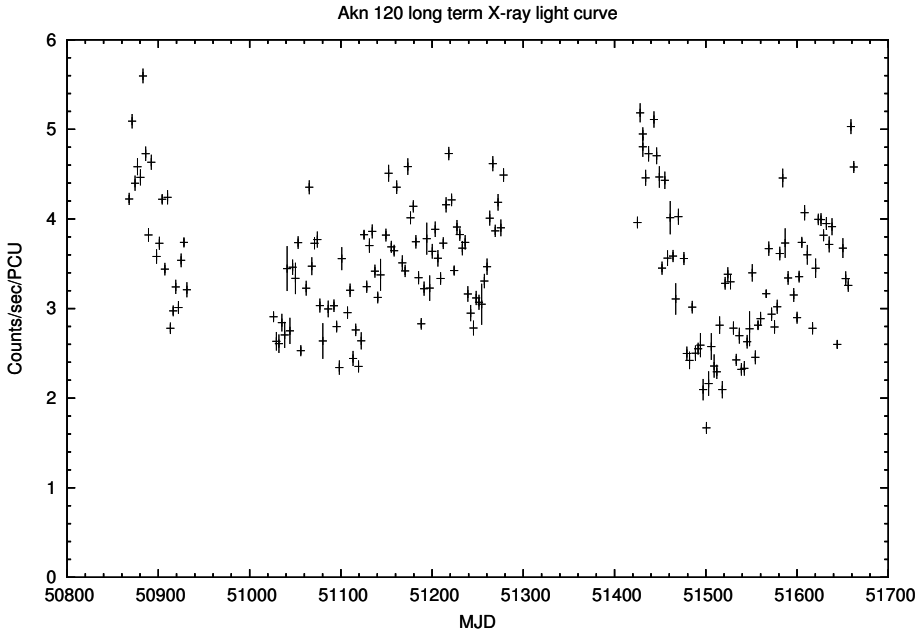

Figure 3.1: Long term X-ray light curve for Akn 120, with monitoring every 3 days for two years.

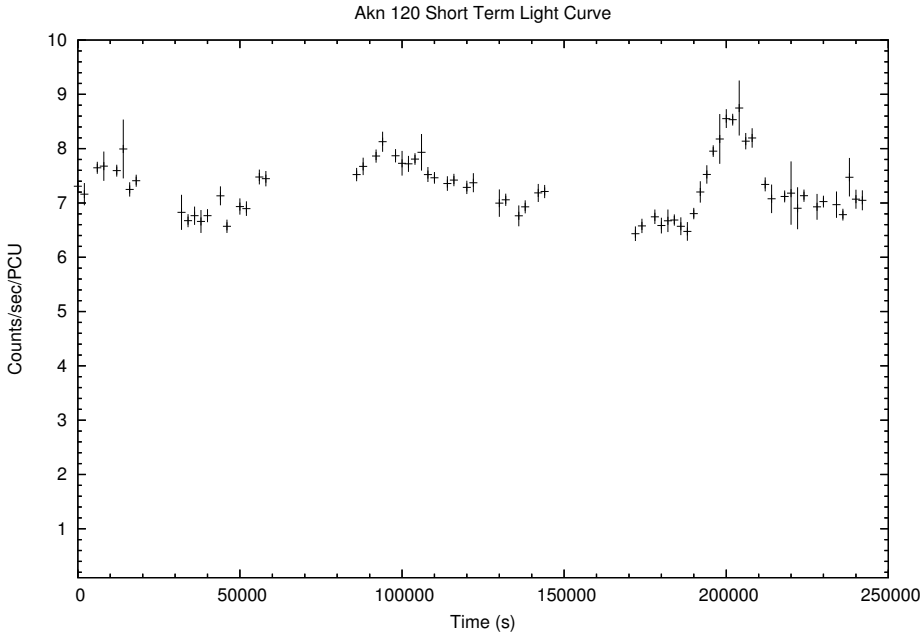

Figure 3.2: Short term light curve for Akn 120, with continuous monitoring for three days. Gaps due to Earth occultation and other observing programs have been linearly interpolated.

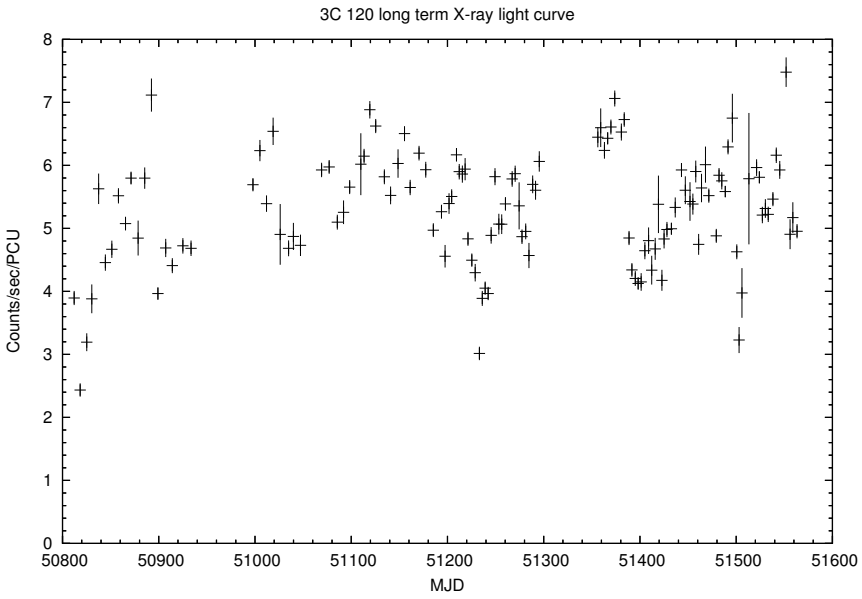

Figure 3.3: Long term X-ray light curve for 3C 120, with sampling every 7 days for approximately 2 years.

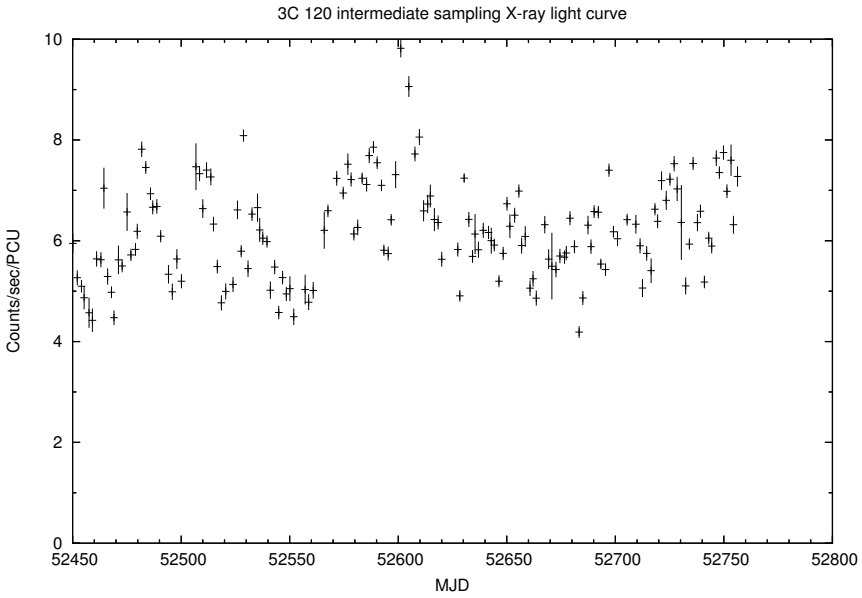

Figure 3.4: Intermediate sampling X-ray light curve for 3C 120, with observations every 2 days for nearly two years.

interpolated linearly. Despite a large number of gaps, overall coverage during the observation was satisfactory and the gaps are spread evenly throughout the light

curve.

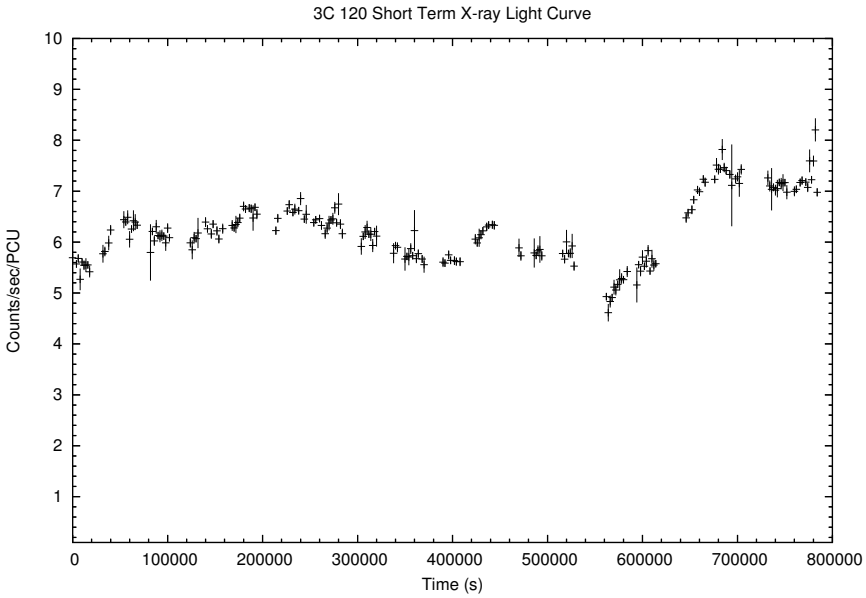

Figure 3.5: Short term X-ray light curve for 3C 120, with nearly continuous monitoring for nine days. Gaps in the light curve due to Earth occultation and other observing programs have been linearly interpolated.

It is well known that 3C 120 possesses a superluminal jet. To examine the possibility of flux contamination from the jet, we have analyzed a 16 ks archival *Chandra* ACIS-I observation. The image (Figure 3.6) clearly shows the central source and a small amount of X-ray emission roughly 25″ to the northwest, which is coincident with the position of the radio lobe labeled as k25 by Harris et al. (2004). The X-ray emission from the nucleus was roughly 18 times stronger than the emission from the lobe. We did not account for the obvious pileup in the nucleus, and thus this value is a lower limit on the strength of the nuclear emission.

VLBA observations have also shown jet structure on milli-arcsecond scales. This jet appears to be inclined at an angle less than 14°, and exhibits superluminal motion

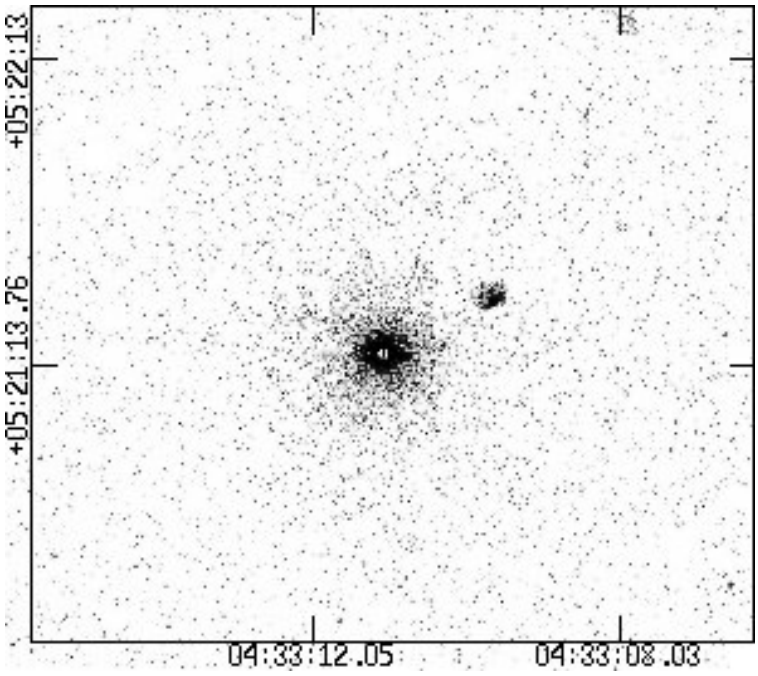

Figure 3.6: Chandra observation of 3C 120. Note small amount of emission from the X-ray jet, and obvious pileup in the center.

with an apparent velocity of $5c$. Because of the small size of the jet, it is impossible to separate the nuclear and jet X-ray emission using current X-ray observatories.

However, spectroscopy can help us to determine whether the X-ray emission that we see comes from the nucleus (accretion disk/corona) or from the jet itself. Ballantyne et al. (2004) have analyzed a 127 ks *XMM/Newton* observation of 3C 120. They find a neutral Fe Kα line with an equivalent width of 53 eV. There is no evidence for a relativistically broadened line. The strength of the Fe Kα line indicates that the majority of the X-ray emission has its origin in an unbeamed source, such as the accretion disk or corona, as opposed to the jet. If the X-ray flux were beamed within a narrow cone, reflection would be unlikely. Ogle et al. (2005) find a half-opening angle for the X-ray continuum of $> 50°$, indicating the narrow jet is not responsible

for the X-ray flux observed.

3.3 3C 390.3

Similar to 3C 120, 3C 390.3 has an X-ray jet. To check for the possibility of contamination from the jet, we have analyzed a 35 ks *Chandra* pointing (Figure 3.7). As before, a small amount of X-ray emission is visible at the position of the radio lobes, however the amount of emission is insignificant compared to that from the nucleus. Also, Gliozzi et al. (2003) noted the presence of a strong Fe Kα line in the X-ray spectrum. Such a line is never seen in blazars, where all of the emission is thought to originate in the jet.

We analyzed archival observations of 3C 390.3 (PI: K. Leighly), with data points once every 3 days from 1999 January 7 until 2001 February 23. The light curve is shown in Figure 3.8. The source is highly variable, varying from 1–7 Counts/sec/PCU during the observations.

We also analyzed the data from Gliozzi et al. (2003), with observations taken once per day from 16 May–11 July 1996 (Figure 3.9). The source declines steadily during the first 40 days of monitoring, then rises slightly during the last 20 days.

Leighly & O'Brien (1997) made a claim for the existence of non-linear variability in this object, based on a comparison of the light curve with the variance over a sliding box with a width of six data points. They found that the variance dropped (i.e. the flux became quiescent) immediately prior to a flare. To verify this claim on

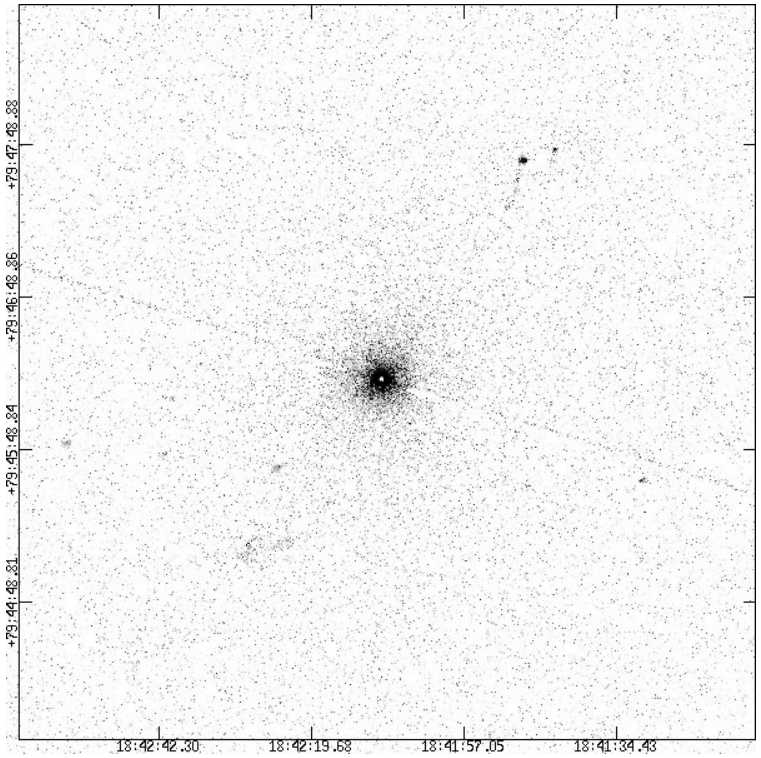

Figure 3.7: Chandra observation of 3C 390.3. Note small amount of emission from X-ray jet seen to the upper right of object.

longer timescales, we have performed a similar analysis, shown in in Figure 3.10.

The data show several dips in the variance, which are labeled in the Figure. With the exception of number 7, none of the dips in the variance precede a flare in the light curve. Also, the largest abrupt rise in the flux, shown at point 4 in the variance curve, has no significant dip in variance preceding it. These results contradict the shorter-term analysis of Leighly & O'Brien (1997), and do not suggest any evidence for non-linear variability in 3C 390.3.

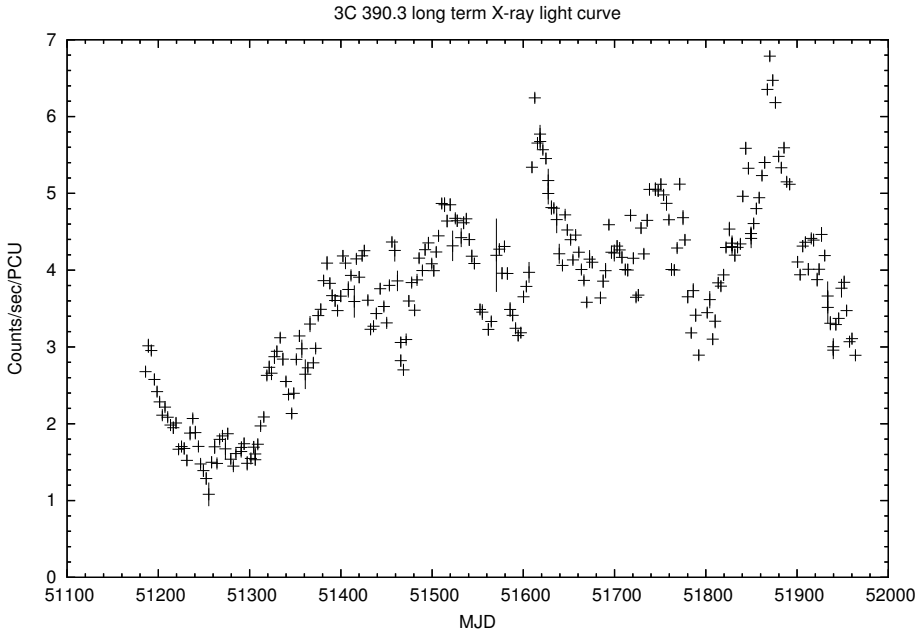

Figure 3.8: Long term X-ray light curve for 3C 390.3, with sampling every 3 days for two years.

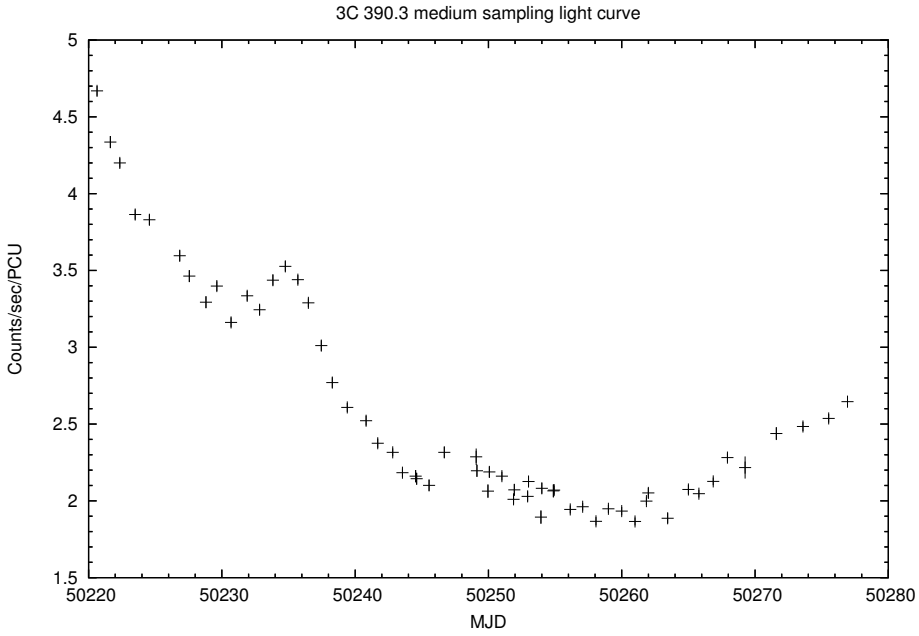

Figure 3.9: Intermediate sampling light curve for 3C 390.3, with observations once per day for 56 days.

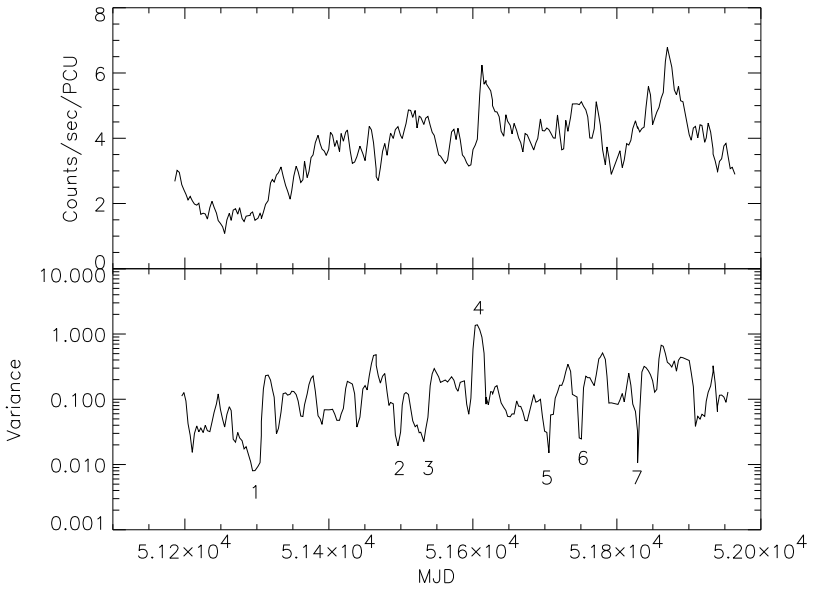

Figure 3.10: X-ray light curve for 3C 390.3 (top), and variance with a sliding box of width $N = 7$ points. Numbers represent dips and maxima in the variance.

3.4 Mkn 509

3.4.1 X-ray Data

For Mkn 509, we have obtained more than 3 years of monitoring, with observations taken every 3 days from 2003 March 27 until 2006 July 29. The source varies in flux by a factor of 2, with some unresolved high frequency variations. Unfortunately we do not have any short-term X-ray data to complement our long-term monitoring.

3.4.2 Optical Data

Utilizing queue observations obtained under the SMARTS observing consortium, we have also been monitoring Mkn 509 optically. Although observations were taken in

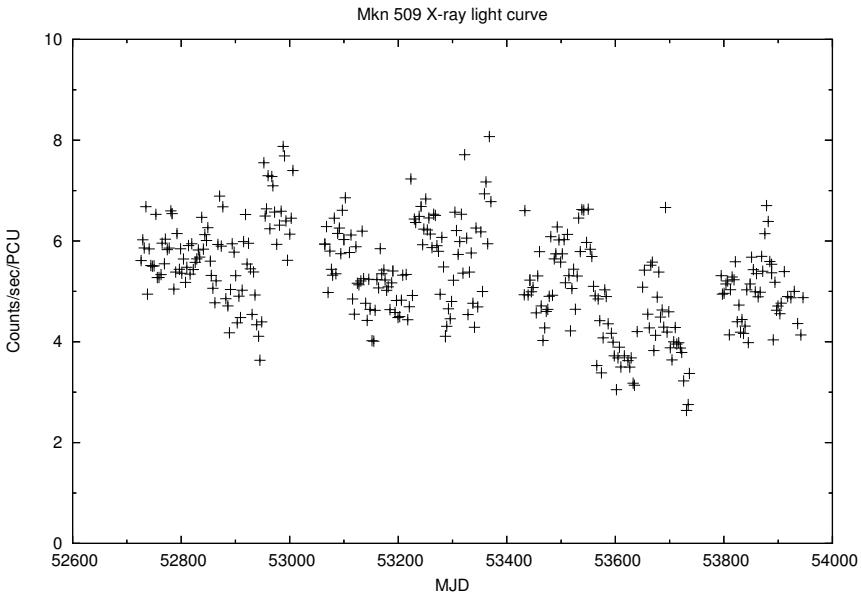

Figure 3.11: RXTE long term light curve for Mkn 509, with sampling every 3 days for nearly three years.

several filters, here we present only the R data. Differential photometry was performed using a number of comparison stars (Figure 3.12).

Figure 3.13 shows the comparison of Mkn 509 with check star A. The source varies by nearly half a magnitude during the observing campaign. We can check the accuracy of our data by comparing 2 check stars (Figure 3.14). In this case we see that the check stars vary by only a few hundredths of a magnitude, and so the variability that we see in Mkn 509 is real.

3.4.3 Cross Correlation

To search for any possible correlation between X-ray and optical fluxes, we must first convert our differential magnitudes into absolute fluxes. We know that check star A has an R magnitude of $R = 13.9$ (Miller 1986), so the magnitude is easily obtained

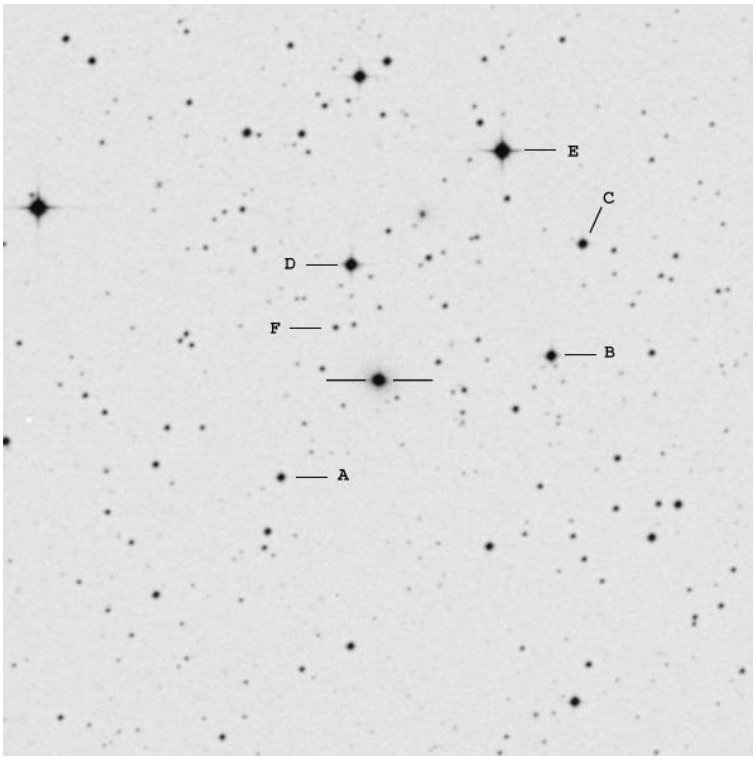

Figure 3.12: Optical finder chart for Mkn 509. Check stars A and B were used in the analysis.

by adding 13.9 to the object–check value derived from the differential photometry.

The general relationship between magnitude and flux is given by:

$$m_1 - m_2 = -2.5 \log \frac{f_1}{f_2} \tag{3.2}$$

For a reference star with magnitude 0 (i.e. Vega), this equation reduces to:

$$f_1 = f_2 10^{-0.4 m_1} \tag{3.3}$$

The factor f_2 is the zero-point flux density at a given wavelength, $F_{\lambda 0}$. We can now re-write the above equation as:

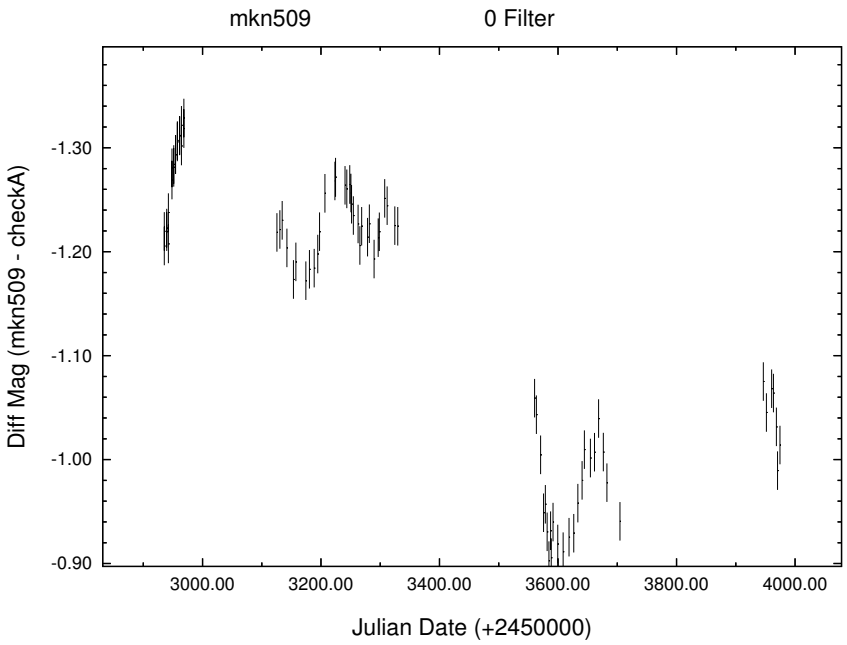

Figure 3.13: Optical variability for Mkn 509, covering approximately 3 years. All data are from the 1.3m telescope at CTIO.

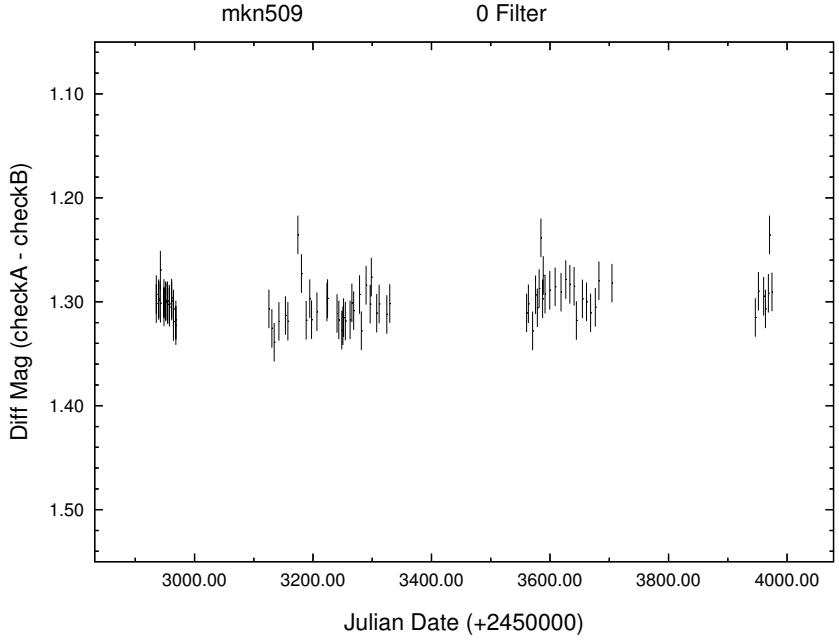

Figure 3.14: Check star A minus check star B for Mkn 509. Note lack of variations when compared to Mkn 509.

$$F_\lambda = F_{\lambda 0} 10^{-0.4m} \tag{3.4}$$

From Cox (2000), we know that $F_{\lambda 0} = 2941$ Jy for the R band, so now we can convert our differential magnitudes into absolute fluxes.

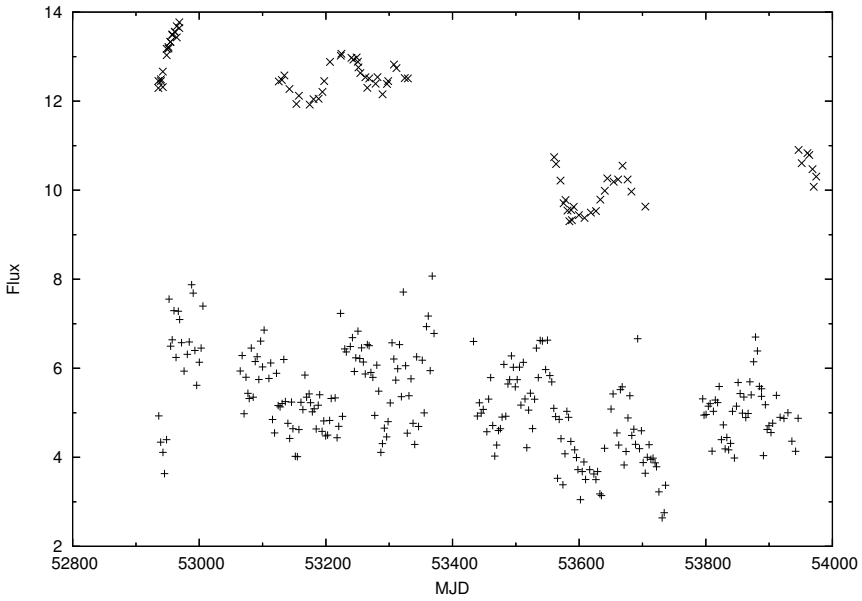

Figure 3.15: Mkn 509 optical (×) and X-ray (+) data plotted on an arbitrary flux scale. Note that the X-ray appears to follow the optical, with a lag of roughly 25 days.

In Figure 3.15, we plot the X-ray and optical fluxes versus time. Note that the optical coverage is not as complete as for the X-ray data, but there are still several significant events. Most noticeable are a 'bump' in the optical flux around MJD 53200, and a dip and a rise around MJD 53600. With a simple examination by eye, these events appear to correlate with the X-ray flux, with the optical leading the X-ray by a bit.

To further investigate the possibility of a correlation between the optical and X-ray flux, we use the Cross Correlation Function (CCF), defined as:

$$\mathrm{CCF}(\tau) = \int a(t)b(t-\tau)dt \tag{3.5}$$

where $a(t)$ and $b(t)$ are the light curves at time t, and τ is the lag time.

The traditional CCF requires evenly sampled data, and can be computationally intensive. Because of observing constraints, neither our X-ray nor optical data are evenly sampled. To solve this issue, we use the Discrete Correlation Function (DCF) of Edelson & Krolik (1988). The DCF allows for cross-correlation of two unevenly sampled data sets.

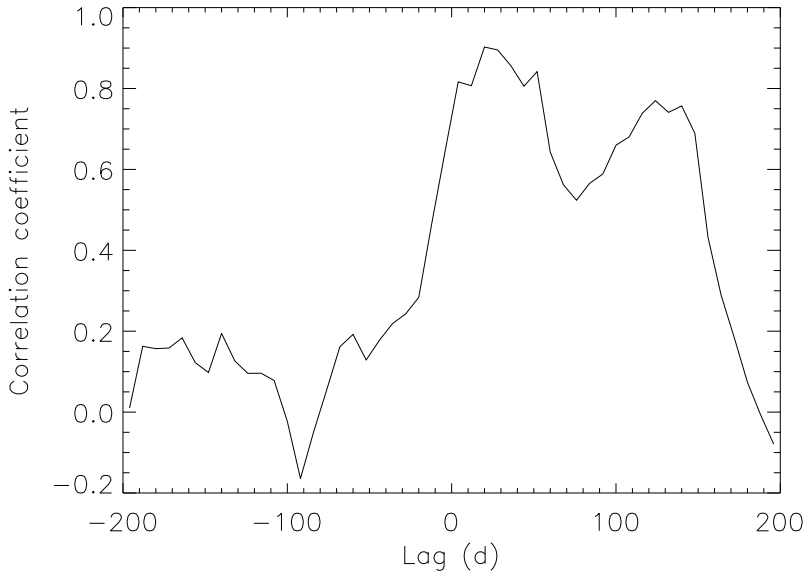

Figure 3.16: X-ray / optical cross correlation function for Mkn 509. Significant correlation appears at 25 and 125 days. The 125 day peak results from gaps in the data.

At 0 lag, the DCF (Figure 3.16) shows only a weak correlation coefficient of 0.5. At positive lags, we see two distinct peaks – one near 25 days, and the other near 125 days. In this case, a positive lag means the optical is leading the X-ray emission.

From visual examination, it seems most likely that the 25 day peak is real, and the 125 day peak is a result of gaps in the light curves. To further explore this possibility, we have offset the X-ray data by 125 days and plotted it against the optical data in Figure 3.17. Note that there is no X-ray coverage for the first group of optical observations. The second and third groups of optical data points also span significant gaps in the X-ray coverage. Based on this, we believe that the peak in the CCF near 125 days is a result of poor sampling in both the optical and X-ray bands.

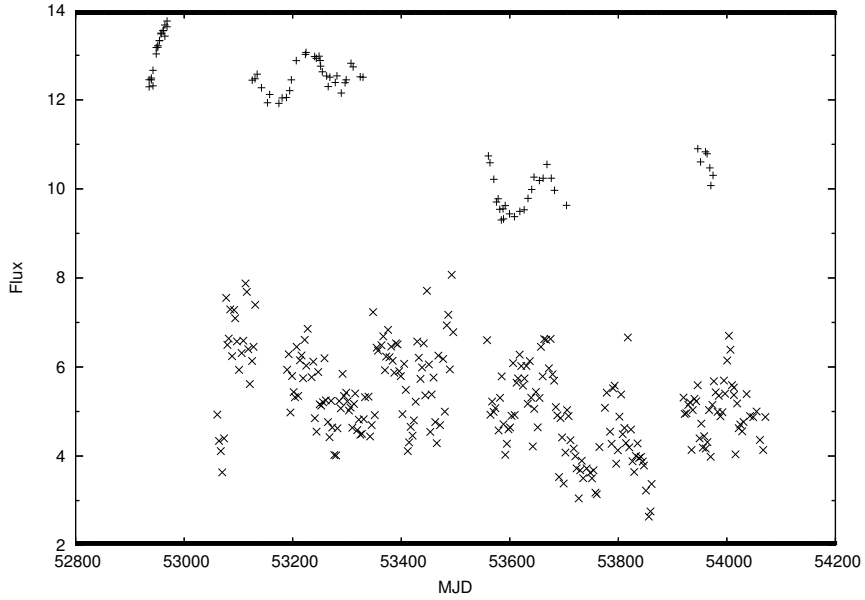

Figure 3.17: Mkn 509 optical (×) and X-ray (+) data. X-ray data have been shifted forward in time 125 days, to check for correlation between the data at that lag.

– 4 –

Analysis

4.1 Fundamentals of Time Series Analysis

Before we can begin a detailed analysis of the light curves presented in Chapter 3, we must first set some definitions regarding time series analyses.

- A *system* is the underlying cause of variability in the object, and is ultimately what we are trying to measure. For an AGN, this could be hot spots in an accretion disk, shocks in a jet, variations in accretion rate, etc.

- A *process* is a stochastic system that is sampled by our observations. The variability process is subject to observational errors and windows, and so determining the underlying system from observations of the process can often be difficult.

- A *model* is often the best way to characterize the variability process, and then relate it to the system through physical knowledge of the object being studied.

Given this, how can we best measure the variability process in an object, and obtain a suitable model? The answer lies in the Fourier transform. Defined as:

$$F(\nu) = \int_{-\infty}^{+\infty} f(t) e^{i2\pi\nu t} dt, \tag{4.1}$$

the Fourier transform displays data as a function of frequency, rather than time. For non-continuous data sets, we can also define a discrete Fourier transform,

$$F_N(\nu) = \sum_{k=1}^{N} f(t_k) e^{i2\pi\nu t_k}, \tag{4.2}$$

which is defined at evenly spaced intervals, $\nu_{\rm min}$, $2\nu_{\rm min}$, $3\nu_{\rm min}$, $\ldots \nu_{\rm Nyq}$, where $\nu_{\rm min}$ is equal to $1/T$ (where T is the total duration of the light curve), and the Nyquist frequency $\nu_{\rm Nyq} = N/2T$, where N is the number of data points.

Note that the Fourier transform contains both real and imaginary components. To extract a physically measurable quantity from the Fourier transform, we can take the modulus squared by multiplying the Fourier transform by its complex conjugate:

$$|F(\nu)|^2 = F(\nu) * \tilde{F}(\nu). \tag{4.3}$$

This is known as the power density spectrum (PDS) of an object, $P(\nu)$. It is interesting to note that the PDS is the Fourier pair of the autocorrelation function (Deeming 1975), i.e.,

$$P(\nu) = \int_{-\infty}^{+\infty} r(\tau) e^{i2\pi\nu t}\, dt = 2 \int_{-\infty}^{+\infty} r(\tau) \cos 2\pi\nu t\, dt, \tag{4.4}$$

where $r(\tau)$ is the autocorrelation function of the light curve, defined as the cross correlation of a function with itself.

The Fourier transform requires evenly sampled data, which is almost never the case with real-world observations. To avoid this issue, we use the Lomb-Scargle periodogram of Scargle (1982). The periodogram provides an estimate of the PDS, and is essentially the same for evenly sampled data.

For a periodic light curve, the power spectrum will show a strong peak at the corresponding frequency. However, AGN light curves do not appear to be periodic. They appear to be far more 'noisy.'

Noise, in the Fourier sense, is defined as having a PDS that is a power law, i.e. $P(\nu) \propto \nu^{-\alpha}$, where α is the power law index. Note that α is usually defined so that a positive value yields a negative power law slope. For different power law slopes, we obtain different light curves.

The simplest case, where $\alpha = 0$, is commonly called white noise. Here, the variability power is spread across all frequencies evenly. Although interesting, this case is physically impossible for AGN, due to the absence of variability power contained at the highest frequencies created by the impossibly small light travel time required to cause such variations. As shown by the simulation in Figure 4.1, the variations seen in the simulation are limited only by the resolution of the computations involved. With infinitely fine time steps, the source would vary on an infinitely small timescale.

For a steeper slope of $\alpha = 2$ we obtain red noise, otherwise known as random walk noise, or Brownian noise. Here the steep power law slope removes the high frequency variations, and we are left with a light curve that varies smoothly and slowly over time,

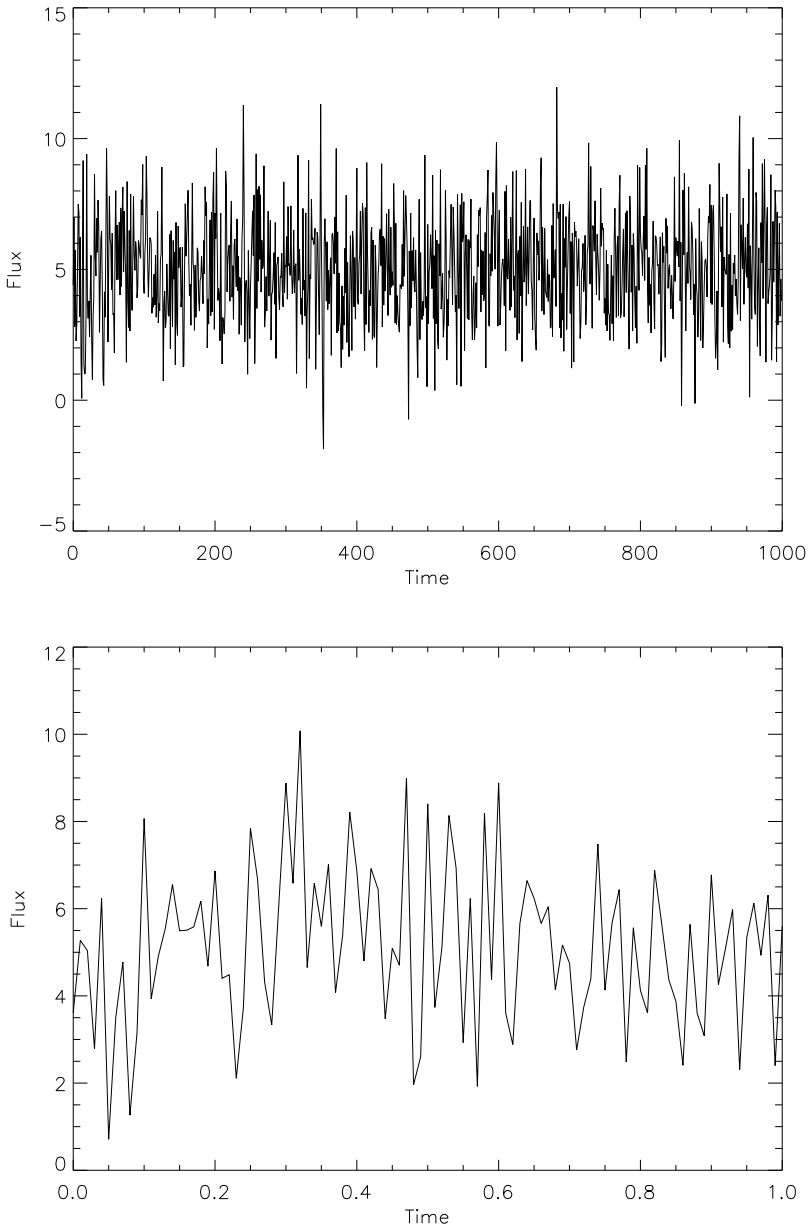

Figure 4.1: White noise light curves, generated from a power law PDS with spectral index of 0. Top panel shows a simulation length of 1000 steps, with data computed at intervals of 1 step. As the computational resolution is increased from 1 step to 0.01 steps, the bottom panel shows that the variability becomes finer as well.

as shown in Figure 4.2. We no longer have a problem with variability on infinitely small time scales; however, the total variability power will diverge as we integrate over all frequencies. No object can have infinitely large variability power, and so this type of noise is unphysical as well.

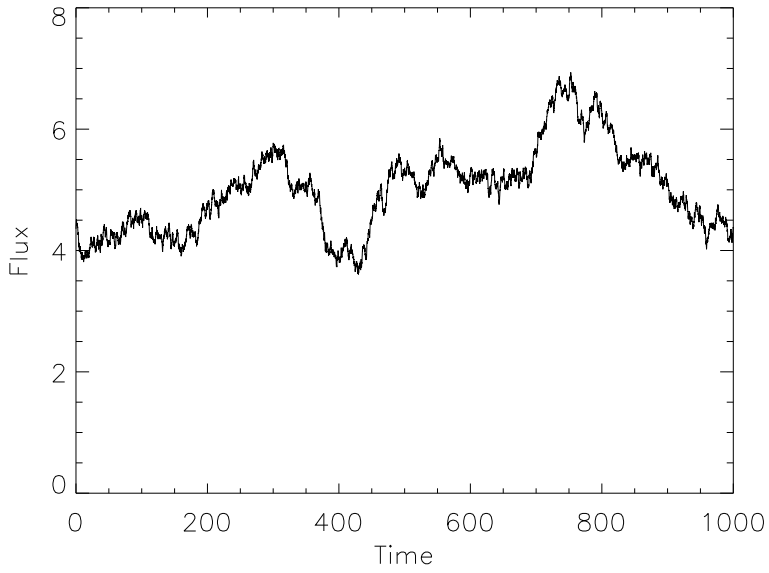

Figure 4.2: Pure red noise light curve, generated from a power law PDS with spectral index of -2. Note the complete lack of high frequency variability.

If we use an intermediate slope of $\alpha = 1$, we obtain what is known as flicker noise, or sometimes pink noise (Figure 4.3). In this case, there is more variability power at low frequencies than at high frequencies, and so the light curve shows large variations at long timescales, with small variations at shorter timescales superimposed.

The case of $\alpha = 1$ represents a special case for physical systems. With a shallower slope, there will still be significant variability power at high frequencies (similar to

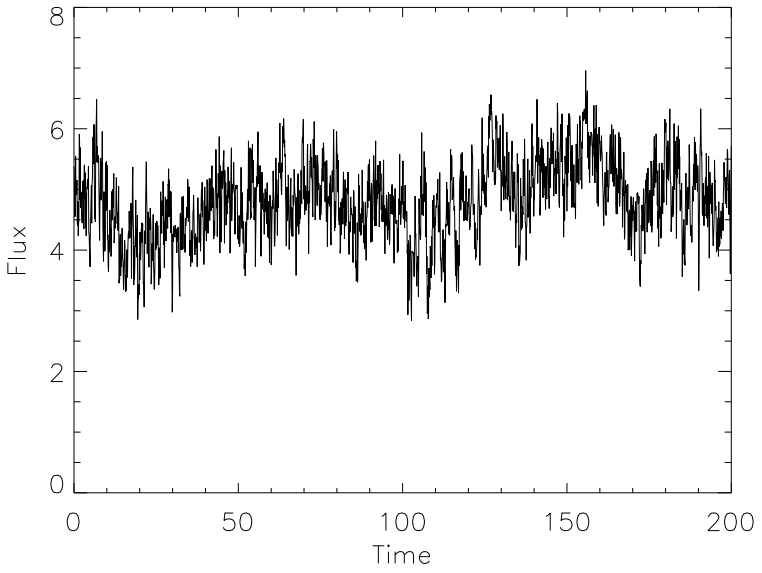

Figure 4.3: Flicker noise light curve, generated from a power law PDS with spectral index of -1.

white noise), making the system physical. However, for steeper slopes of $\alpha > 1$, the total variability power will diverge.

Given all of the above, what can we say about the variability process in AGN? At high frequencies, the power spectrum must have a steep slope of $\alpha > 1$, with some break frequency $\nu_{\rm b}$ below which the power spectrum turns over to a shallower slope of $\alpha < 1$. This type of PDS has been seen before in X-ray binaries. Below we explore the shape of the PDS, and the significance of the break frequency.

4.2 Stationarity

Power spectrum analysis can only be considered meaningful if the underlying variability process is stationary. In the statistical sense, stationary means that the process

does not change over time. But how can this best be measured?

For each light curve, we can measure the mean and variance for small segments, and see if they change over time. However, for any red noise process, the mean and variance will change regardless of stationarity, due to the finite observation length. This can be seen in Figure 4.4. Examining the data by eye, we can see that the mean is significantly higher for days 50–100 when compared to days 100–150. This light curve was generated from a single, stationary model and thus any changes in the mean or variance are a result of the red noise process itself.

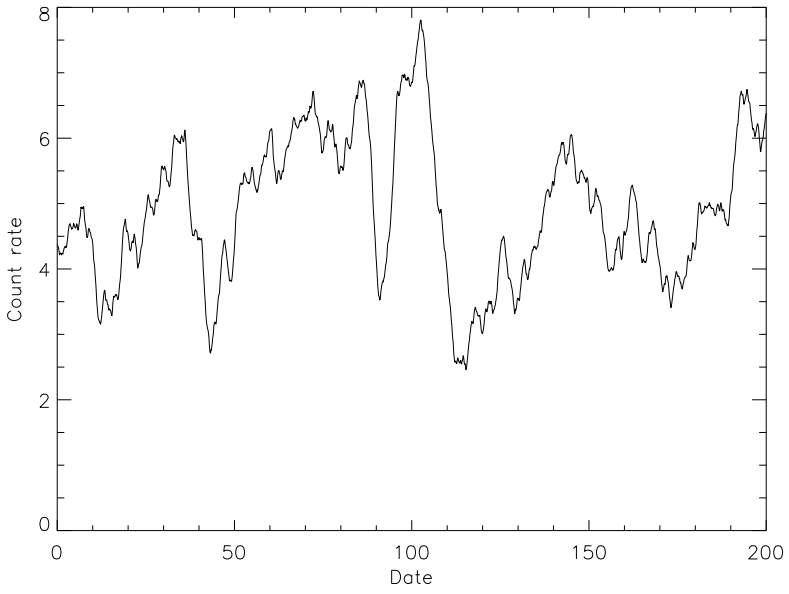

Figure 4.4: Simulated X-ray light curve, generated from a power spectrum with index -1.25 and break at $10^{-5.5}$ Hz.

Similarly, Vaughan et al. (2003a) have examined a 100 ks *XMM* observation of Mkn 766, and measured statistical parameters for bins of 20 points in the light curve.

They find that both the mean and fractional variability change by a factor of 2 during the observation.

Given that the mean and variance can both be expected to change with time for a red noise process, how else can we test for stationarity? Each realization of the variability process is governed by the underlying power spectrum, and so by comparing power spectra for different segments of the light curve, we can effectively test for stationarity.

Papadakis & Lawrence (1995) define the "S" statistic, which measures stationarity in the power spectrum. Briefly, the light curve is divided into two equal halves, the periodogram is computed for each, and then compared using the S statistic, where S is defined as:

$$S(\nu) = \frac{\log P_1(\nu) - \log P_2(\nu)}{\sqrt{\mathrm{var}[\log P_1(\nu)] + \mathrm{var}[\log P_2(\nu)]}}, \tag{4.5}$$

where $P_{1,2}(\nu)$ are the periodograms for each half of the light curve, and $\mathrm{var}[\log P_{1,2}] = 0.31$ (Papadakis & Lawrence 1993). We can then sum over all frequencies to find the test statistic S,

$$S = \frac{1}{N} \sum_{n=1}^{n_{max}} S(\nu_n), \tag{4.6}$$

where N is the total number of frequencies for which we have calculated the periodogram. For two identical periodograms, S will have a Gaussian distribution with

zero mean and unit variance. Or in other words, if $|S| < 1$ we can reasonably assume the variability is stationary.

For our sample, we have calculated S for each long-term light curve, because any changes in the periodogram should be most easily visible on the longest timescales. The results can be seen in Table 4.1. Each object shows $-1 < S < 1$, and so from analyzing the periodogram it seems likely that the the underlying variability process remains stationary during all of our light curves.

Table 4.1: S Test Results

Name	S
Akn 120	0.778
Mkn 509	-0.194
3C 120	-0.324
3C 390.3	0.733

4.3 The rms-flux Relationship

Thus far we have shown that the variance, mean, and fractional variability can be expected to vary over time for a red noise process, while the shape of the periodogram remains constant. We can further investigate the stationarity of our data using the excess variance, $\sigma^2_{\rm XS}$.

Similar to $F_{\rm var}$, $\sigma^2_{\rm var}$ measures the intrinsic source variance, independent of measurement errors. Edelson et al. (2002) define the excess variance as:

$$\sigma^2_{\rm var} = S^2 - \overline{\sigma^2_{\rm err}}, \tag{4.7}$$

where S^2 is the variance (not to be confused with S from above), and $\overline{\sigma^2_{\rm err}}$ is the mean square error for the light curve.

The existence of a linear relationship between the excess variance and the flux level has been well established for X-ray binaries such a Cygnus X-1 and SAX J1808.4–3658 (Uttley & McHardy 2001). Such a relationship has been noted for several Seyfert galaxies as well, such as NGC 4051 and MCG–6-30-15 (Vaughan et al. 2003b).

To test for the presence of an rms-flux relationship in our own data, we have calculated the variance for each light curve with a sliding bin of width 7 data points, similar to Leighly & O'Brien (1997). The excess variance was then calculated, and then averaged along with the flux into bins of width 0.25 counts/sec.

Both of our radio loud objects show a clear correlation between excess variance and flux, with $\sigma_{\rm var}$ increasing as the count rate increases (Figures 4.5 and 4.6). This correlation is well-defined, with Spearman rank-order correlation coefficients of 0.96 for 3C 390.3 and 0.72 for 3C 120. Quantitatively speaking, such an rms-flux relationship will cause the quiescent periods to show less short-term variability, while bright flares will show jagged peaks from an increase in the rms variability. For 3C 120, we have used the intermediate sampling light curve for the rms-flux calculation, because

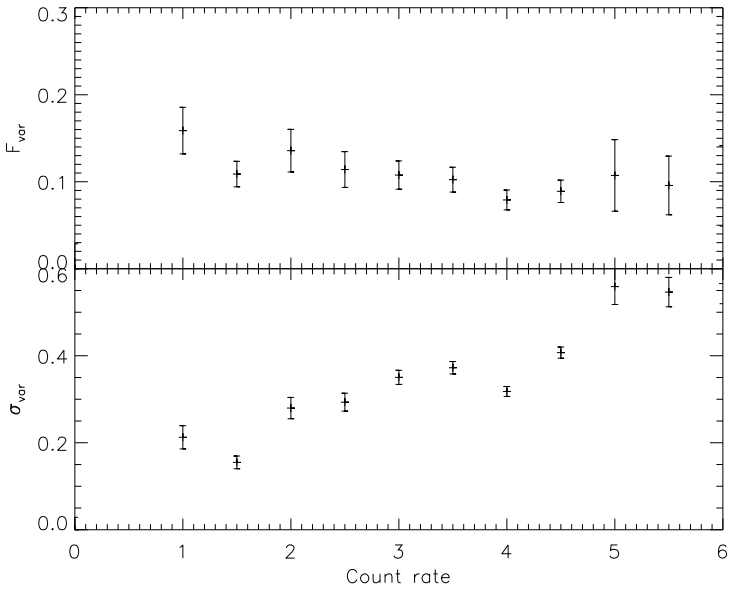

Figure 4.5: $F_{\rm var}$-flux and rms-flux relationship for 3C 390.3.

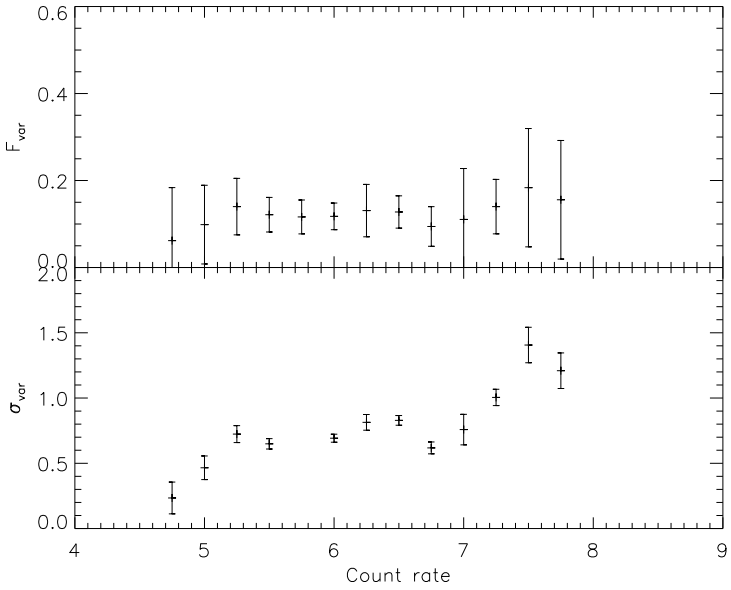

Figure 4.6: $F_{\rm var}$-flux and rms-flux relationship for 3C 120.

it is nearly the same length as the long-term light curve, and offers better sampling by a factor of > 3.

This rms-flux relationship represents a form of non-stationarity, in that the variance changes with flux. This trend can be removed by plotting $F_{\rm var}$ as a function of flux, since the fractional variability is normalized to the flux. When we do this, we see that $F_{\rm var}$ remains relatively constant with respect to the flux.

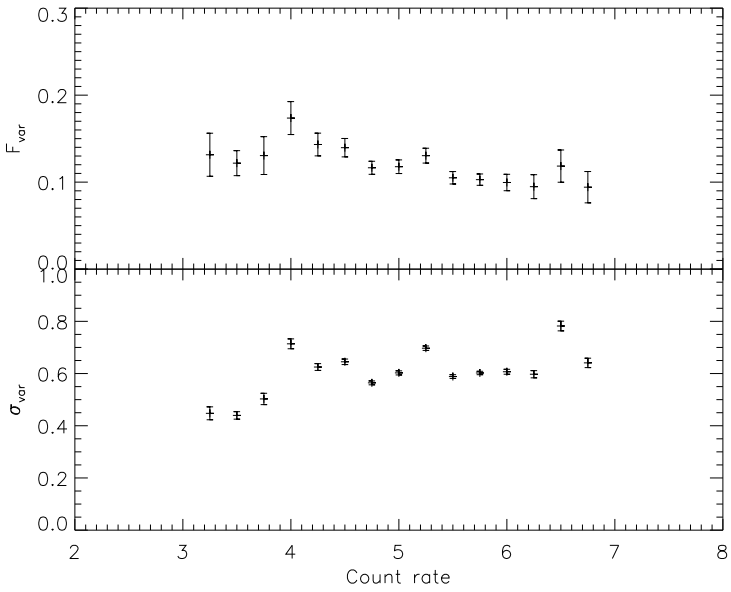

Figure 4.7: $F_{\rm var}$-flux and rms-flux relationship for Mkn 509.

For our radio quiet objects, Mkn 509 and Akn 120, there is no clear evidence of an rms-flux relationship (Figures 4.7 and 4.8). For Akn 120, Figure 4.8 shows possible evidence of a correlation, but only weakly (Spearman r coefficient = 0.50). For Mkn 509, no correlation is seen. In either case, plotting $F_{\rm var}$ against flux shows no correlation.

From this, we can assume that aside from the known rms-flux correlation in our radio loud objects, no other form of non-stationarity is present in the light curves

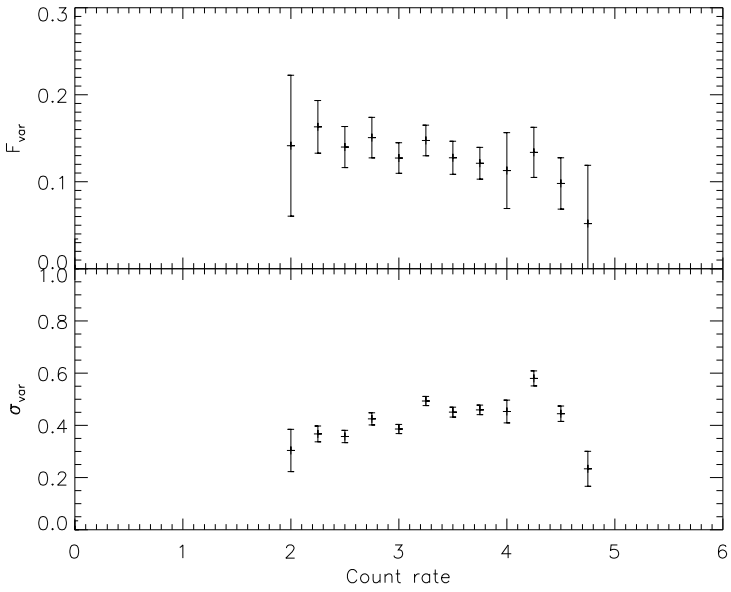

Figure 4.8: $F_{\rm var}$-flux and rms-flux relationship for Akn 120.

and the periodogram remains constant with time. Further details of the rms-flux relationship will be discussed in Chapter 5.

4.4 Computing the Power Density Spectrum

For any discretely sampled, finite length data set, there are many caveats and complications when trying to compute the periodogram. We review some of those difficulties below.

4.4.1 Windowing

The Fourier transform assumes ideal conditions for the data, i.e., continuous sampling and an infinitely long data set. For an actual observed light curve, obviously neither one of these is possible. In that case, the observed data will be modified by a window

function, so that

$$f(t) = r(t)w(t), \tag{4.8}$$

where $r(t)$ is a realization of the process, $w(t)$ is our windowing function, and $f(t)$ is the observed light curve. The Fourier transform of our light curve will then be the convolution of the Fourier transform of the process with the Fourier transform of the window function.

In the most simple case, the window will look like a boxcar function, with zero value before the start of our observations, a value of 1 during the observations, and then back to zero afterward. For a more realistic case of discretely sampled observations, the Fourier transform of the window function will be the Fejer kernel (Priestley 1981), which has a shape very similar to the sinc^2 function. This causes variability power to shift or 'leak' on either side of individual points in the periodogram. This introduces the problems of aliasing and red noise leakage, which are discussed in more detail below.

4.4.2 Aliasing

The periodogram is not calculated above the Nyquist frequency, $f_{\mathrm{Nyq}} = N/(2\Delta T)$, where N is the number of observations, and T is the time between observations. Variability on timescales shorter than T can not be resolved, and so power is shifted or 'aliased' from frequencies above f_{Nyq} to lower frequencies. The aliased power is

reflected about the Nyquist frequency, i.e., shifted from $f_{\rm Nyq}+\Delta\nu$ to $f_{\rm Nyq}-\Delta\nu$ (Uttley et al. 2002).

For a red noise PDS, the amount of variability power drops off steeply with increasing frequency, and so at very high frequencies there will be negligible contribution to aliasing. For a light curve with resolution of T, it can also be assumed that variations at frequencies higher than $N/(2T)$ will be smoothed out and not contribute any significant variability power.

Therefore, we can correct for aliasing by adding a constant amount of variability power to the computed periodogram. The amount of power is given by integrating the estimated periodogram from $f_{\rm Nyq}$ to $2f_{\rm Nyq}$, or

$$P_{\rm alias} = \frac{1}{\nu_{\rm Nyq} - \nu_{\rm min}} \int_{\nu_{\rm Nyq}}^{2\nu_{\rm Nyq}} P(\nu) d\nu. \tag{4.9}$$

Thus, the effects of aliasing can easily be accounted for when computing the periodogram.

4.4.3 Red Noise Leakage

Similarly to the aliasing mentioned above, power is also transferred from low frequencies into the observed frequency range. Due to the power law nature of the variability process in AGN, this power can be greater than the amount of power in the calculated periodogram. There is no simple way to correct for the effects of red noise leakage; however, one solution is to use Monte Carlo simulations, which we discuss in more

detail in §4.5.

4.4.4 Normalization

After computing the periodogram, we need to find an appropriate and meaningful way to normalize it. As in previous works (Uttley et al. 2002; Markowitz et al. 2003a) we use the fractional rms squared normalization,

$$P(\nu) = \frac{2T}{\mu^2 N^2}|F(\nu)|^2 \tag{4.10}$$

where T is the duration of the light curve, μ is the mean count rate, and N is the number of data points. Using this normalization, if we integrate over a frequency range from ν_1 to ν_2, we obtain the fractional variability on timescales from $1/\nu_1$ to $1/\nu_2$. The total fractional variability is thus the integral of the normalized PDS from $\nu_{\rm min}$ to $\nu_{\rm Nyq}$.

The level of Poisson noise in the light curve will be equal to $2(\mu + B)/\mu^2$, where B is the mean background count rate (Uttley et al. 2002). By using a consistent normalization, we can compare power spectra measured with different instruments across different time scales.

4.4.5 Variance of the PDS

As noted in Papadakis & Lawrence (1993), the periodogram possesses the unique property that the rms error of each point is equal to the value of the periodogram

at that point, so that var $[P(\nu)] = P^2(\nu)$. This can be seen in the top panel of Figure 4.9, which was generated from a simulated light curve. All of the scatter seen in the periodogram is intrinsic, i.e. not related to measurement errors.

It would be tempting to try to reduce the variance by using more data points, either from closer sampling or a longer overall data length. However, a larger number of data points only adds to the number of frequencies at which the periodogram is calculated. The variance of those points remains the same.

There are a number of ways around this problem. For a source like an X-ray binary, which is bright and varies on timescales of seconds or less, we can generate a large number of periodograms and then average them together. For an AGN, in which we are interested in variability on timescales of years, this is not possible.

Papadakis & Lawrence (1993) use logarithmic binning to reduce the variance of the periodogram. In that case, the variance is inversely proportional to the number of points in each bin. The bottom panel of Figure 4.9 shows the top panel periodogram, with each bin including a factor of 2 in frequency (0.3 in the logarithm) and a minimum of four points per bin. The variance in the periodogram is now greatly reduced, and we can easily see the original shape of a bending power law.

4.5 Monte Carlo Simulations

To account for the errors on the power spectrum discussed above, we use Monte Carlo simulations to model the underlying variability process. A large number of

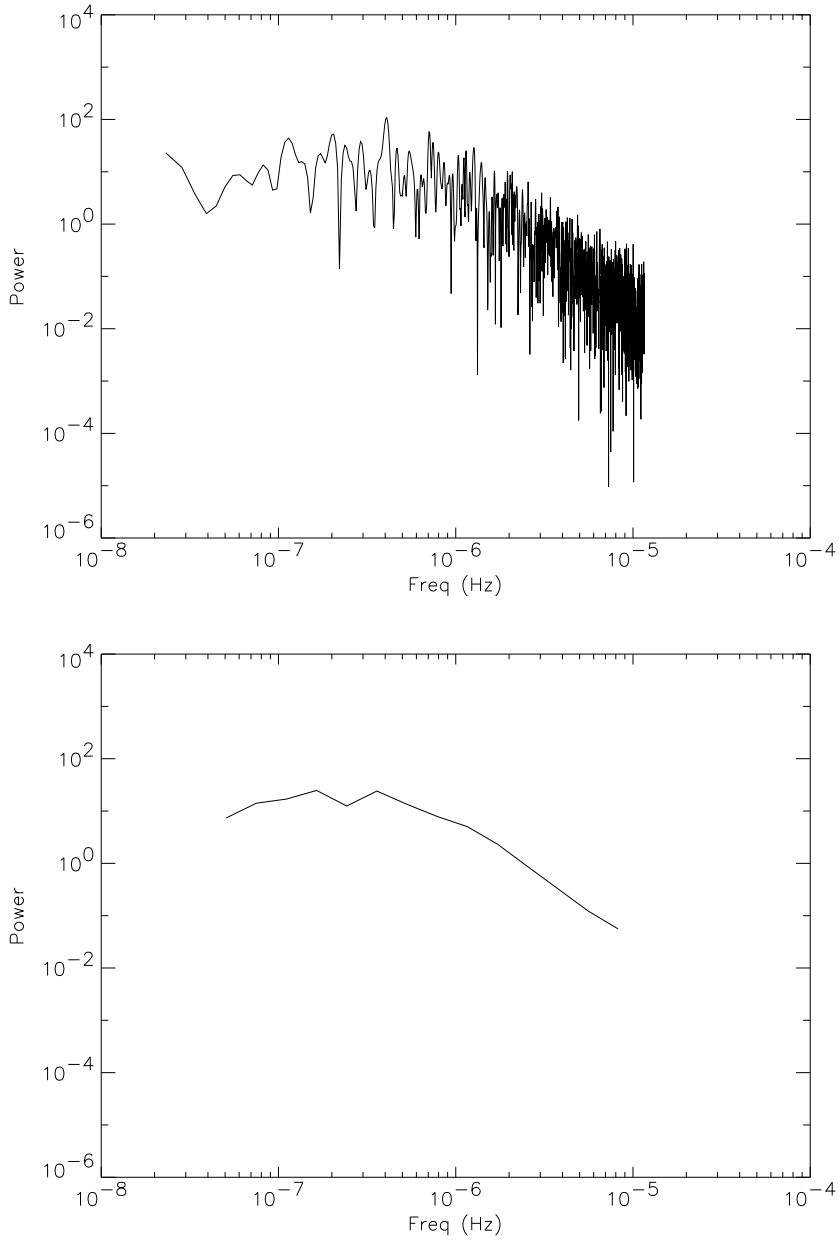

Figure 4.9: Comparison of unbinned (top) and binned (bottom) power spectra. The spectra were generated from simulated data, so the scatter seen in the unbinned spectrum is real, i.e. not a result of measurement errors. Binning the power spectrum by every factor of two, with a minimum of four points per bin, yields a result more closely resembling the original power spectrum.

simulated light curves are generated based on a known power spectrum. The light curves are then sampled in exactly the same fashion as the original light curve, and the periodogram is calculated. The periodograms are then averaged to determine the mean shape of the power spectrum. The spread of simulated powers about the mean can be used to determine errors and goodness of fit of the model.

Such a method was first used by Done et al. (1992) for measuring unevenly sampled *Ginga* light curves. They analyzed only a single light curve of several days duration. Also, they used the χ^2 statistic to measure the goodness of fit, which is not a reliable statistic for reasons discussed below.

The Monte Carlo simulation method was greatly expanded upon by Uttley et al. (2002), and later used by Markowitz et al. (2003b), McHardy et al. (2004), and Uttley & McHardy (2005) for estimating the power spectra of several AGNs (for a slightly different method, see Mueller et al. 2004). We explain the method of Uttley et al. (2002) in more detail below.

We begin by choosing an underlying power spectrum, either a power law or a broken/bending power law. The normalization is a multiplicative factor which is unchanged by any convolution, so we can use an arbitrary normalization and then re-normalize to obtain the best fit to the data later.

For each observed light curve, we simulate N light curves using the algorithm of Timmer & Koenig (1995), which randomizes both the phase and the amplitude of the Fourier transform of the data. This is superior to the method of summing

sine waves of randomized phase in that the power at each frequency is drawn from a χ^2 distribution, as should be the case for a noise process, and is not fixed at the amplitude of the underlying power spectrum.

Ideally, N should be large (~ 1000) to provide the most accurate possible distribution of values; however, we limit N to 100, for computational efficiency. The resolution of the simulated light curves, $\Delta T_{\rm sim}$, should be the same as the initial resolution of our observed light curves, $\Delta T_{\rm bin}$. This is because variations on time scales down to the exposure time will contribute to aliasing. However, for a typical monitoring light curve which consists of 1 ks observations, ensuring that our simulated light curves have 1 ks resolution would be computationally prohibitive.

Instead, we can correct for aliasing in the following ways. First, our simulated light curves have resolution at a fraction of the sampling rate, so that $\Delta T_{\rm sim} < 0.1 \Delta T_{samp}$. For light curves whose power spectra are a power law, the uncertainty in aliasing is dominated by frequencies not much greater than the Nyquist frequency. Second, we can estimate the amount of power at frequencies greater than the Nyquist frequency using the expression:

$$P_{\rm alias} = \frac{1}{f_{\rm Nyq} - f_{\rm min}} \int_{(2\Delta T_{\rm sim})^{-1}}^{(2\Delta T_{\rm bin})^{-1}} P(f) df. \tag{4.11}$$

The values for $P_{\rm alias}$ are typically very small, and are added to the resultant power spectra.

To account for red noise leak, the simulated light curve must be significantly longer

than the observed light curve, so that power at frequencies lower than $f_{\rm min}$ is sampled. To accomplish this, we simulate a single light curve of length NT, which is then split up into N individual segments.

Once the light curve has been simulated, it is then resampled in the same fashion as the observed light curve, and the periodogram is calculated. The periodogram is rebinned using the same method as the observed light curve, binned logarithmically every factor of 1.5, with a minimum of two points per bin. The average periodogram $\overline{P_{\rm sim}}$ is calculated for all segments, with the rms spread of the points giving the error $\Delta\overline{P_{\rm sim}}$.

Given our model average power spectrum, we now need a way to normalize it to the existing data. Comparison of the simulated periodogram with the observed using a traditional χ^2 statistic is not possible, because the error on the observed periodogram is not strictly Gaussian. Instead, we use the statistic $\chi^2_{\rm dist}$, which is defined as

$$\chi^2_{\rm dist} = \sum_f \frac{(\overline{P_{\rm sim}(f)} - P_{\rm obs}(f))^2}{(\Delta\overline{P_{\rm sim}(f)})^2}. \tag{4.12}$$

The total $\chi^2_{\rm dist}$ is calculated by summing over all frequency bins. The best-fitting normalization can be found by re-normalizing $\overline{P_{\rm sim}}$ until $\chi^2_{\rm dist}$ is minimized. During this step we also add in Poisson noise to each periodogram, where the Poisson noise is given by $P_{\rm Poisson} = 2(\mu + B)/\mu^2$, where μ is the mean count rate, and B is the mean background count rate. For non-continuously observed light curves, we must

also multiply by $\Delta T_{\rm samp}/\Delta T_{\rm bin}$.

Given the above, we can now calculate what goodness of fit our values of $\chi^2_{\rm dist}$ correspond to. The $\chi^2_{\rm dist}$ variable is not the same as a standard χ^2 value, because the $P_{\rm obs}$ values are not normal variables, since the number of values averaged in each frequency bin is small. Instead, for each input light curve, we use the N individual simulated periodograms to calculate the distribution of $\chi^2_{\rm dist}$.

For Mkn 509, which has only 1 light curve, we calculate $\chi^2_{\rm dist}$ for each periodogram estimate. For our other objects, which have 2–3 light curves, we choose 1000 random pairs of long, medium, and short term light curves. For each, $\chi^2_{\rm dist}$ is then calculated, and compared with $\chi^2_{\rm dist}$ calculated for the observed light curve. The probability that the model can be accepted is given by the percentage of combinations for which the observed $\chi^2_{\rm dist}$ is greater than that for the simulated periodograms.

Such a method of determining a goodness of fit is well known, and a more general description can be found in §15.6 of Press et al. (1992).

In summary, the method is as follows.

- Calculate the power spectrum of each observed light curve, and bin by factors of 1.5.

- Given a model for the power spectrum, generate N fake curves (where $N > 100$) and re-sample in the same manner as the original light curve.

- Calculate the periodogram for the simulated light curve, and bin in the same manner as the observed periodogram. Average the N separate periodograms, with error bars coming from the rms spread of the simulated power.

- Estimate $\chi^2_{\rm dist}$ for the observed versus the model power spectrum, and re-normalize the model to minimize this value.

- Calculate $\chi^2_{\rm dist}$ for M combinations of simulated periodograms, where $M > 100$. The probability of acceptance is given by the percentage of $\chi^2_{\rm dist}$ for the simulated data which are less than $\chi^2_{\rm dist}$ for the observed data.

4.6 The PDS of Cygnus X-1

One critical assumption in the Monte Carlo simulations involves an assumption of which model to use. As in previous studies, we base our models on observations of the galactic black hole binary Cygnus X-1. With a black hole mass of 10 $M_\odot$ (Belloni & Hasinger 1990), Cygnus X-1 has been studied more than any other X-ray binary.

The PDS of Cygnus X-1 features 2 distinct states: a high/soft state with high flux and a soft (steeper) X-ray spectrum, and a low/hard state with low flux a hard (flatter) X-ray spectrum. Each state also has a markedly different PDS. The high/soft state has a slope of –1 at low frequencies, which breaks to a slope of –2 near 13 Hz. The low/hard state has a slope of 0 at low frequencies, which breaks to a slope of

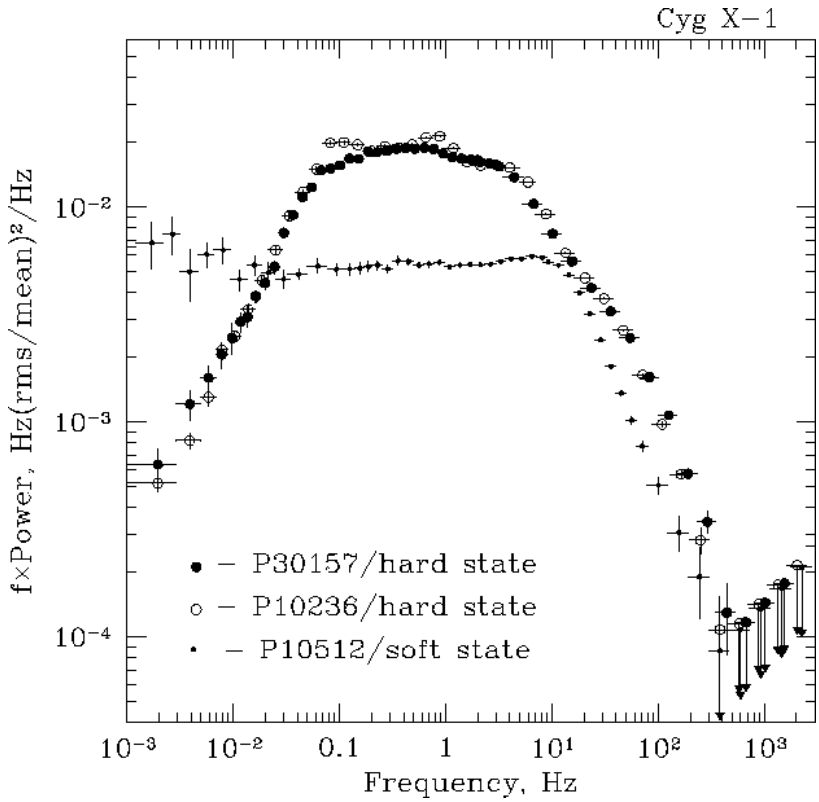

Figure 4.10: X-ray PDS of Cygnus X-1. Note that the y-axis is frequency times power, so that a slope of $\alpha = 1$ appears horizontal. The high/soft state has a single break near 13 Hz, while the low/hard state has breaks at frequencies of 0.2 and 3 Hz. (Revnivtsev et al. 2000)

–1 near 0.2 Hz, and then again breaks to –2 at 3 Hz. The power of both states is illustrated in Figure 4.10. The nature of these states is discussed further in §5.3.

4.7 Results

For each of our objects, we began by fitting a simple power law of the form:

$$P(\nu) = A \left(\frac{\nu}{\nu_0} \right)^{-\alpha}, \tag{4.13}$$

where A is the variability amplitude at frequency ν_0. Power law slopes were tested in the range from –2.5 to –0.5, in increments of 0.1. For each of our objects, we find that a simple unbroken power law can be rejected.

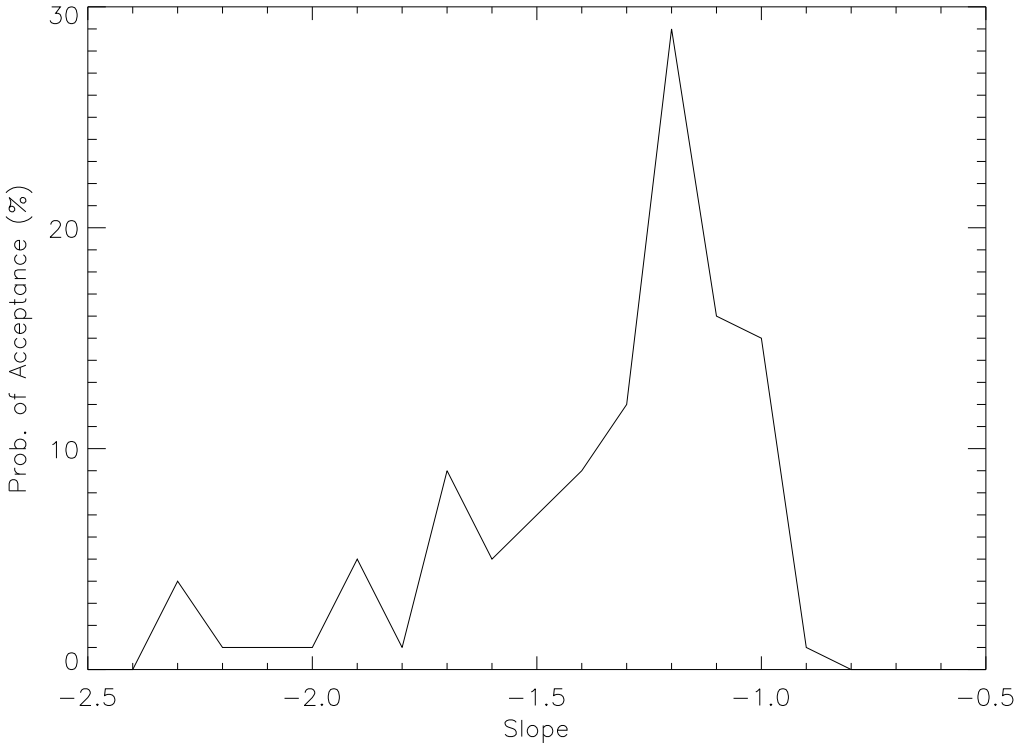

Figure 4.11: Unbroken power law fit probabilities for Mkn 509. The maximum likelihood of acceptance occurs at slope –1.2, with a probability of 29%.

The greatest likelihood of acceptance occurs for Mkn 509, with a 29% probability of acceptance at a slope of –1.2 (Figure 4.11). However it should be noted that the PDS for Mkn 509 only covers 2 decades of temporal frequency, and thus it is more difficult to see changes in the shape of the power spectrum.

For 3C 390.3, we find a very low likelihood of acceptance for a simple power law. The greatest probability occurs at a slope of –1.9, with a probability of only 6%

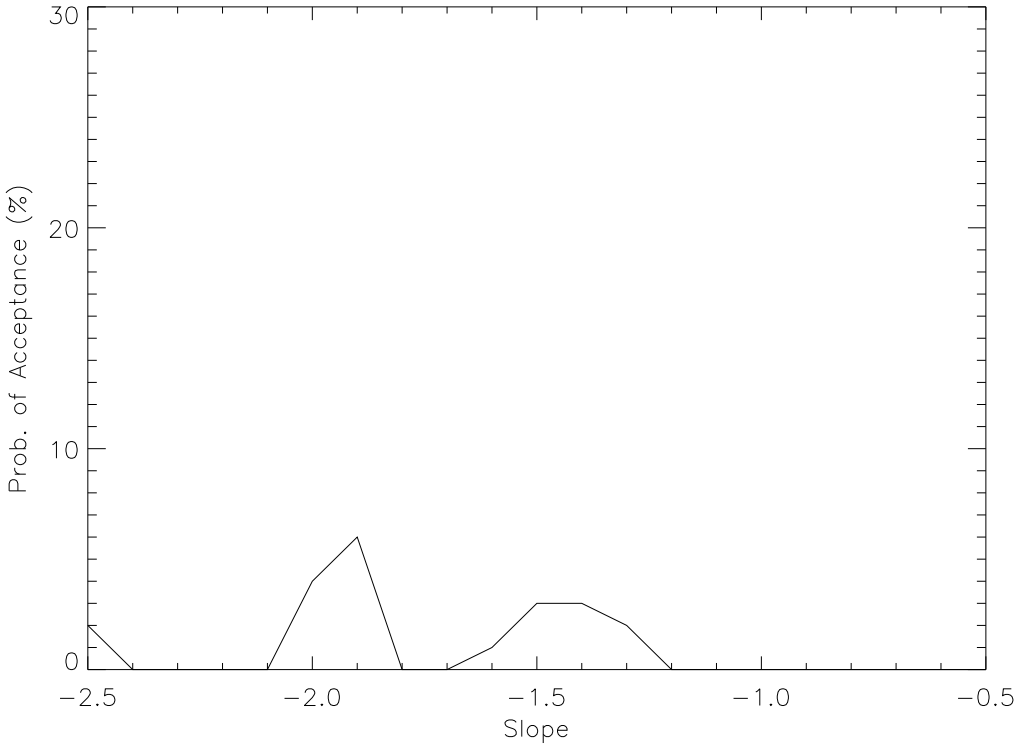

Figure 4.12: Unbroken power law fit probabilities for 3C 390.3 The maximum likelihood of acceptance occurs at slope –1.9, with a probability of 6%.

(Figure 4.12). Note that the value of –1.9 is similar to that reported by earlier analysis efforts that did not account for distortion effects in the power spectrum (Leighly & O'Brien 1997; Gliozzi et al. 2006).

For 3C 120, an unbroken power law provides an extremely poor fit to the data, with a maximum likelihood of acceptance of only 2% at several slopes. For Akn 120, the unbroken model has a maximum probability of acceptance of 16%, at a slope of –1.6 (Figure 4.13).

Given that a power law provides an unacceptable fit to our data ($> 80\%$ for three of our objects and $> 70\%$ for the other), how can we best model our power spectra? The

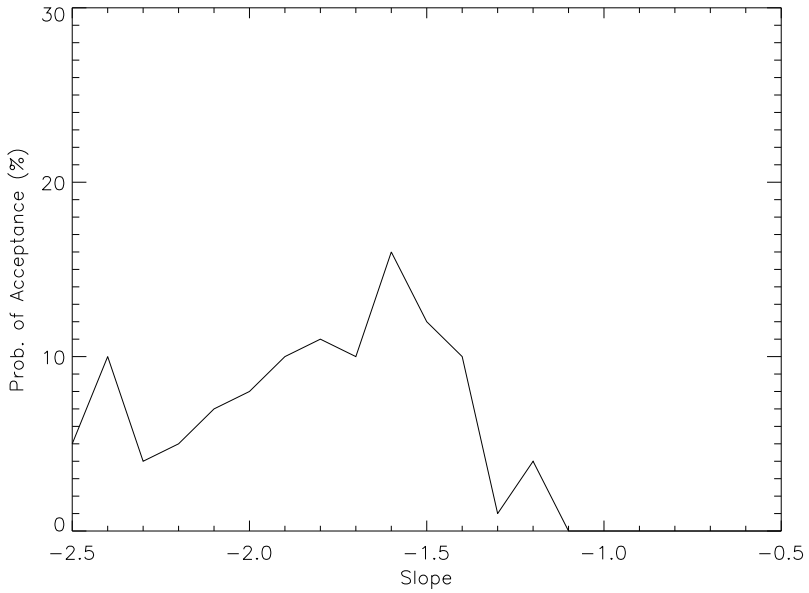

Figure 4.13: Best-fit unbroken power law probability of acceptance for Akn 120. Maximum likelihood of acceptance is 16%, at a slope of –1.6.

galactic X-ray binary Cygnus X-1 has been extensively studied at X-ray wavelengths, and has a well-defined power spectrum in both the low state (Revnivtsev et al. 2000) and the high state (McHardy et al. 2004). Previous studies have shown that AGN have a similar power spectrum, consisting of either a broken power law or a knee model (Edelson & Nandra 1999; Markowitz et al. 2003b; Uttley et al. 2002; McHardy et al. 2004; Uttley & McHardy 2005).

For Cygnus X-1, the knee model is analogous to the low-frequency break seen in the low state, where the PDS flattens to 0 at low frequencies. The broken power law is more similar to a high-frequency break, where the PDS turns over from –1 at low frequencies to a steeper value at high frequencies. More complex models can be used, but as will be shown, these two models provide an adequate fit to the observed data.

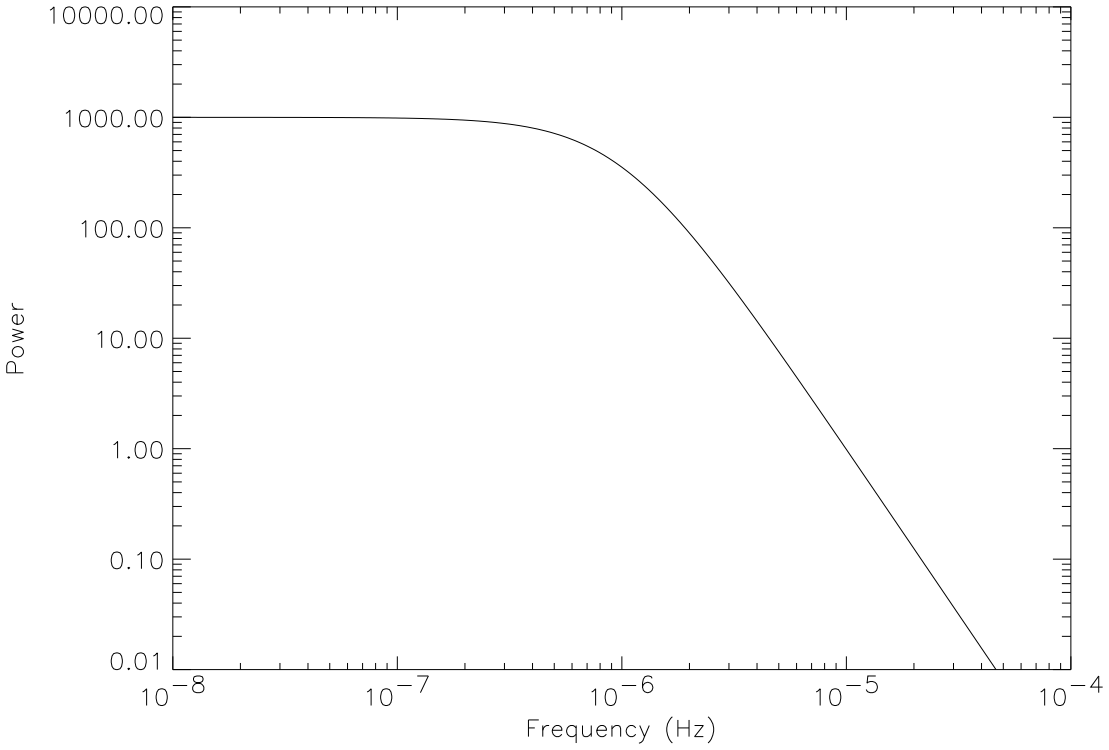

Figure 4.14: Knee model power density spectrum, with zero slope at low frequencies, bending to a slope of –1.5 at 10^{-6} Hz.

We chose to model our data with each type of power spectrum to find the best fit. The knee model takes the form

$$P(\nu) = \left(1 + \left(\frac{\nu}{\nu_{\rm b}}\right)^2\right)^{-\alpha} \tag{4.14}$$

where $\nu_{\rm b}$ is the break frequency, and α is the power law slope above the break. The slope at low frequencies is fixed at zero, while the high frequency slope was varied from –2.5 to –0.5 in increments of 0.1. The break frequency was varied from $\log \nu_{\rm b} = -8 \rightarrow -5$, in increments of 0.17 (a multiplicative factor of 1.5). An example

of this model is shown in Figure 4.14.

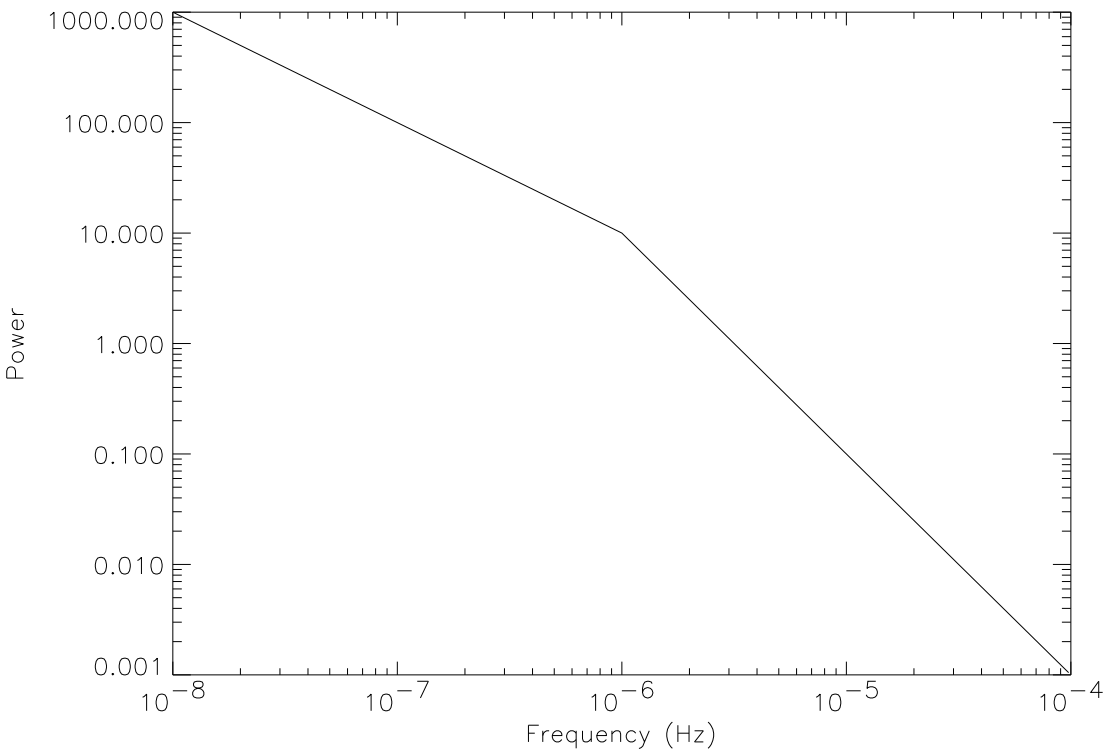

Figure 4.15: Broken power law power density spectrum, with a slope of –1 at low frequencies, breaking to a slope of –2 at a frequency of 10^{-6} Hz.

The broken power law has a well defined break frequency $\nu_{\rm b}$, with one power law slope below the break, and a steeper slope above it. Similar to the power spectrum of Cygnus X-1, and previous efforts (Markowitz et al. 2003b; Uttley et al. 2002), we fix the low-frequency slope of the power law to a value of –1. Similar to the knee model above, the high-frequency slope was allowed to vary from –2.5 to –1.0, with the break frequency varied from $\log \nu_{\rm b} = -8 \rightarrow -5$, in increments of 0.17. An example of the broken power law model is shown in Figure 4.15.

4.7.1 Mkn 509

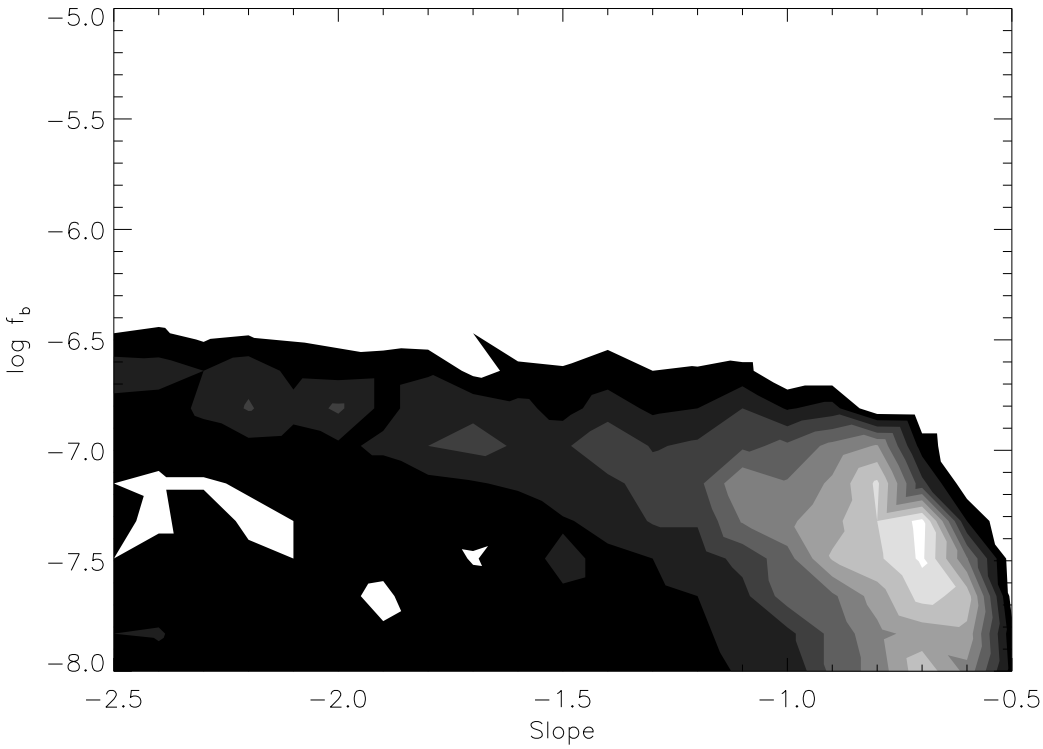

Figure 4.16: Confidence contours for the probability of knee model acceptance for Mkn 509. Contours are at 10, 20, 30, 40, 50, 60, 70, 80, and 90% acceptance. Maximum of 93% acceptance occurs at a slope of –0.7, and a break frequency of $\log f_{\rm b} = -7.32$ Hz, or 241 days.

For Mkn 509, the knee model provided an excellent fit, with a maximum probability of acceptance of 93% occuring at a slope of –0.7, and a break frequency of $\log \nu_{\rm b} = -7.32$ Hz, or 241 days (Figure 4.16. Note that the slope of –0.7 is shallower than the typical value of –1.0 seen in the high state of Cygnus X-1. The simulation provides a good fit to the data, with nearly all of the observed data points falling within the error bars of the simulated spectrum (Figure 4.17).

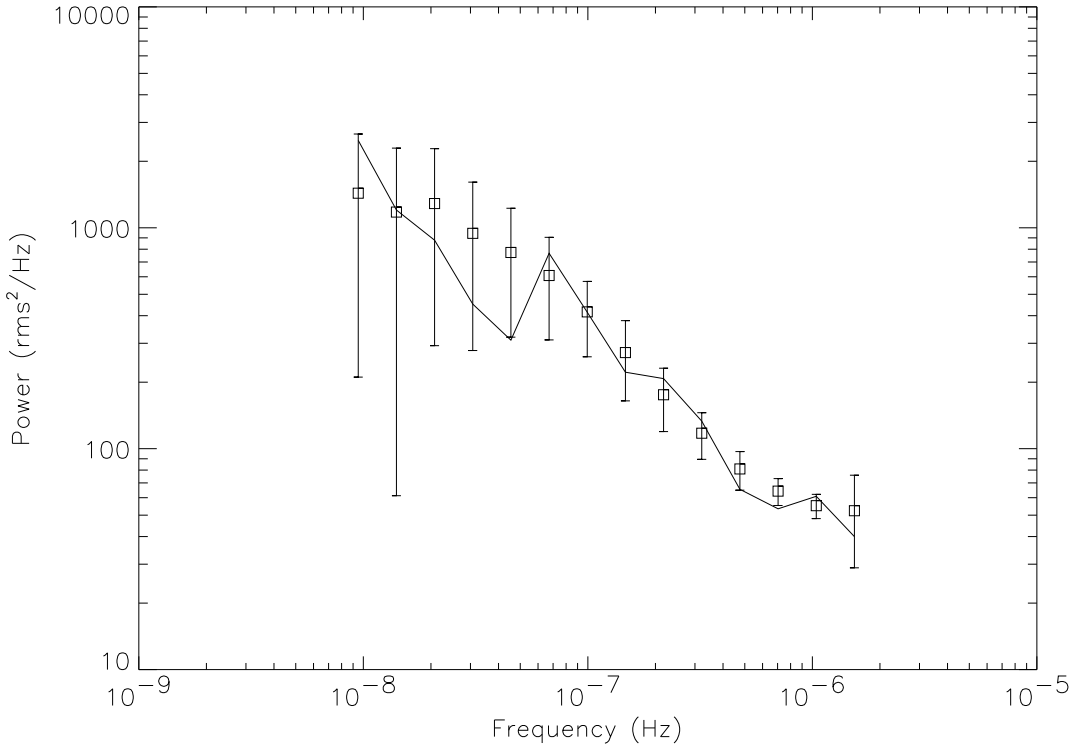

Figure 4.17: Best-fit Monte Carlo knee model simulation for Mkn 509. Solid line represents observed periodogram, squares represent average simulated periodograms, with error bars given by the rms spread of the averaged points. Underlying model power spectrum had a high frequency slope of –0.7, and a break at $\log f_{\rm b} = -7.32$ Hz, or 241 days.

The broken power law model (Figure 4.18) also provides an excellent fit, with a 95% probability of acceptance occuring at a slope of –2.0, and a break frequency of $\log \nu_{\rm b} = -6.47$ Hz, or 34 days. As with the knee model, all of the observed PDS points fall within the error bars of the simulated data (Figure 4.19).

Given that both models fit the data with greater than 90% confidence, is it possible to determine which model fits best? Unfortunately our data for Mkn 509 cover only 2 decades in temporal frequency. The knee model break at 241 days ($\sim 5 \times 10^{-8}$ Hz)

is near the low end of what can be detected with the light curve duration we have. Similarly, the break at 34 days ($\sim 3 \times 10^{-7}$ Hz) is close to the highest observable frequency given a 3 day sampling pattern.

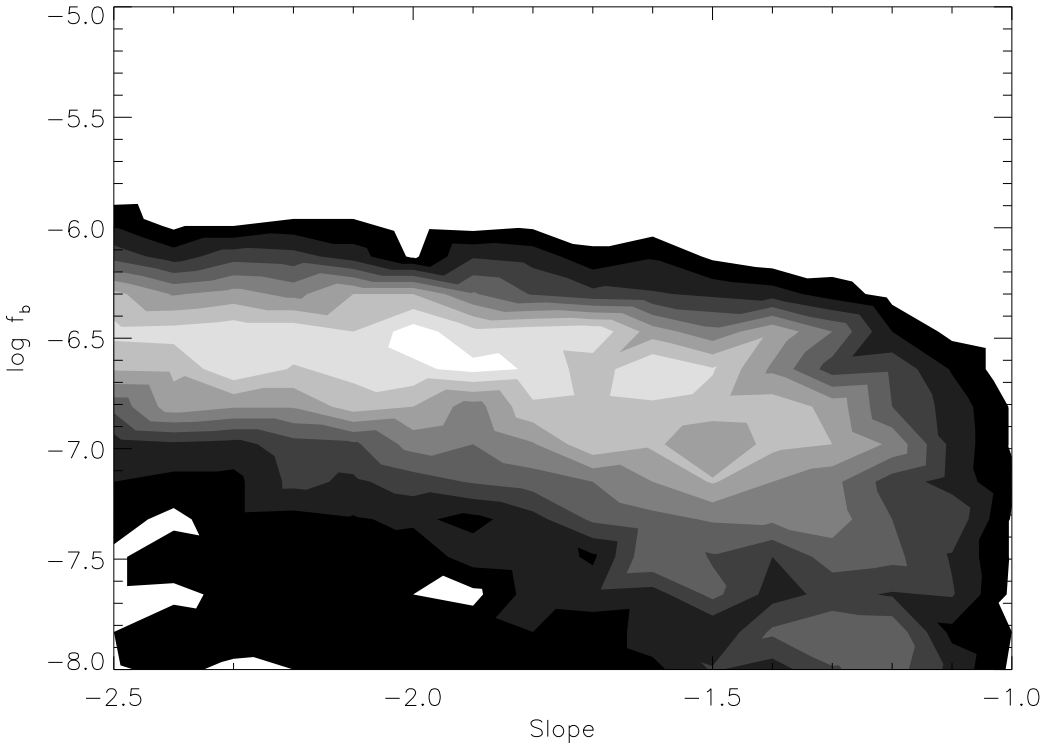

Figure 4.18: Confidence contours for the probability of broken power law model acceptance for Mkn 509. Contours are at 10, 20, 30, 40, 50, 60, 70, 80, and 90% acceptance. Maximum of 95% acceptance occurs at a slope of –2.0, and a break frequency of $\log f_{\rm b} = -6.47$ Hz, or 34 days.

We can, however, use the relationship between break frequency and black hole mass. Using the naive assumption that break frequency scales linearly with black hole mass, and given the well-known PDS and mass for Cygnus X-1, we can estimate what the break frequency would be for Mkn 509. Given a mass of $M = 1.43 \times 10^8$ $M_\odot$ for Mkn 509 from BLR reverberation mapping (Peterson et al. 2004), the high-frequency

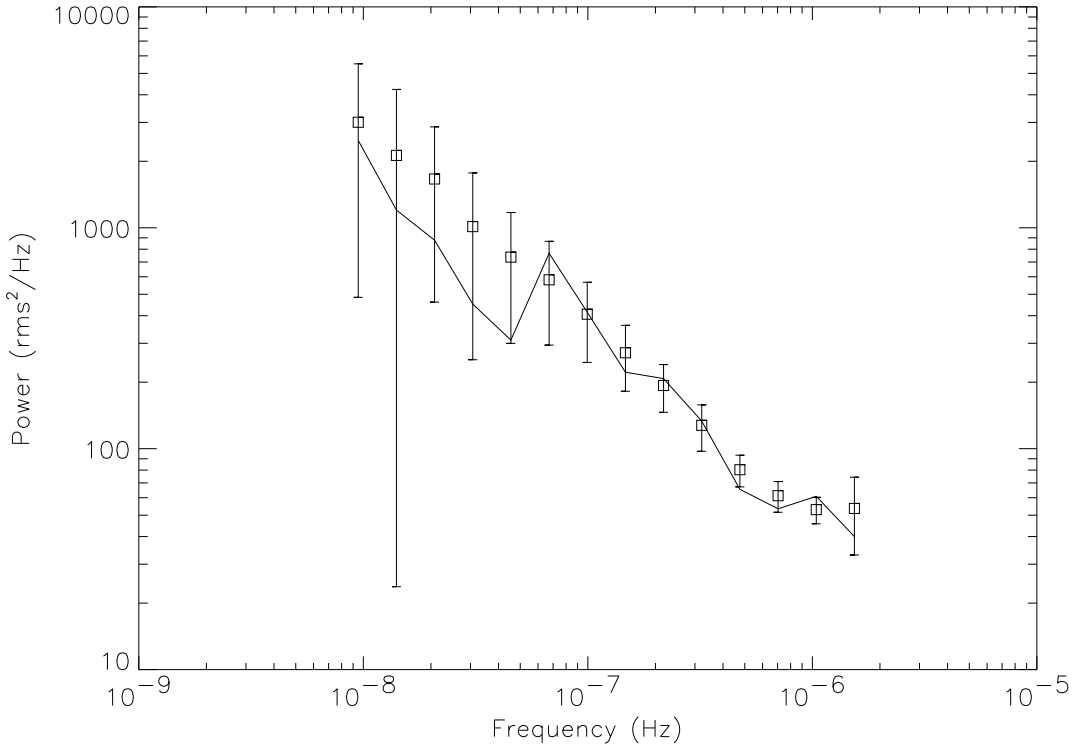

Figure 4.19: Best-fit Monte Carlo broken power law simulation for Mkn 509. Solid line represents observed periodogram, squares represent average simulated periodograms, with error bars given by the rms spread of the averaged points. Underlying model power spectrum had a high frequency slope of –2.0, and a break at $\log f_{\rm b} = -6.47$ Hz, or 34 days.

break of the low/hard state would occur around 50 days. The low-frequency break, where the PDS changes slope from 0 to 1 (analogous to the knee model) would be near 1000 days, and thus definitely not detectable in our light curve. Thus for the moment, it seems the broken power law with a break of 34 days seems more plausible, however further observations with a sampling pattern on the order of several days are necessary to further confirm this break.

4.7.2 3C 390.3

For 3C 390.3, the knee model provides a good fit to both the long-term and intermediate sampling light curves. The maximum probability of acceptance of 81% occurs at a slope of –1.0, and a break frequency of $\log f_b = -7.49$ Hz, or 358 days (Figure 4.20). The overall power spectrum for the best fit result is shown in Figure 4.21.

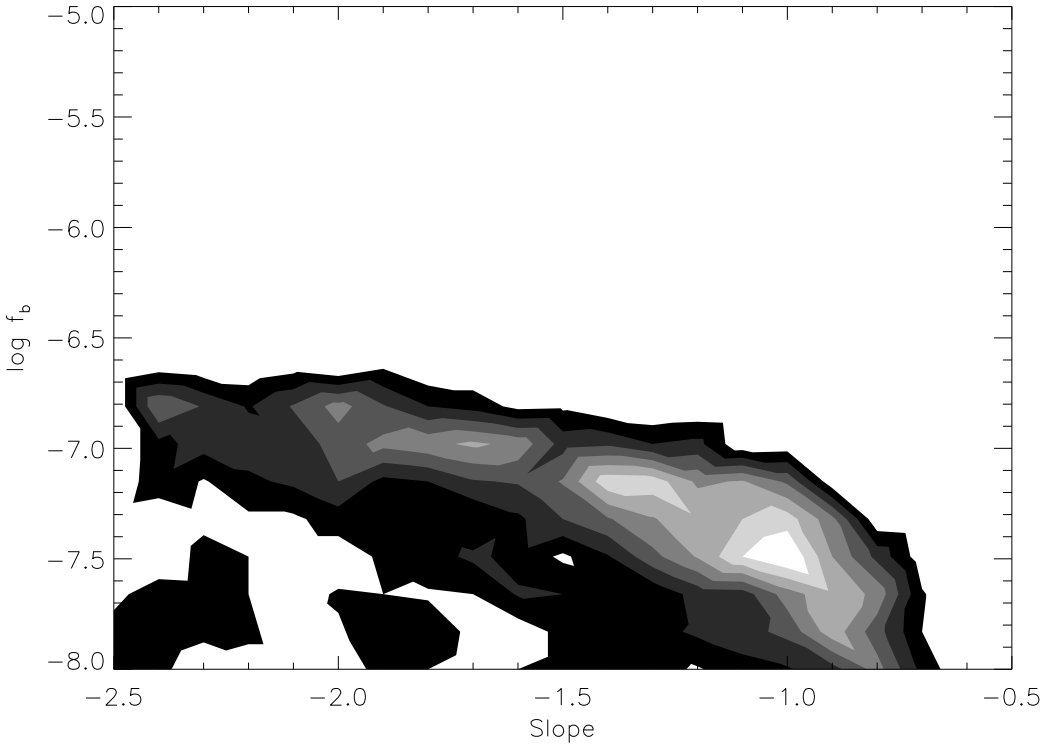

Figure 4.20: Confidence contours for the probability of knee model acceptance for 3C 390.3. Contours are at 10, 20, 30, 40, 50, 60, 70, and 80% acceptance. Maximum of 81% acceptance occurs at slope –1.0, and a break frequency of $\log f_b = -7.49$ Hz, or 357 days.

For the broken power law model, the fit is not quite as good, with a maximum likelihood of acceptance of 50% occurring at a slope of –2.1, and a break frequency of

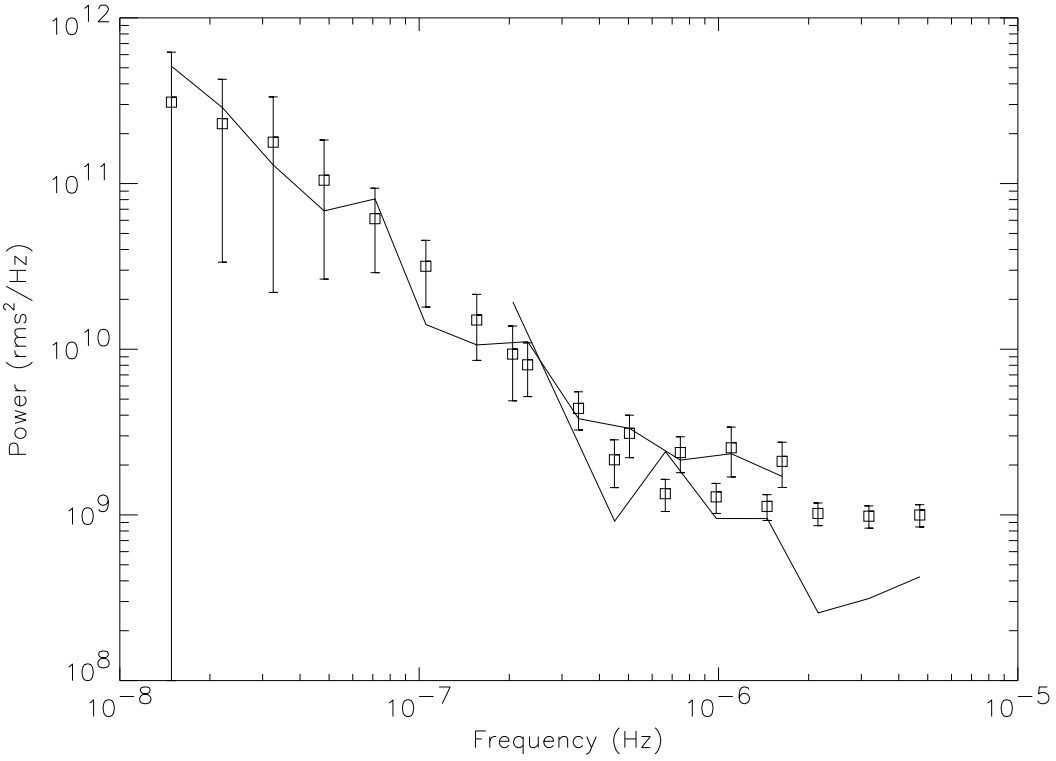

Figure 4.21: Best-fit Monte Carlo knee model for 3C 390.3. Solid lines represent the observed power spectra, squares represent the simulated data, with error bars representing the rms spread of averaged points. Underlying model power spectra has a high-frequency slope of –1.0, and a break frequency of $\log f_b = -7.49$ Hz, or 358 days.

$\log f_b = -6.81$ Hz, or 74 days (Figure 4.22). Observed and simulated results for the best fit values are shown in Figure 4.23.

The knee model has a 30% higher likelihood of acceptance compared to the broken power law, but which is the most realistic for our data set? The knee model break of 357 days corresponds to a frequency of $\sim 3 \times 10^{-8}$ Hz, which is just barely resolvable with our 2 year monitoring campaign. The 74 day break of the broken power law model corresponds to a break at 1.5×10^{-7} Hz, which is right in the middle of the

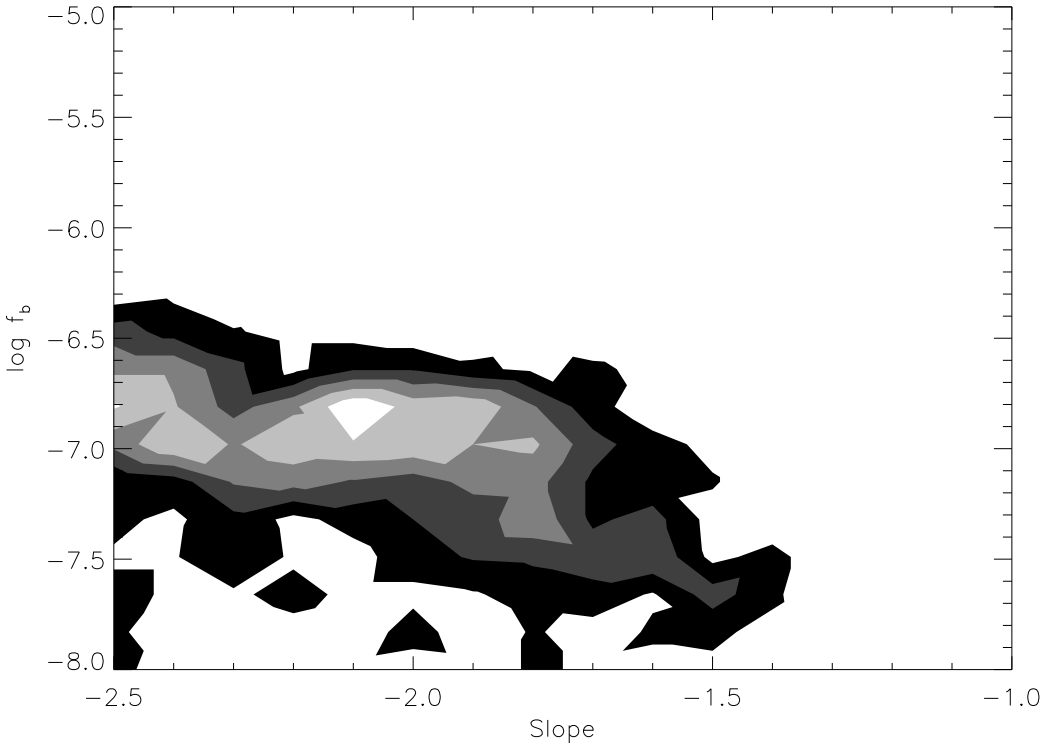

Figure 4.22: Confidence contours for the probability of broken power law model acceptance for 3C 390.3. Contours are at 10, 20, 30, 40, and 50% acceptance. Maximum of 50% acceptance occurs at high-frequency slope –2.1, and a break frequency of $\log f_b = -6.81$ Hz, or 74 days.

frequency range for our observations.

Also, note that for the break frequency/black hole mass relationship discussed in Markowitz et al. (2003b); Uttley & McHardy (2005), and given the mass of 3C 390.3 as 2.87×10^8 $M_\odot$ (Peterson et al. 2004), we would expect to see a high-frequency break at $\sim$ 100 days assuming 3C 390.3 is similar to the low/hard state of Cygnus X-1. For the high state, we would expect to see a break around 30 days. The low frequency break of the low/hard state would be seen around 2000 days, which is well outside the timescale of our observations. It seems most likely that we are seeing either the

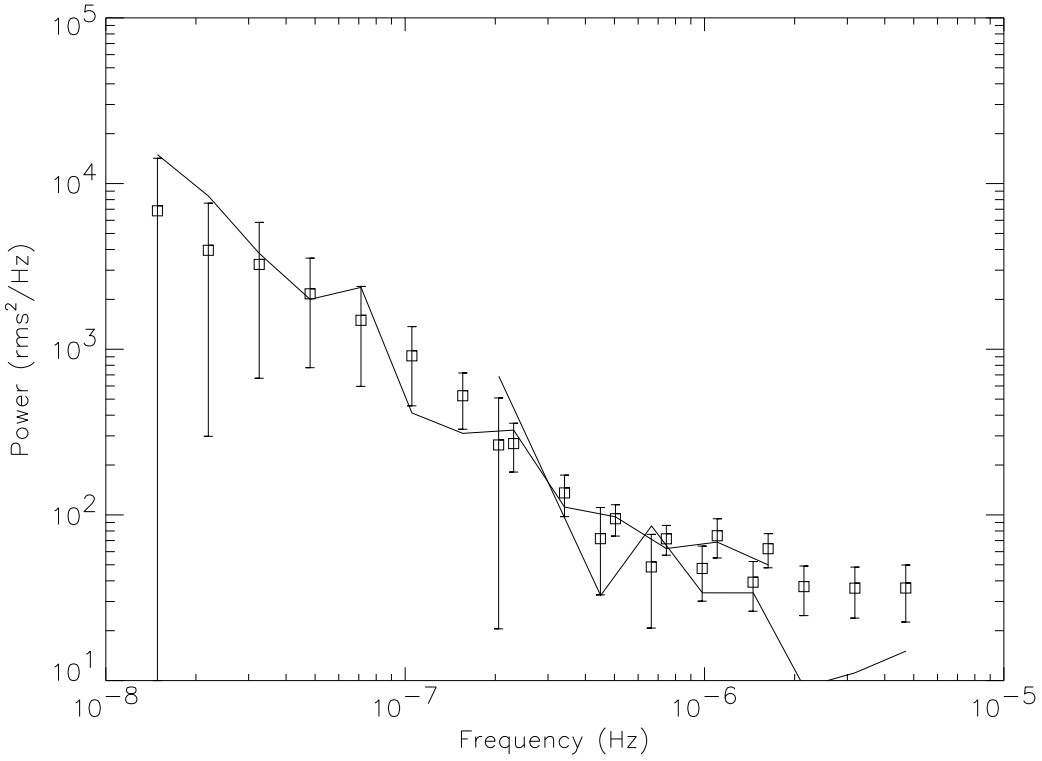

Figure 4.23: Best-fit Monte Carlo broken power law model for 3C 390.3. Solid lines represent the observed power spectra, squares represent the simulated data, with error bars representing the rms spread of the averaged points. Underlying model power spectra has a high-frequency slope of –2.1, and a break frequency of $\log f_b = -6.81$ Hz, or 74 days.

high-frequency break of 3C 390.3 in a low/hard state, or 3C 390.3 is a high state object. This will be discussed more in Chapter 5.

4.7.3 3C 120

For 3C 120, a broken power law model provides a modest probability of acceptance of 17%, at a slope of –1.9, and break frequency $\log \nu_{\rm b} = -6.47$ Hz, or 34 days (Figure 4.24). Examination of the observed and simulated power spectra (Figure 4.25)

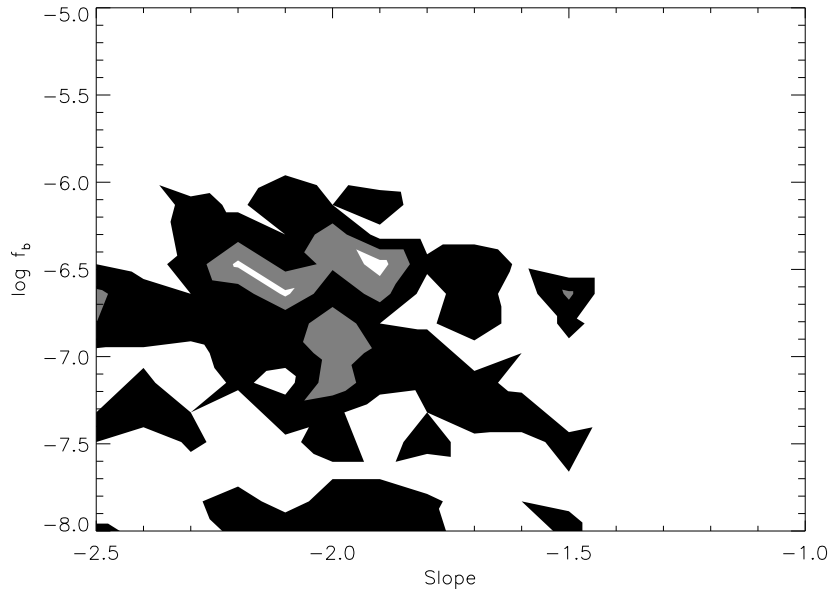

Figure 4.24: Best-fit Monte Carlo broken power law contours for 3C 120. Contour lines are drawn at 5, 10, and 15% probability of acceptance. Maximum likelihood of acceptance of 17% occurs at slope –1.9, and break frequency $\log \nu_{\rm b} = -6.47$ Hz, or 34 days.

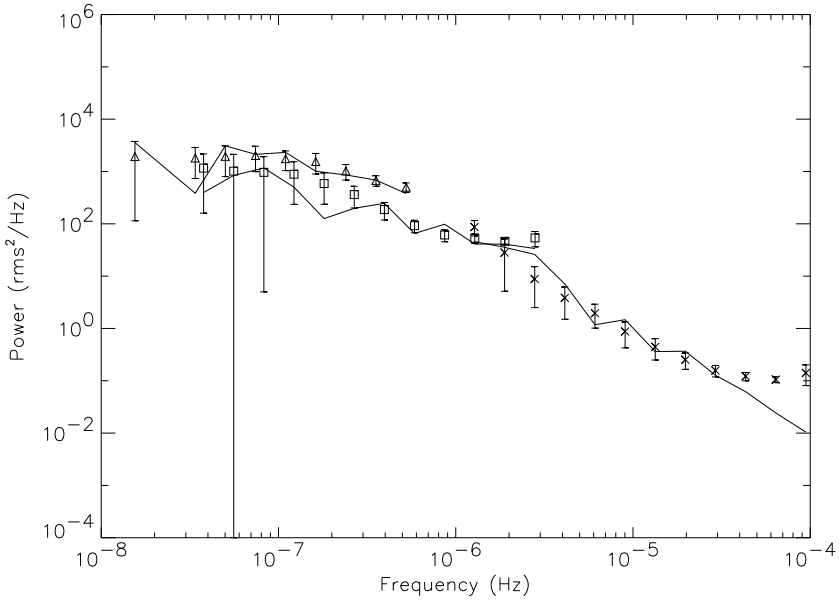

Figure 4.25: Best-fit Monte Carlo broken power law model for 3C 120. Solid lines represent the observed power spectra, while triangles, squares, and crosses represent the simulated data, with error bars representing the rms spread of the averaged points. Underlying model power spectra has a high-frequency slope of –2.0, and a break frequency of $\log f_b = -6.47$ Hz, or 34 days.

shows clear evidence of flattening at low frequencies.

For the knee model, we find a slightly better probability of acceptance, with a maximum of 25% at a slope of –1.0, and break frequency $\log \nu_{\rm b} = -6.98$ Hz, or 110 days (Figure 4.27). From visual inspection of Figure 4.26, the knee model appears to provide a better fit to the data than the broken power law.

Given the large range in temporal frequency covered by our observations (nearly four decades), and the rather poor probability of acceptance given by the models above, we also fit a doubly-broken power law to the data. Ideally, we would test a wide range of slopes and break frequencies to find the best fit to the data. This would be very computationally intensive, however, and thus we limit the range of slopes to that seen in Cygnus X-1. Our doubly-broken PDS model has a fixed slope of 0 at low frequencies, which steepens to –1 above a low-frequency break, and which then steepens again to –2 above a high frequency break. An example of such a model is shown in Figure 4.28. The low-frequency break is allowed to vary from $\log \nu = -8 \rightarrow -6$ Hz, in increments of 0.1 in log space. The high-frequency break is allowed to vary anywhere from a factor of four higher in frequency, up to a factor of 40 higher, in increments of two (i. e. 4× higher, 6× higher, 8× higher, etc.).

Confidence contours for the double-break simulation (Figure 4.29) show a poorer fit than either the knee model or the singly broken power law. The maximum likelihood of acceptance is only 7.1%, and thus we can not say with any confidence that the PDS shows a double break. It is interesting to note, however, that the best-fitting

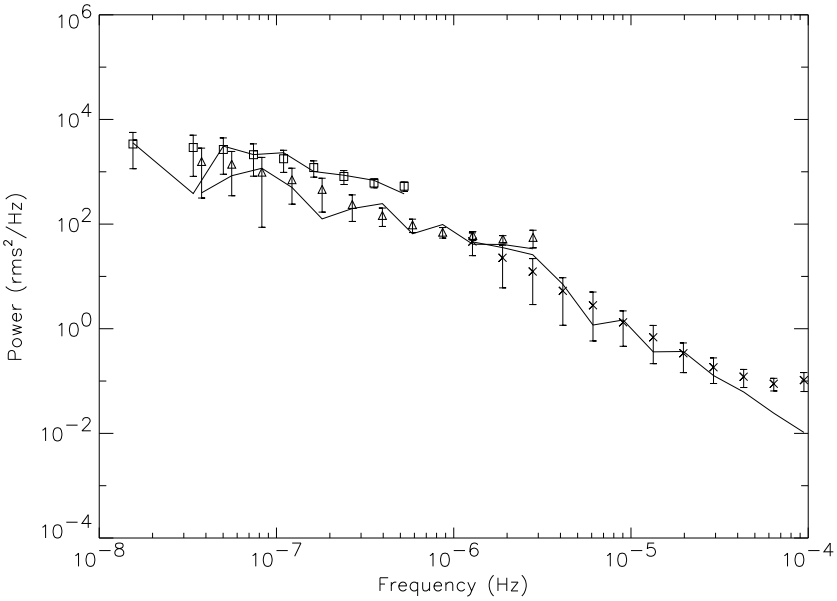

Figure 4.26: Best-fit Monte Carlo knee model for 3C 120. Solid lines represent the observed power spectra, while triangles, squares, and crosses represent the simulated data, with error bars representing the rms spread of the averaged points. Underlying model power spectrum has a high-frequency slope of –1.0, and a break frequency of $\log f_b = -6.98$ Hz, or 110 days.

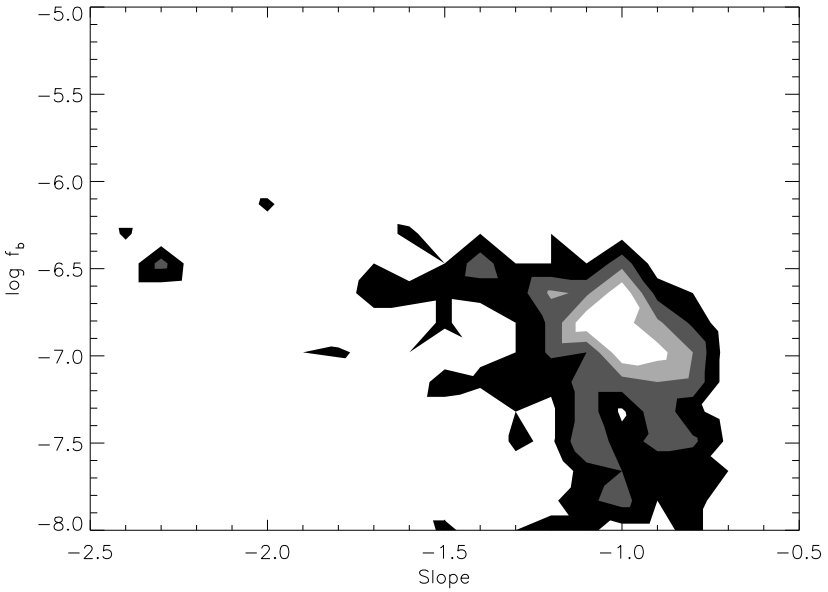

Figure 4.27: Best-fit Monte Carlo knee model contours for 3C 120. Contour lines are drawn at 5, 10, 15, 20, and 25% probability of acceptance. Maximum likelihood of acceptance of 25% occurs at slope –1.0, and break frequency $\log \nu_{\rm b} = -6.98$ Hz, or 110 days.

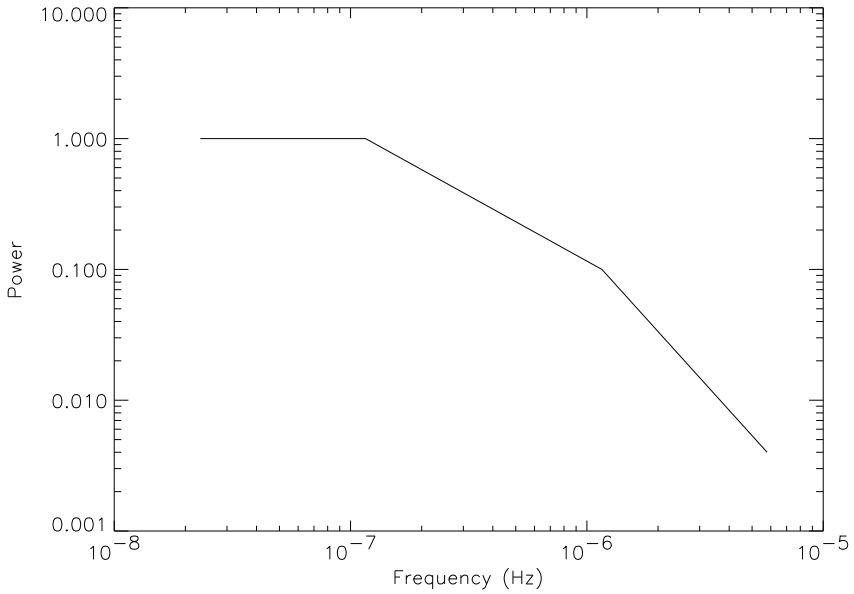

Figure 4.28: Example of a doubly-broken PDS. Slope breaks from 0 to –1 at a timescale of 100 days , and then steepens to –2 at a timescale of 10 days.

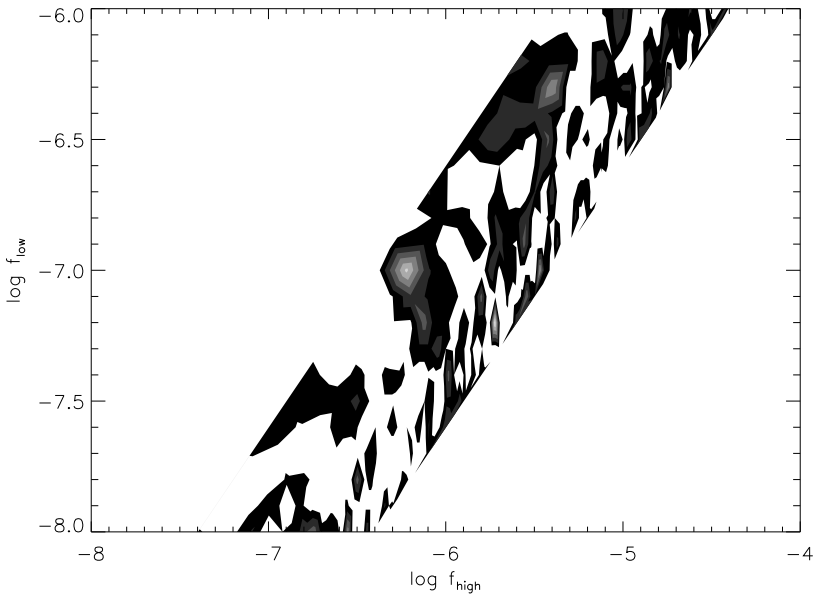

Figure 4.29: Doubly broken power law contours for 3C 120. Slopes were fixed at 0, –1, and –2. Contours are drawn at 1, 2, 3, 4, 5, 6, and 7% probability. Maximum likelihood of acceptance of 7.1% occurs at break frequencies of $\log \nu_{\rm b} = -7.2$ and –5.7, or timescales of 183 and 6.1 days, respectively.

breaks occur at timescales of 183 and 6.1 days, which are very close to the values expected from scaling the low/hard state break frequency in Cygnus X-1.

4.7.4 Akn 120

Our two light curves for Akn 120 give us coverage at different regions in frequency space, with a gap in between. Despite this, we can still fit our data with both the knee model and broken power law and check for goodness of fit.

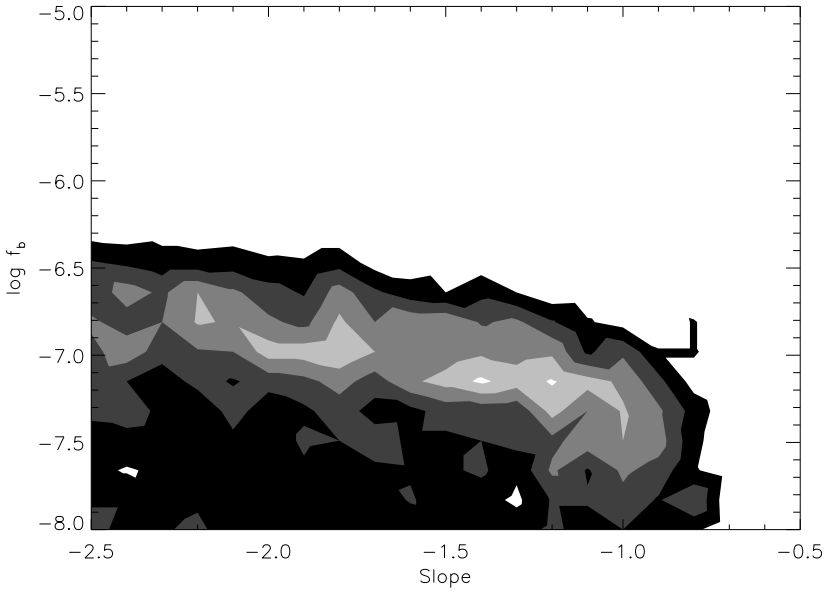

Figure 4.30: Best-fit Monte Carlo simulation knee model contours for Akn 120. Contours are drawn at 10, 20, 30, 40, and 50% probability of acceptance. Maximum likelihood of acceptance is 52%, at a slope of –1.4 and break frequency $\log \nu_{\rm b} = -7.15$ Hz, or 163 days.

The knee model provides a maximum likelihood of acceptance of 52%, at a slope of –1.4 and break frequency $\log \nu_{\rm b} = -7.15$ Hz, or 163 days (Figure 4.30). The power spectrum (Figure 4.31) shows clear evidence of flattening at the lowest frequencies. At

high frequencies, our calculations show a large spread in the simulated periodograms, as evidenced by the large error bars on the data points. The most likely cause is the large amount of aliasing introduced by significant gaps in the short term light curve. The short-term light curve for 3C 120 also has a significant number of gaps, but its longer duration (9 days versus 3), combined with shorter and more evenly spaced gaps serve to reduce the scatter seen in the simulations.

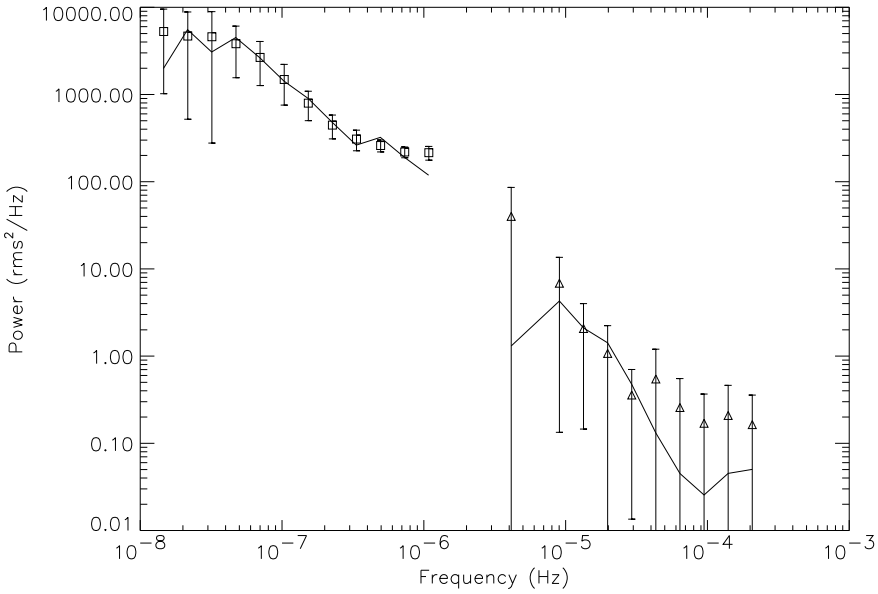

Figure 4.31: Best-fit Monte Carlo knee model for Akn 120. Solid lines represent observed power spectra, while triangles, and squares represent the simulated data, with error bars representing the rms spread of the averaged points. Underlying model power spectra has a high-frequency slope of –1.4, and a break frequency of $\log f_{\rm b} = -7.15$ Hz, or 163 days.

For a broken power law, we find a similar likelihood of acceptance of 47%, at a slope of –2.2 and break frequency $\log \nu_{\rm b} = -6.98$ Hz, or 110 days (Figure 4.32). Similarly to the knee model, we see a large amount of scatter in the short term

simulated periodograms (Figure 4.33).

Given the relatively similar probabilities of acceptance for the above models, which one provides the most reasonable fit to the data? Peterson et al. (2004) find a mass of 1.50×10^8 $M_\odot$ for Akn 120. As for 3C 390.3, we can use the break frequency of Cygnus X-1 to estimate what the break should be for a galaxy of that mass. For the low/hard state, we would expect the high frequency break to occur near 60 days, and the low frequency break to occur near 1200 days. For the high/soft state, we expect the break should be near 10 days.

Clearly the break frequency of 110 days given by the broken power law model is the best fit to the expected value. It therefore seems most likely that the break we are seeing in the power spectrum is analogous to the high-frequency break seen in the low/hard state of Cygnus X-1.

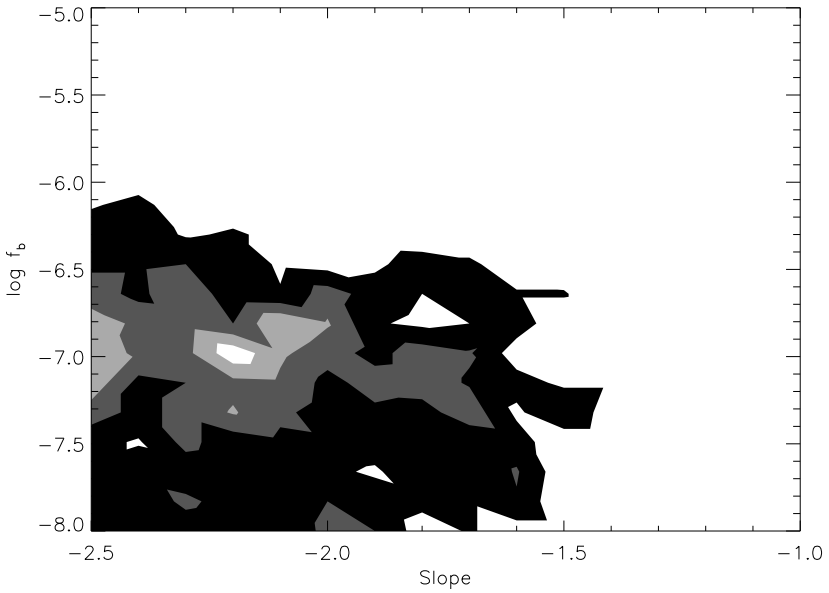

Figure 4.32: Best-fit Monte Carlo simulation broken power law model contours for Akn 120. Contours are drawn at 10, 20, 30, and 40% probability of acceptance. Maximum likelihood of acceptance is 47%, at a slope of –2.2 and break frequency $\log \nu_{\rm b} = -6.98$ Hz, or 110 days.

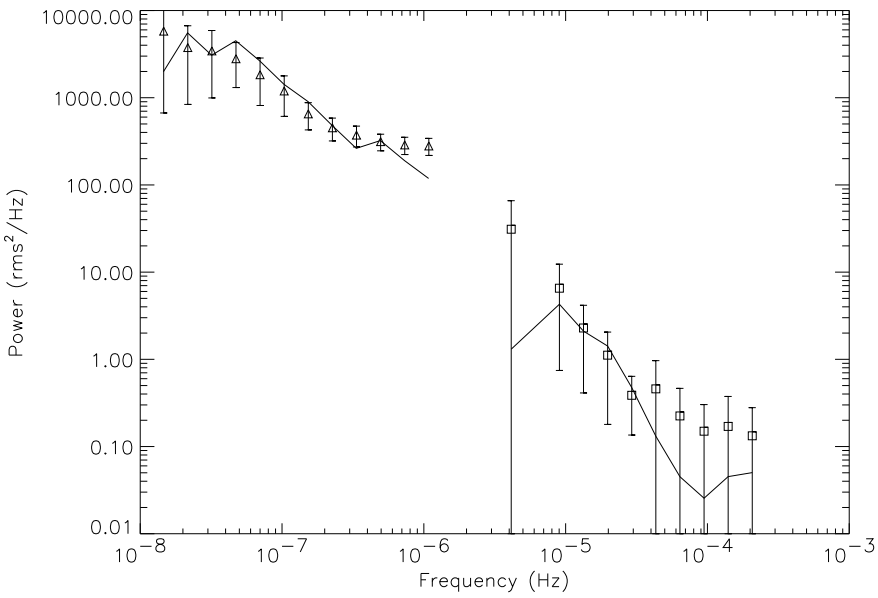

Figure 4.33: Best-fit Monte Carlo broken power law model for Akn 120. Solid lines represent observed power spectra, while triangles and squares represent the simulated data, with error bars representing the rms spread of the averaged points. Underlying model power spectra has a high-frequency slope of –2.2, and a break frequency of $\log f_{\rm b} = -6.98$ Hz, or 110 days.

– 5 –

Conclusions

For each of a sample of four objects, we have presented results of a multi-year X-ray monitoring campaign. All objects show significant variability on both long and short timescales. For Mkn 509, optical monitoring shows that the X-ray variability is closely correlated with the X-ray flux, with the optical emission leading the X-ray by ~ 25 days. A simple power law provides a poor fit to the PDS of each object, with a high probability of rejection. Instead, we find a broken power law provides a better fit, with break timescales on the order of a few weeks. For 3C 120, the break we see is most likely the low-frequency break of a doubly broken power law. Additionally, we find that the two radio-loud objects in our sample show a linear rms-flux relationship, while the two radio-quiet objects do not. Below, we discuss some of the implications of our results.

5.1 Optical/X-ray Lags in Mkn 509

At present, there is no clear picture regarding the correlation of X-ray emission with other wavelengths in Seyfert galaxies. Maoz et al. (2002) monitored NGC 3516 in the optical and X-ray for 5 years, and found no clear correlation. X-ray and UV monitoring of NGC 7469 showed no correlation between those wavelengths (Nandra et al. 1998), while Miller & Ferrara (1999) found a strong correlation between X-ray

and optical flux in Akn 120, with no lag. Uttley et al. (2005) examined long-term X-ray and optical variations in NGC 5548, and found a strong correlation, again with zero lag.

For Mkn 509, the optical flux appears to lead the X-ray flux by 25 days (§3.4.3), with a correlation coefficient of ~ 0.9. Additionally, the fractional variability of the optical data is similar to the X-ray data, with $F_{\rm var} = 19.42\%$ for the X-ray light curve and $F_{\rm var} = 11.83\%$ for the optical. Note that the flux from the host galaxy has not been subtracted, and so the optical $F_{\rm var}$ is likely higher. On short timescales, however, the X-ray data show greater variability than the optical. Given the above, we can ask what may produce this effect.

The most obvious choice is a light crossing time from the optical to the X-ray emitting region; however, for that hypothesis 25 days would be too great. Kaspi et al. (2000) found the size of the Broad Line Region (BLR) in Mkn 509 to be 20 light days, a figure close to the observed lag. However, the continuum emission arises nearer to the accretion disk, and so the similarity of these timescales is purely coincidental.

Assuming all the above sources are essentially similar in nature, the most likely scenario is that the X-ray and optical variations follow more fundamental variations in the accretion flow, such as changes in the accretion rate or instabilities in the disk. As the disturbance in the accretion disk moves inward, it first moves through the optical emitting region, and then later the X-ray region closer to the black hole. The additional high-frequency variability seen in the X-rays could come from the

decreased light-travel time closer to the black hole, or from an additional component closer to the central engine.

If the lag is due to changes in the accretion flow, wouldn't we expect to see a lag in all Seyfert galaxies? Probably not, since the mass of the black hole in Mkn 509 is 1.43×10^8 $M_\odot$ (Peterson et al. 2004), roughly an order of magnitude larger than previously studied objects. Many of the relevant timescales (orbital, thermal, viscous) increase linearly with black hole mass, so we would expect to see a lag on the order of 2–3 days for other, less massive Seyferts. Given that previous campaigns have typically involved weekly sampling, or more intensive sampling, but for only a few days, it is distinctly possible that the data would appear be correlated with zero lag (not sampling frequently enough) or uncorrelated (not sampling for long enough).

5.2 Accretion Timescales

For each object, we have detected a break in the power spectrum at a timescale of a few months. A summary of our results is given in Table 5.1.

Table 5.1: Break Timescales for Object Studied

Name	Prob. of Acceptance (%)	α	Break Timescale (d)	Model
Mkn 509	95	$2.0^{+0.1}_{-0.1}$	34^{+17}_{-11}	Broken power law
3C 390.3	50	$2.1^{+0.1}_{-0.1}$	74^{+37}_{-25}	Broken power law
3C 120	25	$1.0^{+0.1}_{-0.1}$	110^{+37}_{-25}	Knee
Akn 120	47	$2.2^{+0.1}_{-0.1}$	110^{+55}_{-37}	Broken power law

The timescales detected are somewhat larger than the typical value of a few days found by Uttley et al. (2002) and Markowitz et al. (2003b), however three of our galaxies have masses $> 10^8$ $M_\odot$, a value roughly an order of magnitude larger than the typical Seyfert galaxy. For 3C 120, the break detected at 110 days is most likely the low-frequency break of a low/hard state PDS, which would correspond to a typical high-frequency break near 6 days.

Edelson & Nandra (1999) discuss a number of timescales which may be related to the break frequency. The shortest timescale is the light-crossing time, given by:

$$t_{\rm lc} = 0.011(M/10^7\ {\rm M}_\odot)(R/10R_S)\ {\rm days}, \tag{5.1}$$

where R is the radius of the emission, and R_S is the Schwarzschild radius. For all of our objects, t_{lc} is much too small to correspond with the observed break frequencies.

For an α-disk (Shakura & Sunyaev 1973), there are several other relevant timescales we can consider (**?**). The viscous timescale is given by:

$$t_{\rm viscous} = 53000(R/H)^2(\alpha/0.01)^{-1}(M/10^7\ {\rm M}_\odot)(R/10R_S)^{3/2}\ {\rm days}, \tag{5.2}$$

where H is the height of the accretion disk, and α is the viscosity parameter which relates the shear stress to the pressure. In this case, any reasonable values for a thin accretion disk would yield a timescale orders of magnitude too large to correspond with the break timescale.

More relevant are the thermal and sound crossing timescales, given by:

$$t_{\rm thermal} = 5.3(\alpha/0.01)^{-1}(M/10^7\ {\rm M}_\odot)(R/10R_S)^{3/2}\ {\rm days,\ and} \tag{5.3}$$

$$t_{\rm sound} = 33(R/100H)(M/10^7\ {\rm M}_\odot)(R/10R_S)^{3/2}. \tag{5.4}$$

With the thickness of the disk, α, and the distance at which X-rays are emitted as variable parameters, either of these timescales provides a good match with the break timescale.

5.3 Variability States

The black hole X-ray binary Cygnus X-1 has 2 distinct variability states: a high/soft state with a high flux and soft (steeper) X-ray spectrum, and a low/hard state with low flux and hard (flatter) X-ray spectrum. The power spectra of these two states are also different. The high/soft state has a slope of –2 at high frequencies, which flattens to a slope of –1 with a break near 13 Hz (Revnivtsev et al. 2000). The low/hard state has a slope of –2 at high frequency, which breaks to –1 near 3 Hz, and then breaks again to a slope of 0 near 0.2 Hz. The transition between states is thought to be a function of accretion rates, with Cygnus X-1 switching from the low/hard state to a high/soft state above $\sim 2\%$ of the Eddington accretion rate. At higher accretion rates, the inner edge of the disk moves inward. The softer spectrum is a result of increased thermal emission from higher disk temperatures, and the shorter light-crossing time

allows for greater variability amplitudes on shorter timescales.

Previous efforts (Markowitz et al. 2003b; McHardy et al. 2004) have connected the accretion rate in AGNs with such spectral states. NLS1s, thought to accrete at a very high fraction of their Eddington rate, have previously shown a high/soft state PDS (McHardy et al. 2004). However, Uttley & McHardy (2005) showed that is not always the case, with the Seyferts NGC 3227 and NGC 5506 both showing high/soft state power spectra, but hard X-ray spectra. Additionally, nearly all of the AGNs for which power spectra have been measured are accreting at a rate greater than 2% of the Eddington rate.

In Table 5.2, we give masses, luminosities, and accretion rates for each of our objects. With the exception of 3C 120, each object has an accretion rate of a few percent of the Eddington rate, which is typical for Seyfert galaxies. Note that there is some discrepancy in the black hole mass of 3C 120. Peterson et al. (2004) use reverberation mapping and find that $\log M = 7.74$ $M_\odot$, while Kaspi et al. (2000) finds $\log M = 7.42$ $M_\odot$, and Wandel et al. (1999) give $\log M = 7.49$ $M_\odot$. All of these yield a fairly high accretion rate, relative to the Eddington value. However Bettoni et al. (2001) find $\log M = 8.03$ $M_\odot$ using stellar velocity dispersions. Using this value, the accretion rate is only 16% of the Eddington limit, a more reasonable value. Given that Bettoni et al. (2001) use a different method when compared with previous results, and given the similarities in the reverberation mapped masses, we use the value of $\log M = 7.74$ $M_\odot$ given by Peterson et al. (2004).

Table 5.2: Masses and Luminosities for Objects Studied

Name	$\log L_{\rm bol}^{a}$	$M/10^6$ $M_\odot{}^{b}$	$L/L_{\rm Edd}$
3C 390.3	44.88	287 ± 64	0.021
3C 120	45.35	55.5^{+31}_{-22}	0.313
Akn 120	44.91	150 ± 19	0.043
Mkn 509	45.03	143 ± 12	0.059

[a] from Woo & Urry (2002)
[b] from Peterson et al. (2004)

The power spectra for all of our objects appear to correspond with the low/hard state of Cygnus X-1, despite accreting at a rate higher than the 2% value where Cygnus X-1 switches to a high/soft state. Looking at the X-ray spectra for all of our objects, we find photon indices of $\Gamma = 1.7 - 2.0$, which is typical for the low/hard state. The high/soft state typically shows values of $\Gamma > 2.5$, similar to what is seen in NLS1s. One notable exception is NGC 3227, a Seyfert 1 with $\Gamma = 1.6$ but a high/soft state PDS (Uttley & McHardy 2005).

Figure 5.1 shows the relationship between count rate and spectral slope for 3C 390.3. Fitted with a simple power law plus absorption, the photon index does not change from the median value of $\Gamma = 1.75$ as the count rate increases. All of our objects show a similar result, with the spectral slope remaining constant with regards to flux.

All of our objects show a low/hard state PDS, with a hard X-ray spectrum, despite having an accretion rate higher than that seen in the high/soft state of Cygnus X-1. For 3C 120, the accretion rate is more similar to that seen in NLS1s, however the PDS and spectrum place it firmly within the camp of broad line galaxies. As suggested by

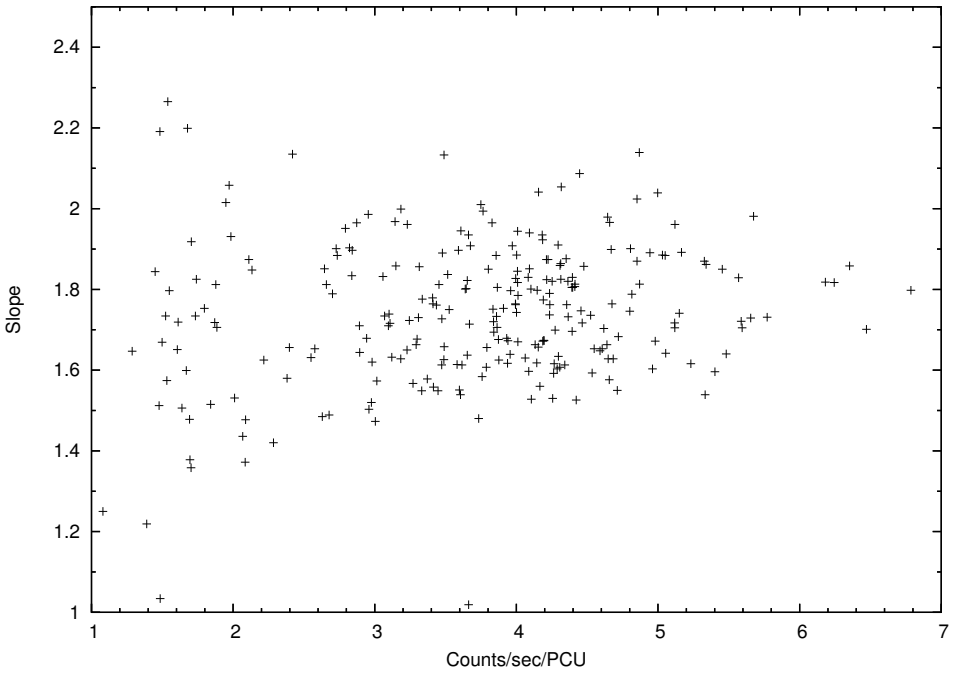

Figure 5.1: Count rate vs. spectral slope for 3C 390.3. Note that spectral slope does not appear to change significantly with increasing count rate, and remains near the mean value of $\Gamma = 1.75$. Increased scatter at low count rates is most likely due to poor photon statistics.

Uttley & McHardy (2005), the relationship between accretion rate, spectral shape, and variability state may not be as simple as previously thought.

5.4 The rms-flux Relationship

In Chapter 4, we discussed the rms-flux relationship for each object in our sample. We found that for the radio loud galaxies, 3C 120 and 3C 390.3, there was a relationship between flux and rms variability. For the radio quiet objects, Mkn 509 and Akn 120, no relationship was seen.

The presence of an rms-flux relationship in two of our objects allows us to exclude

the shot noise model as the underlying variability process, because the shot noise model predicts stationarity of both the PDS shape and amplitude.

Uttley & McHardy (2001) have found a similar rms-flux relationship for NGC 4051, NGC 5506, and MCG–6-30-15, although on timescales of only days. With a small, yet diverse sample of a NLS1, Seyfert 1, and Seyfert 2 galaxy, their results suggest that the rms-flux relationship is not limited to just one class of AGN.

5.5 Mass-Break Frequency Relationship

Table 5.3: Previously Calculated Break Frequencies[a]

Name	PDS Break (d)	Ref[b]	Mass (10^6 $M_\odot$)	Ref[b]	$L_{\rm bol}/L_{\rm Edd}$	Ref[b]
Fairall 9	28.9	M03	255	P04	0.053	W02
NGC 5548	18.3	M03	67.1	P04	0.080	W02
PG 0804+761	12	P03	693	P04	0.010	W02
NGC 4151	9.2	M03	13.3	P04	0.032	W02
NGC 3516	5.8	M03	42.7	P04	0.036	W02
NGC 3783	2.9	M03	29.8	P04	0.068	W02
NGC 5506	0.89	U05	100	O99	0.026	XBC
MCG–6-30-15	0.15	M05	4.5	M05	0.062	R97
NGC 3227	0.059	U05	42.2	P04	0.014	W02
Mrk 766	0.023	V03	3.5	B05	0.62	XBC
NGC 4051	0.019	M04	1.91	P04	0.15	W02
NGC 4395	0.006	V05	0.05	V05	0.008	L99
Akn 564	0.005	P02	2.6	B04	3.04	R04

[a] Adapted from Uttley & McHardy (2005)
[b] References used: M03 - Markowitz et al. (2003b); P03 - Papadakis et al. (2003); U05 - Uttley & McHardy (2005); M05 - McHardy et al. (2005); V03 - Vaughan et al. (2003a); M04 - McHardy et al. (2004); V05 - Vaughan et al. (2005); P02 - Papadakis et al. (2002); P04 - Peterson et al. (2004); O99 - Oliva et al. (1999); B05 - Botte et al. (2005); B04 - Botte et al. (2004); W02 - Woo & Urry (2002); R97 - Reynolds et al. (1997); L99 - Lira et al. (1999); R04 - Romano et al. (2004); XBC - assuming a factor of 36.6 for the bolometric correction from 2–10 keV X-ray luminosity

Markowitz et al. (2003b) were the first to explore the relationship between break frequency and black hole mass. Using masses from reverberation mapping, they found a significant correlation between the two. Most notably, the relationship appears to scale linearly from the break frequency seen in Cygnus X-1, assuming a black hole mass of 10 $M_{\odot}$ in that object.

Since then, break frequencies have been found for over a dozen objects (see Uttley & McHardy 2005, for a compilation). Despite some scatter, the correlation holds remarkably well, especially considering the values are being scaled over six orders of magnitude. A complete list of known break timescales, masses, and Eddington accretion rates is given in Table 5.3.

We plot previously known break frequencies versus our new results in Figure 5.2. All of our objects agree well with linear scaling from the low/hard state of Cygnus X-1, and help to fill in the high-mass portion of the diagram. For 3C 120, we adopt a high-frequency break of 6 days, based on the detected low-frequency break of 110 days, and the ratio of ~ 20 seen between the high- and low-frequency breaks in Cygnus X-1.

5.6 Future Work

Although the *RXTE* observatory is showing its age, it remains a viable option for AGN monitoring for at least the next year or two. Intensive long-look observations of Mkn 509 and 3C 309.3 will help extend the range of our power spectra of those objects by several orders of magnitude. Additionally, observations of Akn 120 with

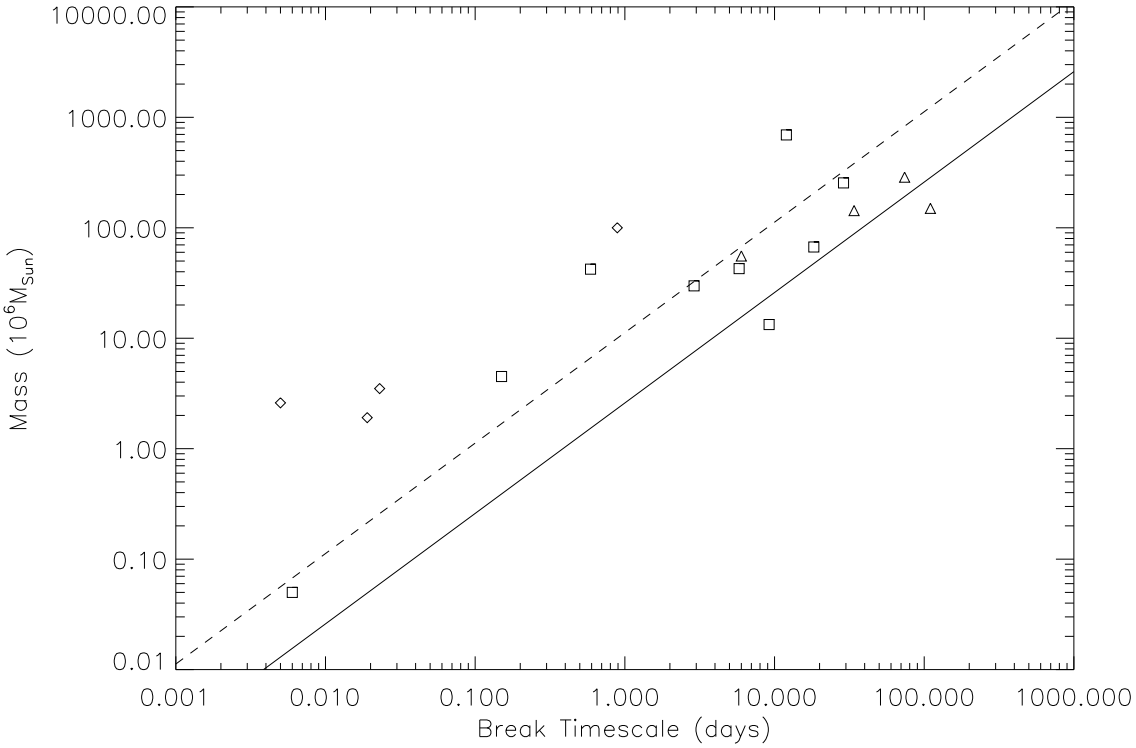

Figure 5.2: PDS break timescale versus mass. Previously known breaks are represented by squares for traditional Seyferts and diamonds for NLS1s, while break timescales for our objects are represented by triangles. The solid and dashed lines represent extrapolation of the break timescales for the low/hard and high/soft states of Cygnus X-1, respectively.

sampling on the order of several hours would help to fill in the power spectrum of that object.

With the demise of *RXTE*, the prospects for long-term monitoring of extragalactic sources remain uncertain. *Chandra* and *XMM-Newton* are both capable of providing continuous observations of 10^5 s duration, but repeated monitoring is not feasible. *GLAST*, scheduled to be launched in Oct. 2007, will provide complete observations of the γ-ray sky every few hours, however Seyfert galaxies are most likely not γ-

ray emitters. The *Swift* γ-ray burst explorer is already devoting some of its time to observations of AGN, however *Swift* is not capable of the flexible scheduling available with *RXTE*.

References

Antonucci, R. R. J., & Miller, J. S. 1985, ApJ, 297, 621

Arakelian, M. A. 1975, Soobshcheniya Byurakanskoj Observatorii Akademiya Nauk Armyanskoj SSR Erevan, 47, 43

Ballantyne, D. R., Fabian, A. C., & Iwasawa, K. 2004, MNRAS, 354, 839

Belloni, T., & Hasinger, G. 1990, A&A, 227, L33

Bettoni, D., Falomo, R., Fasano, G., Govoni, F., Salvo, M., & Scarpa, R. 2001, A&A, 380, 471

Boller, T., Brandt, W. N., Fabian, A. C., & Fink, H. H. 1997, MNRAS, 289, 393

Botte, V., Ciroi, S., di Mille, F., Rafanelli, P., & Romano, A. 2005, MNRAS, 356, 789

Botte, V., Ciroi, S., Rafanelli, P., & Di Mille, F. 2004, AJ, 127, 3168

Cooke, B. A. et al. 1978, MNRAS, 182, 489

Cox, A. N. 2000, Allen's Astrophysical Quantities, 4th Ed. (New York: AIP Press)

Deeming, T. J. 1975, Ap&SS, 36, 137

Dewangan, G. C., Boller, T., Singh, K. P., & Leighly, K. M. 2002, A&A, 390, 65

Dietrich, M. et al. 1998, ApJS, 115, 185

Done, C., Madejski, G. M., Mushotzky, R. F., Turner, T. J., Koyama, K., & Kunieda, H. 1992, ApJ, 400, 138

Edelson, R., & Nandra, K. 1999, ApJ, 514, 682

Edelson, R., Turner, T. J., Pounds, K., Vaughan, S., Markowitz, A., Marshall, H., Dobbie, P., & Warwick, R. 2002, ApJ, 568, 610

Edelson, R. A., & Krolik, J. H. 1988, ApJ, 333, 646

Fabian, A. C. et al. 2002, MNRAS, 335, L1

Foltz, C. B., Peterson, B. M., Capriotti, E. R., Byard, P. L., Lawrie, D. G., & Bertram, R. 1981, ApJ, 250, 508

Forman, W., Jones, C., Cominsky, L., Julien, P., Murray, S., Peters, G., Tananbaum, H., & Giacconi, R. 1978, ApJS, 38, 357

French, H. B., & Miller, J. S. 1980, PASP, 92, 753

Gliozzi, M., Papadakis, I. E., & Räth, C. 2006, A&A, 449, 969

Gliozzi, M., Sambruna, R. M., & Eracleous, M. 2003, ApJ, 584, 176

Greenstein, J. L., & Schmidt, M. 1964, ApJ, 140, 1

Harris, D. E., Mossman, A. E., & Walker, R. C. 2004, ApJ, 615, 161

Kaspi, S., Smith, P. S., Netzer, H., Maoz, D., Jannuzi, B. T., & Giveon, U. 2000, ApJ, 533, 631

Kembhavi, A. K., & Narlikar, J. V. 1999, Quasars and active galactic nuclei : an introduction (Cambridge, UK: Cambridge University Press)

Khachikian, E. Y., & Weedman, D. W. 1974, ApJ, 192, 581

Leighly, K. M., & O'Brien, P. T. 1997, ApJ, 481, L15

Levine, A. M., Bradt, H., Cui, W., Jernigan, J. G., Morgan, E. H., Remillard, R.,

Shirey, R. E., & Smith, D. A. 1996, ApJ, 469, L33

Lira, P., Lawrence, A., O'Brien, P., Johnson, R. A., Terlevich, R., & Bannister, N. 1999, MNRAS, 305, 109

Longair, M. 1997, High Energy Astrophysics, Vol. 2, 2nd Ed. (Cambridge: Cambridge University Press)

Lutz, M. 2001, Programming Python (Sebastopol, CA: O'Reilly & Associates, Inc.)

Maoz, D., Markowitz, A., Edelson, R., & Nandra, K. 2002, AJ, 124, 1988

Markowitz, A., & Edelson, R. 2004, ApJ, 617, 939

Markowitz, A., Edelson, R., & Vaughan, S. 2003a, ApJ, 598, 935

Markowitz, A. et al. 2003b, ApJ, 593, 96

Marscher, A. P., Jorstad, S. G., Gómez, J.-L., Aller, M. F., Teräsranta, H., Lister, M. L., & Stirling, A. M. 2002, Nature, 417, 625

McHardy, I. M., Gunn, K. F., Uttley, P., & Goad, M. R. 2005, MNRAS, 359, 1469

McHardy, I. M., Papadakis, I. E., Uttley, P., Page, M. J., & Mason, K. O. 2004, MNRAS, 348, 783

Miller, H. R. 1979, A&AS, 35, 387

——. 1986, AJ, 91, 665

Miller, H. R., & Ferrara, E. C. 1999, Bulletin of the American Astronomical Society, 31, 698

Mueller, M., Madejski, G., Done, C., & Zycki, P. 2004, in AIP Conf. Proc. 714: X-ray Timing 2003: Rossi and Beyond, ed. P. Kaaret, F. K. Lamb, & J. H. Swank,

190–193

Mushotzky, R. F., & Marshall, F. E. 1980, ApJ, 239, L5

Nandra, K., Clavel, J., Edelson, R. A., George, I. M., Malkan, M. A., Mushotzky, R. F., Peterson, B. M., & Turner, T. J. 1998, ApJ, 505, 594

Noble, J. C. 1995, Ph.D. Thesis, Georgia State University

Nousek, J. A. et al. 1998, in Proc. SPIE Vol. 3444, X-Ray Optics, Instruments, and Missions, ed. R. B. Hoover & A. B. Walker

O'Brien, P. T. et al. 1998, ApJ, 509, 163

Ogle, P. M., Davis, S. W., Antonucci, R. R. J., Colbert, J. W., Malkan, M. A., Page, M. J., Sasseen, T. P., & Tornikoski, M. 2005, ApJ, 618, 139

Oliva, E., Origlia, L., Maiolino, R., & Moorwood, A. F. M. 1999, A&A, 350, 9

Papadakis, I. E., Brinkmann, W., Negoro, H., & Gliozzi, M. 2002, A&A, 382, L1

Papadakis, I. E., & Lawrence, A. 1993, MNRAS, 261, 612

——. 1995, MNRAS, 272, 161

Papadakis, I. E., Reig, P., & Nandra, K. 2003, MNRAS, 344, 993

Peterson, B. M. 1997, An Introduction to Active Galactic Nuclei (Cambridge: Cambridge University Press)

Peterson, B. M. et al. 2004, ApJ, 613, 682

Peterson, B. M., Korista, K. T., & Wagner, R. M. 1989, AJ, 98, 500

Pounds, K., Reeves, J., O'Brien, P., Page, K., Turner, M., & Nayakshin, S. 2001, ApJ, 559, 181

Pounds, K. A., Nandra, K., Fink, H. H., & Makino, F. 1994, MNRAS, 267, 193

Press, W. H., Teukolsky, S. A., Vetterling, W. T., & Flannery, B. P. 1992, Numerical Recipes in C. The Art of Scientific Computing (Cambridge: Cambridge University Press)

Priestley, M. B. 1981, Spectral Analysis and Time Series (London: Elsevier Academic Press)

Revnivtsev, M., Gilfanov, M., & Churazov, E. 2000, A&A, 363, 1013

Reynolds, C. S., Ward, M. J., Fabian, A. C., & Celotti, A. 1997, MNRAS, 291, 403

Romano, P. et al. 2004, ApJ, 602, 635

Sanders, D. B., Phinney, E. S., Neugebauer, G., Soifer, B. T., & Matthews, K. 1989, ApJ, 347, 29

Scargle, J. D. 1982, ApJ, 263, 835

Schmidt, M. 1963, Nature, 197, 1040

Seyfert, C. K. 1943, ApJ, 97, 28

Shakura, N. I., & Sunyaev, R. A. 1973, A&A, 24, 337

Singh, K. P., Westergaard, N. J., Schnopper, H. W., Awaki, H., & Tawara, Y. 1989, in ESA SP-296: Two Topics in X-Ray Astronomy, Volume 2: AGN and the X Ray Background, ed. J. Hunt & B. Battrick, 1053

Stalin, C. S., Gopal Krishna, Sagar, R., & Wiita, P. J. 2004, Journal of Astrophysics and Astronomy, 25, 1

Sturm, E., Hasinger, G., Lehmann, I., Mainieri, V., Genzel, R., Lehnert, M. D., Lutz, D., & Tacconi, L. J. 2006, ApJ, 642, 81

Tanaka, Y. et al. 1995, Nature, 375, 659

Timmer, J., & Koenig, M. 1995, A&A, 300, 707

Turner, T. J., George, I. M., Nandra, K., & Turcan, D. 1999, ApJ, 524, 667

Uttley, P., & McHardy, I. M. 2001, MNRAS, 323, L26

——. 2005, MNRAS, 363, 586

Uttley, P., McHardy, I. M., & Papadakis, I. E. 2002, MNRAS, 332, 231

Uttley, P., McHardy, I. M., & Vaughan, S. 2005, MNRAS, 359, 345

Vaughan, S., Edelson, R., Warwick, R. S., & Uttley, P. 2003a, MNRAS, 345, 1271

Vaughan, S., Fabian, A. C., & Nandra, K. 2003b, MNRAS, 339, 1237

Vaughan, S., Iwasawa, K., Fabian, A. C., & Hayashida, K. 2005, MNRAS, 356, 524

Wandel, A., Peterson, B. M., & Malkan, M. A. 1999, ApJ, 526, 579

Webb, J. R., Smith, A. G., Leacock, R. J., Fitzgibbons, G. L., Gombola, P. P., & Shepherd, D. W. 1988, AJ, 95, 374

Weedman, D. W. 1977, ARA&A, 15, 69

Woltjer, L. 1959, ApJ, 130, 38

Woo, J.-H., & Urry, C. M. 2002, ApJ, 579, 530

Zakamska, N. L. et al. 2006, AJ, 132, 1496

Zensus, J. A., & Pearson, T. J. 1988, in IAU Symp. 129: The Impact of VLBI on Astrophysics and Geophysics, ed. M. J. Reid & J. M. Moran, 7

Appendices

– A –

Source Code

A.1 pypeline.py

```
#!/usr/bin/env python

pydir = '/usr/local/PEGA/pypeline'
storagedir = '/nfs/sync2/pega_data/xray'

import os, string, sys, time, ftplib, shutil, glob, popen2
from math import sqrt

#os.putenv('PYTHONPATH','%s/lib' % (pydir))

global obsIDdir, logdir, target, propID, obsID

def handleDownload(block):
        file.write(block)

#Create function to run OS commands
def getCommandOutput(command):
        child = os.popen(command)
        data = child.read()
        err = child.close()
        if err:
                raise RuntimeError, '%s failed with error code %d' \
                        % (command, err)
                print '\nTHIS IS VERY BAD!!!'
                sys.exit(1)
        return data

#Retrieve data via FTP
def retrieve(propID, targetID, target, pgpkey):
        currentdir = os.getcwd()
        global datadir
        datadir = storagedir + '/' + target
```

```
        ftpsite = 'ftp://legacy.gsfc.nasa.gov/xte/data/archive/ \
PGPData/'
        input = open(pydir + '/.pgpfiles', 'r')
        datafiles = ['']
        pgpfiles = string.split(input.read())
#Download only those files that are needed
        for entry in pgpfiles:
                if entry[:8] == propID + '-' + targetID:
                        datafiles.append(entry)
        input.close()
        datafiles = datafiles[1:]

        try:
                os.mkdir(datadir + '/' + target + '/rxte/P' + propID)
        except OSError:
                print 'Downloading data to ' + datadir + '/rxte/P' + \
propID
                getfiles = ['']
                gotdir = datadir + '/rxte/P' + propID
                gotfiles = glob.glob('%s/%s*' % (gotdir, propID))
                for line in datafiles:
                        flag = 0
                        for nextline in gotfiles:
                                nextline = nextline[-14:] + '.tar.pgp'
                                if line == nextline:
                                        flag = 1
                        if flag == 0:
                                getfiles.append(line)
                getfiles = getfiles[1:]
                if getfiles == []:
                        print 'No new files need to be downloaded for\
%s\n' \
                                % (target)
                        return None
        else:
                print 'Creating data directory ' + datadir + \
'/rxte/P'+ propID
                getfiles = datafiles

        print 'Connecting to FTP server at legacy.gsfc.nasa.gov'

        from ftplib import FTP
```

```
        try:  ftp = FTP('legacy.gsfc.nasa.gov')
        except ftp.all_errors, error:
                print 'Cannot connect, possibly HEASARC is having \
downtime?'
                print error
                sys.exit(1)
        else:
                try:  ftp.login()
                except ftp.all_errors, error:
                        print 'Cannot login: ', error
                        sys.exit(1)
        ftp.cwd('/xte/data/archive/PGPData/')

#Download, decrypt, and untar each file
        for filename in getfiles:
                os.chdir(datadir+ '/rxte')
                global file
                print '\nDownloading file ' + filename
                file = open(filename, 'wb')
                ftp.retrbinary('RETR ' + filename, handleDownload)
                file.close()
                print 'Decrypting file...'
                os.putenv('PGPPASS', pgpkey)
                getCommandOutput('gpg %s' % (filename))
                os.putenv('PGPPASS', '9999')
                print 'Extracting data...'
                filename = filename[:-4]
                os.system('tar -xf ' + filename)
                os.remove(filename + '.pgp')
                os.remove(filename)
                os.chdir(currentdir)
        ftp.close()

        try:
                os.mkdir(datadir + '/rxte/P' + propID + '/pypeline')
        except OSError:
                pass

#Create FMI file for each observation
        for line in getfiles:
                os.chdir(datadir + '/rxte/P' + propID)
                obsID = line[:-8]
```

```
                try:
                        os.mkdir(datadir + '/rxte/P' + propID + \
'/pypeline')
                except OSError:
                        pass
                os.mkdir(datadir + '/rxte/P' + propID + '/pypeline/' \
+ obsID)
                os.chdir(obsID)
                shutil.copyfile('FMI', '../FMI')
                os.chdir(datadir + '/rxte/P' + propID)
                getCommandOutput('recofmi level=1 delete=yes . > \
/dev/null')
                os.chdir(obsID)
                analyze(obsID, target)

        os.chdir(currentdir)

#Analyze each downloaded observation
def analyze(obsID, target):
        modelfile = glob.glob('%s/*.mdl' % (pydir))[0]
        propID = obsID[:5]
        fmidir = datadir + '/rxte/P' + propID
        logdir = fmidir + '/pypeline/' + obsID
        obsIDdir = fmidir + '/' + obsID
        appidlist = pydir + '/appidlist'
        os.chdir(fmidir)
        print '\nAnalyzing obsID %s' % (obsID)
        print 'Generating filter file with xtefilt... '
        getCommandOutput('xtefilt -s -c -a %s -o %s -p %s -t 16 > \
                %s/xtefilt.log' % (appidlist, obsID, fmidir, logdir))

        os.chdir(obsIDdir)
        std2 = glob.glob('pca/FS4a*')[0]
        filterfile = glob.glob('stdprod/*.xfl')[0]
        bkg = std2[:-4] + '_bkg'
        print 'Generating background files with pcabackest...'

        getCommandOutput('pcabackest infile=%s/%s outfile=%s/%s \
                filterfile=%s/%s modelfile=%s saahfile=%s/ \
pca_saa_history modeltype=both interval=16 \
propane=no layers=yes gaincorr=no gcorrfile=-\
fullspec=no syserr=no clobber=yes \
```

```
timeslop=128 > %s/pcabackest.log' % \
(obsIDdir, std2, logdir, bkg[4:], obsIDdir, \
filterfile, modelfile, pydir, logdir))

        print 'Generating good time interval with maketime...'
        input = open(pydir + '/expression.txt', 'r')
        expression = string.split(input.read(), '\012')[0]
        input.close()
        getCommandOutput('maketime infile=%s/%s outfile=%s/basic.gti \
                expr="%s" name=NAME value=VALUE time=TIME compact=no \
                clobber=yes' % (obsIDdir, filterfile, logdir, \
expression))

#For observations with no GTI, skip
        if string.split(getCommandOutput('fdump infile=%s/basic.gti[1]\
                outfile=STDOUT columns="START STOP" prhead=no \
showcol=no showrow=no rows=- more=yes wrap=yes \
pagewidth=200' % (logdir)), '\012')[3:-1] == []:
                print 'obsID has no goodtime, skipping extraction...'
                return

        print 'Extracting light curves and spectra for data files...'
        getCommandOutput('saextrct infile=%s/%s gtiorfile=APPLY \
                gtiandfile=%s/basic.gti outroot=%s/layer1 \
accumulate=ONE timecol=TIME columns=@%s/layer1.cols \
binsz=16 printmode=BOTH lcmode=RATE spmode=SUM
timemin=INDEF timemax=INDEF timeint=INDEF \
chmin=INDEF chmax=INDEF chint="0-44" chbin=INDEF \
bailout=yes clobber=yes > %s/extract.log' % (obsIDdir,\
std2, logdir, logdir, pydir, logdir))

        print 'Extracting light curves and spectra for background \
files...'
        getCommandOutput('saextrct infile=%s/%s gtiorfile=APPLY \
                gtiandfile=%s/basic.gti outroot=%s/layer1_bkg \
accumulate=ONE timecol=TIME columns=@%s/layer1.cols \
binsz=16 printmode=BOTH lcmode=RATE spmode=SUM
timemin=INDEF timemax=INDEF timeint=INDEF chmin=INDEF\
chmax=INDEF chint="0-44" chbin=INDEF bailout=yes \
clobber=yes > %s/extract_bkg.log' % \
(logdir, bkg[4:], logdir, logdir, pydir, logdir))
```

```
        getCommandOutput('lcmath infile=%s/layer1.lc bgfile=%s/\
layer1_bkg.lc outfile=%s/layer1_net.lc multi=1 \
multb=1 addsubr=no > /dev/null' % \
(logdir, logdir, logdir))

        os.chdir(logdir)
        print 'Generating spectral response file...'
        getCommandOutput('pcarsp -f %s/layer1.pha -a %s/%s -l LR1 \
-j y -p "0,2" -m y > %s/pcarsp.log' % (logdir, \
obsIDdir, filterfile, logdir))

        respfile = glob.glob('*.rsp')[0]

#Change FITS response keywords
        os.system('fparkey %s layer1.pha respfile' % (respfile))
        os.system('fparkey layer1_bkg.pha layer1.pha backfile')

        reduce(logdir, target)


#Extract counts and spectrum from each light curve
def reduce(logdir, target):
        os.chdir(logdir)

        print 'Getting FITS header keywords...'

#Figure out mean MJD of observation
        mjdrefi = float(string.split(getCommandOutput('fkeyprint \
                layer1_net.lc[0] MJDREFI exact=yes'), '\012')[5][10:31])
        mjdreff = float(string.split(getCommandOutput('fkeyprint \
                layer1_net.lc[0] MJDREFF exact=yes'), '\012')[5][10:31])
        mjdref = mjdrefi + mjdreff

#Figure out exposure time
        exptime = 0.0
        goodtimes = string.split(getCommandOutput('fdump \
infile=basic.gti[1] outfile=STDOUT \
columns="START STOP" prhead=no showcol=no showrow=no \
rows=- more=yes wrap=yes pagewidth=200'), '\012')[3:-1]
        for line in goodtimes:
                exptime = exptime + float(string.split(line)[1]) - \
                        float(string.split(line)[0])
```

```
                mjd = mjdref + ((float(string.split(line)[0]) + \
                        float(string.split(line)[1]))/2.0)/86400.0

#Figure out mean count rate and error
        stats = string.split(getCommandOutput('fstatistic layer1_net.lc \
                RATE -'), '\012')
        rate = float(stats[1][50:])
        try: error = float(stats[2][50:])
        except ValueError:
                print 'obsID does not have significant goodtime, \
                        skipping further analysis'
                return
        num = float(stats[5][50:])
        error = error / (2.0 * (sqrt(num)))

        print 'Fitting spectrum in xspec...'

#Fit spectrum in xspec using TCL script
        getCommandOutput('xspec - %s/autofit.xcm > xspec.log' % (pydir))
        input = open('fit_result.dat', 'r')
        slope = float(input.readline())
        slope_err = slope - float(input.readline())
        flux = float(input.readline())
        input.close()

#Write all data to a text file
        outputlist='%.4f \t %d \t %.3e \t %.3f \t %.3f \t %.3f \t \
%.3f \n' % (mjd, exptime, flux, slope, slope_err, \
rate, error)
        output = open('%s/%s.log' % (datadir, propID), 'a')
        output.write(outputlist)
        output.close()
        print 'Output written to %s/%s.log' % (datadir, propID)

#Main function which runs pypeline
def runpypeline():
        start_time = time.time()
        global propID
        for line in open('obsid.list', 'r').readlines():
                if line[0] == '#':
                        continue
                propID, targetID, target = string.split(line)
```

```
                pgpfile = propID + '.key'
                try:
                        pgpkey = string.split(open(pgpfile, \
'r').readline(), '\012')[0]
                except IOError:
                        print 'PGP key file not found, or you do not \
have read permission for the PGP key \
for propID: ' + propID
                        continue
                print 'propID   =', propID
                print 'targetID =', targetID
                print 'target   =', target
                print 'PGP key  =', pgpkey
                retrieve(propID, targetID, target, pgpkey)
        stop_time = time.time()
        runtime = stop_time - start_time
        print '\n\nPypeline completed after %.2f seconds of \
computation.' % (runtime)

if __name__ == '__main__':
        runpypeline()
```

A.2 stationary.pro

```
PRO stationary,infile

        date=0D & exptime=0L & flux=0L & slope=0L & sloperr=0L & $
counts=0D counterr=0D
        ;Read in values using C. Markwardt's transread procedure
        transread,UNIT,date,counts,counterr,filename=infile
        date=date-date[0]

        ;Split the data up
        date1=[0]
        counts1=[0]
        date2=[0]
        counts2=[0]

        FOR i=0,n_elements(date)-1 DO BEGIN
                IF date[i] LE max(date)/2. THEN BEGIN
                        date1=[date1,date[i]]
                        counts1=[counts,counts[i]]
                ENDIF
                IF date[i] GE max(date)/2. THEN BEGIN
                        date2=[date2,date[i]]
                        counts2=[counts2,counts[i]]
                ENDIF

        ENDFOR

        date2[0] = date2[1]
        counts2[0] = counts2[1]
        print,n_elements(date1),n_elements(date2)
        print,max(date1)-min(date1),max(date2)-min(date2)

        ;Compute binned periodogram for first half
        scargle,date1,counts1,obs_om1,obs_psd1
        obs_om1 = obs_om1/(2.*3.14159)
        obs_om1 = obs_om1/86400.
        obs_om1=alog10(obs_om1)
        rebinlc,obs_om1,obs_psd1,obs_freqs1,obs_power1,dt=0.3,minnum=4
        obs_freqs1=10^obs_freqs1

;Compute binned periodogram for second half
```

```
        scargle,date2,counts2,obs_om2,obs_psd2
        obs_om2 = obs_om2/(2.*3.14159)
        obs_om2 = obs_om2/86400.
        obs_om2=alog10(obs_om2)
        rebinlc,obs_om2,obs_psd2,obs_freqs2,obs_power2,dt=0.3,minnum=4
        obs_freqs2=10^obs_freqs2

;Calculate S value
        S = fltarr(n_elements(obs_freqs1))
        FOR i=0,n_elements(S)-1 DO BEGIN
                S[i]=(alog10(obs_power1[i])-alog10(obs_power2[i]))$
/0.7874
        ENDFOR

        Stotal = 1/sqrt(n_elements(S)) * total(S)
        print,'S=',Stotal

RETURN
```

A.3 simulate.pro

```
PRO simulate,date,counts,counterr,simslope,break,bintime

        ;set initial date to 0, and use days for all units (faster
; than secs)
        date=date-date[0]
        time=date
        daybreak=(10.^(break))*86400.
        npoints=fix((max(date)-min(date))/bintime)*1000.
        print,'npoints=',npoints

        ;calculate, write, and plot PDS for observed data
        scargle,date,counts,obs_om,obs_psd
        obs_om = obs_om/(2.*3.14159)
        obs_om = obs_om/86400.
        obs_psd=(2.*(max(time)-min(time))*86400.)/(mean(counts)*$
mean(counts)*n_elements(counts)*n_elements(counts))*$
obs_psd
        obs_om=alog10(obs_om)
        rebinlc,obs_om,obs_psd,obs_freqs,obs_power,dt=0.17,minnum=2
        obs_freqs=10^obs_freqs
        file_mkdir,string(simslope)+string(break)
        outfile=filepath('observed',root_dir=$
                '/nfs/hubble/marshall/akn120/presp/long', $
                subdir=string(simslope)+string(break))
        openw,3,outfile
        FOR i=0,n_elements(obs_freqs)-1 DO printf,3,obs_freqs[i],$
obs_power[i]
        close,/all


        ;calculate true variance of light curve
        lc_variance = variance(counts) - variance(counterr)

        ;now make a huge fake light curve
        timmerlc,faketime,fakerate,dt=(bintime/10),mean=MEAN(counts),$
                seed=5.6415,sigma=sqrt(lc_variance),slope=-simslope,$
                break=daybreak,nt=npoints*1.1

        ;calculate Poisson noise
        z=findgen(100)*(bintime/100.)+(bintime/100.)
```

```
        pz=(1+(z/daybreak)^2)^(simslope)
        p_alias=int_tabulated(z,pz)
        p_alias=p_alias*(1/((1/(2*bintime))-(1/(max(time)))))

        bintime=fltarr(n_elements(time))
        binrate=fltarr(n_elements(time))
        ;cycle through entire fake data set
        basecount=long(1)
        pm=fltarr(100,20)
        ;do 100 loops for 100 segments
        FOR j=0,99 DO BEGIN
                print,'Computing PDS ',j
                ;step through all points in curve and rebin
                FOR i=0,n_elements(time)-1 DO BEGIN
                        ;bin points
                        FOR k=long64(basecount),basecount+npoints/100 $
DO BEGIN
                                IF time[i] gt faketime[k-1] and $
                                time[i] lt faketime[k] then BEGIN
                                        bintime[i]=faketime[k]
                                        binrate[i]=fakerate[k]
                                ENDIF
                        ENDFOR
                ;move to next segment in curve
                ENDFOR
                plot,bintime,binrate
                basecount=basecount+npoints/100
                faketime=faketime-max(time)
                faketime=faketime-faketime[basecount]

                ;calculate pds and write here
                bintime=bintime-bintime[0]
                bintime=bintime*86400.
                scargle,bintime,binrate,om,psd
                ;add aliasing and poisson noise
                psd=psd+p_alias
                psd=psd+0.2*(mean(binrate)+mean(counterr))/$
(mean(binrate)*mean(binrate))
                om=om/(2.*3.14159)
                om=alog10(om)
                rebinlc,om,psd,freqs,power,dt=0.17,minnum=2
                freqs=10^freqs
```

```
                IF j eq 0 THEN avg_psd=power ELSE avg_psd=avg_psd+power
                FOR k=0,n_elements(avg_psd)-1 DO pm[j,k]=power[k]

                file_mkdir,string(simslope)+string(break)
                outfile=filepath(string(j)+'.pds',root_dir=$
                        '/nfs/hubble/marshall/akn120/presp/long',$
                        subdir=string(simslope)+string(break))
                openw,1,outfile
                FOR i=0,n_elements(freqs)-1 DO printf,1,freqs[i],$
power[i]
                close,/all
        ENDFOR

        avg_psd = avg_psd / 100.0

;Calculate PDS error
        pds_err=fltarr(n_elements(avg_psd))
        FOR i=0,n_elements(pds_err)-1 DO pds_err[i]=sqrt($
variance(pm[*,i]))

;Find minimum chi^2 value
        chi_min=1.0E+50
        norm=0.0
        FOR n=-2.0,6.0,0.01 DO BEGIN
                x=10.^(n)
                norm_psd=avg_psd*x
                norm_err=pds_err*x
                chi_dist=0.0
                FOR i=0,n_elements(avg_psd)-1 DO BEGIN
                        chi_dist=chi_dist+(norm_psd[i]-obs_power[i])*$
                        (norm_psd[i]-obs_power[i])/(norm_err[i]*$
norm_err[i])
                ENDFOR
                IF chi_dist lt chi_min THEN BEGIN
                        chi_min=chi_dist
                        norm=x
                ENDIF
        ENDFOR

;Write all values to files
        outfile=filepath('contour.dat',root_dir=$
```

```
        '/nfs/hubble/marshall/akn120/presp/long')
    openw,4,outfile,/append
    printf,4,simslope,break,chi_min
    close,/all

    outfile=filepath('average',root_dir=$
        '/nfs/hubble/marshall/akn120/presp/long',$
        subdir=string(simslope)+string(break))
    openw,2,outfile
    FOR i=0,n_elements(freqs)-1 DO printf,2,freqs[i],$
        (avg_psd[i])*norm,(pds_err[i])*norm
    close,/all

    outfile=filepath('normalization',root_dir=$
        '/nfs/hubble/marshall/akn120/presp/long',$
        subdir=string(simslope)+string(break))
    openw,3,outfile
    printf,3,norm,chi_min
    close,/all

    set_plot,'ps'
    device,filename=filepath('plot.ps',root_dir=$
       '/nfs/hubble/marshall/akn120/presp/long',$
       subdir=string(simslope)+string(break))
    plot,obs_freqs,obs_power,/xlog,/ylog
    oplot,freqs,avg_psd*norm,psym=6
    errplot,freqs,(avg_psd-pds_err)*norm,(avg_psd+pds_err)*norm
    device,/close


RETURN
END
```

– B –

Reducing RXTE Data

This document provides a brief explanation on how to reduce data from the RXTE X-ray observatory. Most of the information here is intended for analysis of AGN data. If you are looking at bright sources, or wish to do high temporal frequency analysis (timescales less than a hundred seconds), you will need to look elsewhere.

NOTE: Most of the software tools used in this analysis are part of the FTOOLS package. In order to use them, you must either put the following lines in your `.bashrc` file, or run them each time:

```
export HEADAS=/usr/local/xray/headas/i686-pc-linux-gnu-libc2.2
source $HEADAS/headas-init.sh
```

Most of the commands described below can have all of their parameters given to them via command line switches. For the sake of simplicity, I will avoid this, but if you want to write a script or something like that you can look up all the switches in the user guide for that program.

For help with most of the commands described here, FTOOLS provides the a utility called `fhelp`. It works similar to the man pages: just type `fhelp` followed by the name of a command for information on how to run it. All of the websites mentioned in the text are listed in the Resources section at the end. If you have any other questions, feel free to ask me.

B.1 Intro to RXTE

The Rossi X-ray Timing Experiment (RXTE) was launched in late 1995, for the purpose of analyzing the timing properties of sources such as active galaxies, X-ray binaries, and other extreme objects. Although perhaps not producing the flashy results and pretty pictures of an observatory such as HST, RXTE has provided a tremendous amount of useful information, especially to the AGN community. Its high timing resolution, large energy window, and flexible observing schedule naturally lend themselves to the types of data analysis that PEGAns perform on a regular basis.

B.1.1 Detectors and Modes

RXTE carries three detectors on board: the Proportional Counter Array (PCA), the High Energy X-ray Timing Experiment (HEXTE), and the All-Sky Monitor (ASM). The ASM scans roughly 80% of the sky each orbit, looking for transient X-ray sources. The HEXTE consists of two clusters of four scintillation detectors each, with a collecting area of 1.6 square meters and a time resolution of 8 microseconds. Neither the ASM nor the HEXTE will be discussed here.

For the vast majority of AGN timing analysis, the PCA instrument is used. The PCA is an array of 5 proportional counter units (PCUs), numbered 0-4. Because of various issues, typically only the first three of the PCUs are kept on; PCUs 3 and 4 are switched on and off occasionally. Also, each PCU consists of three separate layers of detectors. The first layer is the most sensitive, and is typically the only one used.

This also helps to cut down on readout noise from the other 2 layers. Therefore, this document deals with how to reduce PCA data using PCUs 0-2 and layer 1.

Note that beginning in early 2000, PCU1 began to malfunction as well. Therefore, more recent observations may have intermittent data from PCU1. Info on how to deal with this will be dealt with in the FAQs.

The PCA also contains a wide variety of data collection modes, such as Good Xenon, Standard2, Fourier, etc. Some of these modes (such as the Fourier mode) are so complex that even the RXTE Guest Observer Facility (GOF) has yet to provide a suitable method for data analysis. However, for our purposes, the Standard2 data mode is all we will need. In fact, the GOF stresses that Standard2 is the only data mode you should ever need, unless you want time resolution less than 16s (which we don't).

B.1.2 Retrieving Data

The RXTE data archive is located at the HEASARC website, and the w3Browse interface is used to choose which data sets you want. Enter in the object name or coordinates you want to look for, the coordinate epoch (if necessary), and choose a range of observation dates if you want. Check the 'RXTE' box in section 2, and then in section 3 make sure that 'Archived data and observations' is the only box checked. You can take a look at proposed observations if you want, but if you are looking for data that information will only clutter up your screen.

The default search will bring up a bunch of RXTE data catalogs, when we only

want the public data. So choose 'More Options' at the bottom, and uncheck all of the choices except 'XTE Public Archived Data.' Now submit your search, and it should return all of the public archived observations of your object (note: the site is often slow). Browse now shows you the ObsID for each one, the start and stop times, and some other info. Check which observations you want to retrieve.

There are a wide range of data products available, ranging from GIF previews of light curves and spectra to full datasets, which include nearly all of the spacecraft telemetry during that time. The intermediate level products contain just the data from the instruments, along with a few bare bones files needed for analysis. Thanks to an update in w3Browse, many intermediate level observations can now be tarred into a single file. Yay! So intermediate level products are now the best choice.

Browse will now create a tar file (or files) from all of the data sets you selected, which can take a while. This tar file can now be downloaded and stored in your data directory. When extracted, it will create the directory hierarchy from the observing cycle (if necessary) on down through the proposer ID and individual ObsIDs. Note that the proposer ID directory will probably NOT have an FITS Master Index (FMI) file, you will have to generate one (explained below).

B.1.3 Data Files and Directory Structures

Previous X-ray observatories such as ROSAT and ASCA stored their data in just a few files. However, because of the numerous instruments on board RXTE and various operating modes, as well as the high time resolution of those instruments, the data

files which come from an observation are often large in both size and complexity.

The top level of directories is based on the proposer ID number for each observation. These are labeled as P followed by a number. One of our proposer numbers is 70162, so any data from one of our observations would be in the directory P70162. Below that are the ObsID directories, which are the ID numbers for each individual observation. They have a form such as 70162-01-07-00. So an individual observation directory would be like: P70162/70162-01-07-00. There can be many ObsID's for each proposal directory. Note that if you have data spanning multiple observing cycles (years), it may be in separate proposer ID directories. These must be analyzed separately, and then you can combine the data later by putting the names of the light curves in a list, and giving that to `lcurve`. (§B.3.1.2)

The actual data from the observation are stored within each ObsID directory. The ObsID directory contains several subdirectories, such as pca, hexte, orbit, and so on. These directories contain all of the data files for those instruments, as well as the position of the spacecraft during the observation, and other important information. Methods of finding which files you need will be discussed later.

Within each ObsID directory, there should be an FMI file. The FMI is somewhat similar to a traditional FITS header, in that it contains standard information about the observation. However, it also contains pointers to all of the data files. Each directory, including the proposer ID directory, should have an FMI file. Chances are good that if you downloaded your data from the archive, each ObsID will have an

FMI, but the proposer ID directory won't. So how do you make an FMI file? You use the `recofmi` ftool.

`recofmi` needs an FMI file to reconstruct, so if there isn't one in the directory you want, just copy one from any place (it doesn't matter where). The format you use is:

```
]$ recofmi level=N delete=yes dirpath
```

where `dirpath` is the path to the directory whose FMI file you want to make, `level=N` is the number of levels you want it to go down (typically N=1), and `delete=yes` tells it to overwrite the old FMI information. You should have FMI files in each directory in your data hierarchy, down through the proposer ID level, down to the individual ObsID directories.

B.1.4 Background Issues

The PCA is a non-imaging detector with a field of view of approximately 1 degree. It collects all X-rays from a 1 square degree patch of sky, whether they come from your object or not. Because of the non-imaging nature of the PCA, background can't simply be subtracted from a sky annulus as in optical photometry. Also, there are other sources of noise caused by the South Atlantic Anomaly (SAA), and the decay of various radioactive elements within the spacecraft itself.

Because of this, care must be taken to ensure proper background subtraction. Models are generated using blank-sky and earth pointings, and are distributed at the HEASARC website. For the latest news on background models and subtraction, please refer to the PCA Digest.

B.2 Extracting Light Curves and Spectra

Once you have your data downloaded and un-tarred, you need to extract the information you want. One of the nice things about X-ray data is that each photon is time-tagged and has its energy measured as it arrives. So for a given observation, you can extract both a light curve and a spectrum. Photometry and spectroscopy at the same time!

B.2.1 REX - the Easy Way

Rex is a perl script which is designed to make the extraction process as simple as possible. It's great for doing large numbers of ObsID's at once. Unfortunately, if it messes up then you still have to go back and do those ObsIDs individually, and then merge their results with the rest of the data. Rex is definitely the easiest way to do RXTE data analysis, so unless something goes horribly wrong, you should use Rex whenever possible.

B.2.1.1 Setting up Rex

As with anything else, you should always keep your raw data in a directory separate from where you perform the analysis. I usually make a directory called `analysis` on the same level as the proposer ID directories.

Rex requires a few files to run, the first of which is `aux.tar`. This file is available at:

`ftp://legacy.gsfc.nasa.gov/xte/software/rex/aux.tar`

and should be extracted in the directory where you will do all of your analysis. `aux.tar` provides Rex with some of the parameters it needs for data extraction, as well as a list of keywords that should be in the header of each data file.

Rex sets default extraction parameters of an Earth elevation angle > 10 degrees, pointing offset < 0.02 degrees, PCUs 0, 1, and 2 on, time since SAA passage > 30 minutes, and electron noise < 0.1 units. These are all pretty good, but can be changed by editing the file `aux/expressions.txt`.

We also need a background model for subtraction from the data. Check the PCA digest to see which one is most appropriate for the time of your observations. The voltage on the PCA has been adjusted several times, creating 5 different epochs of background modeling. Thanks to the installation of FTOOLS v5.2, we can now use background files which span all 5 epochs.

Once you find the appropriate background model (or models) and download them, edit the `model.files` file in the `aux` directory. It should contain a list of all the background models you will need for that reduction, giving the path from the directory where you run Rex. You will also need the most recent version of the `pca_saa_history` file, which can be obtained at the PCA digest website.

B.2.1.2 Run Rex, Run!

If you have your extraction parameters and background files all set up, then you are ready to run rex! The command to do this is simply `rex`. Of course, all the

parameters can be input with switches from the command line, but otherwise rex will prompt you for them.

The first thing `rex` asks for is the path to the directory containing the FMI. This should be the path to the highest level directory you have for your data, typically the proposer ID directory. Next `rex` asks for the target, the default of all is a good choice. Then choose if you want a light curve, spectrum, or both. If you don't need one, then don't waste time and precious electrons by making `rex` do them both.

`rex` then prompts for channels for light curve extraction. If you only want a light curve for a certain energy range, you can look up the channel-energy conversion table at the PCA digest website, and put in the values for the range you want. Otherwise, the default is fine. The next choice is for PCU layer, and the default of 1 is good.

Next is the root name of products. If you want some kind of prefix for them, then enter one. Otherwise, your data products will be given a standard name (and will overwrite any previous extraction).

After this, `rex` should go to work and extract all of your data. If it encounters an error, it will notify you and write it to a log file, which you can look at later. Note that if `rex` skips an ObsID, you will either have to fix the problem and run `rex` again on all the data, or do that observation manually and then merge the results with the rest of `rex`'s output.

B.2.1.3 Rex's Output

So what exactly did `rex` leave you with? In your analysis directory, you should have:

- `layer1.pha` - layer 1 spectrum from all ObsIDs
- `layer1_bkg.pha` - layer 1 background spectrum from all ObsIDs
- `layer1_ch0-27.lc` - layer 1 1-10 keV light curve for all ObsIDs
- `layer1_ch0-27_bkg.lc` - layer 1 bkgd light curve for all ObsIDs
- `layer1_ch0-27_net.lc` - layer 1 bkgd. subtracted light curve

Rex will also create directories for each individual ObsID in your analysis directory, which will contain the above files for each ObsID. A directory for each ObsID will also be created in your `aux` directory, which will contain all the background files and GTIs for that ObsID, as well as a list of all background files and std2 data files for that particular ObsID (the relevance of these things will be explained later, although you don't really need them unless you have to do a manual extraction).

Should `rex` encounter an error, it will note that in one of the log files it generates. These can be found in the aux/ObsID directories, and `rex` will tell you the log file you need to look at when the error occurs.

So that's it. Now you should have your spectra and light curve for all of your observations. Skip ahead to section 3 now, if you'd like.

B.2.2 Xselect - the Bad Way

Up until recently, nearly all X-ray data reduction was done with a program known as `xselect`, written by the friendly folks at GSFC. The great thing about `xselect` was

its flexibility, allowing you to extract data from ROSAT, ASCA, or RXTE all in the same program. Nowadays, observatories such as Chandra and XMM have their own data reduction software (CIAO and SAS respectively), which can be a pain to learn.

Although all of the RXTE reduction can be done using individual ftools commands, it's often simpler to do everything at once in `xselect`.

B.2.2.1 Getting Ready for Xselect

As before, you should do all your analysis in a directory separate from your data. Before we begin, we will need to create a filter file, which will allow us to filter data using criteria like Earth elevation angle, number of PCUs on, etc. Each ObsID has its own individual filter file, but we want to create a master filter for all of the observations we are looking at. To do this we use two programs: the XTE data finder (XDF) and `fmerge`.

To start XDF, just type `xdf` in your analysis directory. It will bring up a nice GUI interface which easily lets you browse through all the data directories. The first thing we need to do is give `xdf` the path to your highest level FMI file. Enter in the path in the box that says 'Path' at the top, in the center of the window. Make sure that your path doesn't end with a /, otherwise that will cause some issues. Now click the 'Make ObsList' button, and the Observations window should fill up with info about all of the observations you have selected.

Presumably you want to look at all of them, so click the 'All/None' button underneath the Observations window. They should all be highlighted now. In the

Subsytems window, scroll down and choose '15 Standard Products', and click the 'Make AppIdConfigList' button. The AppIdConfigList window should now fill up with choices. About 10 choices down, you will see 'Filter File.' Highlight this, and click on the 'Make FileList' button at the top of the window. You will now see a list of all your filter files in the 'FITS Files' window at the bottom of the screen.

We are now ready to save this list. Click the 'All/None' button under the 'FITS Files' window to highlight them all. Now enter a name for your filter file in the 'File Name' box at the top. I usually call my filter something obvious like `filter.list`. Then click 'Save FileList' at the top of the window. All of the filter file names should now be written to your `filter.list` file as a list.

We also need to create a list of all our Standard2 mode data files. To do this in `xdf`, go back to the 'Subsystems' window and un-highlight '15 Standard Products', and select '1 PCA'. Now click the 'Make AppIdConfigList' button, and choose 'Standard2f' from the list of AppIds/Configurations. Now click the "Make FileList" button, and XDF will create a list of all the data files we want. Select them all, and then enter a name in the File Name box. Something like `std2.xdf` is good, then click 'Save FileList' to save them all. We are now finished with XDF, so you can exit the program.

Before we begin, we need to merge all of our individual filter files into one. To do this, we use the `fmerge` ftool. To run it, the format is:

```
]$ fmerge @filter.list filter.xfl @column.list lastkey='TSTOP'
```

where `@filter.list` is the list of filter files we created in `XDF`, `filter.xfl` will be the name of our combined filter, `@column.list` is the name of all the column keywords we want put in the new filter (typically found in `aux/filter.cols`), and `lastkey='TSTOP'` tells fmerge when to stop merging the files.

B.2.2.2 Running Xselect

Now we are ready to start, so type `xselect` to fire up the program. It will prompt you for a session name, the default is fine. Notice that the mission is currently set to ASCA; we need to change this. So type `set mission xte` to change the mission to RXTE. To change the instrument, type `set inst pca` to change to the PCA. Now we need to point `xselect` to our data, so type `set datadir`. Give it the top level directory of your data, which will probably be the proposer ID directory.

To see all of your observations, type `make obscat` to create an observation catalog. Hit enter when asked to choose a filter to select the default, and then `xselect` should show you a list of all your observations. You now need to pick which ones you want. Assuming you want all of them, enter `choose 1-**`. If you want only certain ones, enter `choose "1-2,4-6"` or something similar. Make sure to use quotes if you are giving it a list of more than one. `xselect` should indicate that your selected data files are now in use.

The default binsize for Standard2 data is 16 seconds. To change the binning time, type `set binsize xx`, where `xx` is your desired binning size. Note that the binning time cannot be smaller than 16s.

`xselect` by default will extract data from all 5 PCUs and all 3 layers of each PCU. This is bad. To change this, enter the command:

```
> filter detector "01* 11* 21*"
```

where the 0, 1, and 2 are the PCU numbers we want, 1 is the layer we want, and the * allows both the right and left halves of the layer. Note again that you will have to re-extract after filtering out the unwanted PCUs.

If you want to only look at a certain energy, use `filter pha_cut` to select which PHA energy channels you want. A channel-energy conversion table can be found at the PCA digest website.

If you wish to change the selection criteria (and you should), we need to use the filter file that was created earlier. Type `set mkfdir` and point `xselect` to the directory where your filter file is stored. Then enter your selection criteria, such as:

```
> select mkf "ELV .gt.  10.0 .AND. NUM_PCU_ON .eq.  3 .AND. OFFSET
↪ .lt.  0.2 .AND. TIME_SINCE_SAA .gt.  30 .AND. ELECTRON0 .lt.  0.1"
```

will only select data with an Earth elevation angle > 10 degrees, with 3 PCUs on, with pointing offset < 0.2 degrees, time since SAA passage > 30 minutes, and electron noise < 0.1.

Now we are finally ready to extract a light curve and a spectrum. To do this, type `extract all`. Then `xselect` will go through and extract a light curve and spectrum for each observation. To view them after extraction, type `plot curve` or `plot spectrum`. If you decide to change any of the parameters, keep in mind that

you will have to re-extract the curve and spectrum.

When you are ready to save, type `save curve` and `save spectrum` to save your source light curve and spectrum. Now we are ready to move on to the background files. Don't exit `xselect` just yet, we'll need to come back to it in a minute.

B.2.2.3 Creating Background Files

Before we get started, you will need to download the appropriate background file. Typically, this will be the faint-mode 'L7' all-epoch file, available from the PCA digest page. Also, make sure to get the `pca_saa_history file`, which is needed to correct for SAA noise. You will also need your list of Standard2 FITS files from `xdf`, so make sure you have done that already.

Now we are ready to use `pcabackest`. To do this open up another xterm window and run `runpcabackest`. This is a perl script which calls `pcabackest` to process all your data. The first thing `runpcabackest` asks for is your list of Standard2 mode files, so enter in the name of that. Next it prompts for a name for the list of background files. Something like `bg_00.files` is good. Next it wants a suffix for the background files. `bkg` is good, just so you know they are background files. Then enter in the name of your XTE filter file, and then either the name of the background model you are using. For the rest of the choices, the defaults are fine, but make sure to give it the correct path to your `pca_saa_history` file.

`runpcabackest` should go through all your data and create background files for everything, and store the names of those files in the `bg_00.files` list. It may ask if

you should update the parameter file and you can say yes so that your choices will be saved as the defaults for next time. Now we can extract background light curves and spectra in `xselect`.

Returning to `xselect`, you can now read in the list of files generated by `pcabackest`. If your background files are in a different directory, use `set datadir` to point `xselect` there. Then enter:

```
> read events "bg_00.files"
> choose 1-**
```

to read in all background files and select them. `xselect` may ask if you want to clear filters. You should probably say no, since you will want the same filters for your background as you had for your source data. Now you can extract your background light curve and spectrum, so type `extract all` to do that. Then save them both, making sure to give them a suffix like `_bkg` so you know they are background files. You may now exit `xselect`.

The spectra are now ready for analysis; all we need is a response matrix, which will be covered in section 3.2.1. For the light curves, we need to subtract the background light curve from our source+bkgd light curve. For this, we use the `lcmath` ftool. The format is:

```
]$ lcmath infile bgfile outfile multi multib
```

where `infile` is our source+background light curve, `bgfile` is the name of the background light curve, `outfile` is the name of the background subtracted light curve we

want, and `multi` and `multib` are scaling factors for the 2 input light curves. Typically these should both be set to 1. `lcmath` will also ask if it should add instead of subtract. Say no, unless for some bizarre reason you want to add the files together.

That's it, now we have complete spectra and light curves, ready for analysis.

B.2.3 Manually - the Ugly Way

BEWARE ALL YE WHO ENTER HERE!

So why would you ever want to extract your data manually? Possible choices include:

- You like to eat broken glass
- You think IRAF is too easy
- You want to write a script like `rex` to automate things
- You are El Nerdo Supremo

What follows below isn't pretty, but it's how things work. I will assume that you have read the sections on extraction using `rex` and `xselect`, so that I don't have to repeat myself. I'm a lazy, lazy man.

B.2.3.1 Filtering and Making GTIs

First, use `xdf` to get the list of Standard2 files, and also get a list of all the filter files, as we did with `xselect`. Combine the filter files with `fmerge`, just as before. Now

we are ready to pick out the times that we want to look at. To do this, we'll create a GTI (good time interval) file.

This is done with the program `maketime`. Run it, and you will be prompted for the name of your filter file. Enter that in, and then enter the name of your output GTI file. Something simple like `basic.gti` is good. Next `maketime` asks for your selection expression, which is the important part of running this program. `maketime` takes selection criteria in either C or Fortran format. So for a decent criteria, you could enter something like:

```
ELV > 10 && OFFSET < 0.2 && NUM_PCU_ON = 3 && ELECTRON0 < 0.1
↪ && (TIME_SINCE_SAA > 30 || TIME_SINCE_SAA < 0.0)
```

For the rest of the choices, you can choose the defaults, although you should answer `no` on the flag question. `maketime` will now create your GTI file.

Assuming we only want to extract from the top layer of PCUs 0, 1, and 2, we need a way to tell the extractor. So we'll create a text file called `pcu012_layer1.col` which contains the following text:

```
X1LSpecPcu0
X1RSpecPcu0
X1LSpecPcu1
X1RSpecPcu1
X1LSpecPcu2
X1RSpecPcu2
```

Make sure this file ends with a carriage return. These are the identifier codes for each anode of the first layer of the three detectors, and we'll need them when extracting our products.

B.2.3.2 Extracting

The program used to extract spectra and light curves from the data files is `saextrct`. Note that this command should not be confused with `seextrct`, which is used to extract data taken in science event mode, which is not covered here. `saextrct` takes quite a few parameters. For full documentation, see the `fhelp` page.

Let's go ahead and run `saextrct` by typing `saextrct` at a shell prompt. The first thing you are asked for is the input file name. This should be your list of data files, so enter `@std2.xdf`, or whatever you called your file list.

`saextrct` next asks for the list of GTI files to be OR'ed with the infile. Each data file has its own GTI defined, although I'm not quite certain what that is. We want to use our own GTI that we created, so just enter a – and hit enter so that we don't use the default. Now it asks for the name of the GTI file to be AND'ed with infile. Give it the name of the GTI file that you created earlier with `maketime`.

Next `saextrct` asks for the root name of your output files. You can enter something like `pca`, or the name of your object, whatever floats your boat. The output files will be given `.lc` and `.pha` suffixes. The next choice is to accumulate one or many columns in the extraction. The default of one is a good choice.

Now `saextrct` asks for the name of the time column. This is self-explanatory,

so just choose the default of `TIME`. The next prompt is for the names of columns to be accumulated. We only want data from PCUs 0-2, layer 1, so we will enter in the name of the file we created before, prefaced by an @: `@pcu012_layer1.col`

`saextrct` next prompts for the binsize in seconds. Standard2 data have a minimum binsize of 16 seconds, so you shouldn't enter a value smaller than this. If you want something larger, that's fine, but remember you won't be able to make it smaller again if you want.

`saextrct` asks if you want to output a light curve, spectrum, or both. Pick whichever option you want.

Next `saextrct` asks for the type of binning for the light curve. The default of `rate` is fine, as it divides the total amount of counts accumulated in each bin by the binsize, giving you the count rate. For the spectrum, `sum` is good, as it gives the total number of accumulated counts in each bin.

Now `saextrct` asks for the maximum acceptable intensity for the light curve and spectrum. We don't care how bright our AGN gets so the default of `indef` is fine. The next two input choices, Column titles for sum and mean written as header keywords, don't apply to RXTE data and so you should just choose the defaults.

Now `saextrct` asks for the start and end time for the summation. If you want to cut off the ends of your data you can do so here, otherwise the defaults of `indef` are fine. Next you are prompted to input time intervals for extraction. If you want to look at a specific time interval in your data, you can enter the times here. Otherwise,

the default of `indef` will extract all of your data.

The next choice is for minimum and maximum energy bins in the spectrum. If you want to look at only certain energies, you can choose that. Be careful that binned energy channels are different from unbinned energy channels. To convert between the two, use the perl script `chantrans`. See the `fhelp` page for more info on how to do that. If you want to look at all energies, just choose the default of `indef`. Any energy ranges you don't want can be taken out later in `xspec`.

`saextrct` also asks for the energy channels to be retained. Presumably we want to look at all our data, so again choose the default of `indef`.

After entering in all of your preferences (which can also done via command line switches), `saextrct` will go through and extract all of the light curves and spectra you wanted.

There are a few other parameters which, although not prompted for, can sometimes be useful. Check out the `fhelp` file if you think you might be missing something.

B.2.3.3 Background Files

So now we have extracted our light curves and spectra for the data. We now need to do the same thing for background data. As explained above, go through and create your background files using `pcabackest`. Now go through and run `saextrct` as before, only give it your list of background files instead of the data file list. Make sure to change the name of the output files, so that you don't overwrite your previous data.

Now run `lcmath` again, just as for xselect, to create a back- ground subtracted light curve. Congratulations, you have just created light curves and spectra for all your observations, doing it the hard way!

B.3 Analysis of Light Curves and Spectra

Now that we have our data ready to analyze, we need to use separate programs to look at both the light curves and the spectra. Those programs are `xronos` (pronounced chronos) and `xspec`. Whereas `xspec` is pretty much standard in X-ray spectral analysis, `xronos` is not quite as widely used. If you have another method you would like to use when analyzing your light curve(s), a method of converting from FITS to ASCII format will be discussed below.

B.3.1 xronos

`xronos` consists of the following independent tasks:

`autocor` - calculates auto correlation

`crosscor` - calculates cross correlation

`efold` - creates epoch-folded light curve, hardness, and color-color

`efsearch` - finds best chi-squared period by folding the light curve

`listdata` - lists data file on the screen

`lcstats` - calculates statistical variables in a time series

`lcurve` - creates light curves, hardness, and color-color plots

`powspec` - creates power spectrum density

`timeskew` - calculates time skewness for a time series

`xronwin` - creates a window file for xronos tasks

`ascii2flc` - creates xronos FLC file from an ASCII input file

`flc2ascii` - dumps FLC file into a QDP-readable ASCII file

`lcmath` - subtracts or adds 2 binned light curves

`rbf2fits` - converts EXOSAT rate buffer format into FITS

`earth2sun` - changes time to solar system barycenter

Most of these tasks are pretty useful, but I will only focus on a few of them: `lcurve`, `autocor`, and `powspec`. For information on the rest, use the `fhelp` command to get more info, or check out the `xronos` user's guide.

B.3.1.1 I Hate `xronos`!

Don't worry, a lot of people share your feelings. Personally, I think it's a good way to examine your data, without having to do a detailed scientific analysis on it. But if for some other reason you want to manipulate your data in another program, that's fine. You can use the `listdata` or `flc2ascii` programs to display your data. `listdata` will give you columns with bin, day, time, duration (of the bin), counts, count error, and number of exposures. `flc2ascii` will give you a QDP plot file which can be easily plotted, but it's a little more difficult to get just raw columns of data.

B.3.1.2 Using `lcurve`

Since we have already extracted background subtracted light curves, now we can use the `lcurve` program to look at them, and rebin them if we want. To get started, just type `lcurve` at the prompt. It will first ask for the number of time series you want to look at. Just enter 1; if you want to look at more than one curve, put their names in a list file. Next `lcurve` asks you for the filename, so enter in the name of your light curve, or the name of your list file prefaced with an @. This is useful if you have several light curves from different observing cycles that you want to view.

`lcurve` will read in your data, and show you some information about it. Then it will ask for the name of a window file. A window file lets you select only a particular time interval, however presumably we want to look at all of the times contained in our data. So just enter a – to indicate the default window.

Binning data will now be displayed for your curve. If you have used the default parameters during extraction, your data will most likely have 16s bins. If you want to change the binning you can do so here, however note that your new binning time can not be smaller than your current bin size. `xronos` tries to rebin the data so that there are 512 bins. If you don't want this, then enter in either your own bin size, or `indef` to keep the old bin size.

Now `lcurve` asks for the number of bins you want to look at. If for some odd reason you want to create multiple, smaller light curves, enter in whatever number you want. Otherwise, look at the maximum number of newbins/interval it displays,

and enter in this value.

`lcurve` will now ask for the name of an output file. If you want to save your data, enter a name. Otherwise, just enter a space and hit enter. Now you will be prompted on whether or not you want to plot your data. If you say no, `lcurve` will create the light curve and exit. If you answer yes, `lcurve` will ask for the pgplot device (`/xw` for Xwindows, `/ps` for postscript, etc). You can use the PLT commands to mess around with your data, and make a pretty curve for yourself.

B.3.1.3 Using `autocor`

The `autocor` program is used to create an autocorrelation function from a given light curve. It uses an FFT algorithm to create the ACF; if you want to use a direct Fourier algorithm, you can check the `fhelp` file or user's guide for details on that. To get started, just type `autocor`.

You will be prompted for the name of the light curve you want to analyze, or you can also enter an @list of light curves. Next `autocor` will ask for the window file you want to use. As before, just enter a blank space for no window. `autocor` will then ask for the binning parameters. This is the same as the `lcurve` program, you can change them if you wish. Now `autocor` asks if you want to rebin your results. This can sometimes be handy if you will be plotting your results on a logarithmic scale, see the `fhelp` page for more information on that. If you're not sure, just enter a zero. Next `autocor` asks for an output file name. If you want to save your ACF in FITS format, give a name. And finally, `autocor` asks if you want to plot your data. This

works in the same way as `lcurve`.

Now you have your auto correlation function! Note that it is only given for positive time delay. There is no way that I know of to have an ACF for both positive and negative time delays in `autocor`.

B.3.1.4 Using `powspec`

The `powspec` program works much the same way as `lcurve` and `autocor`, so I won't go into much detail. The main caveat is that if you choose to rebin your data, the newbin time must be an integer multiple of your minimum (original) binning time. Note that you may want to rebin your data using geometrical binning, which will give you a logarithmic scale along the time axis (see the `fhelp` page or user's guide for info). `powspec` is a really lousy program, and ignores a lot of the important issues when creating a PDS. I wouldn't really recommend it, but it's there if you want to have a look. In my opinion, Numerical Recipes contains a much better method for creating a PDS.

This is just a small taste of what `xronos` can do. There are many parameters and options for each task, some of which are hidden. If you are planning on using `xronos` for high quality data analysis, make sure to read the user's guide so that you don't miss anything critical. It's only 65 pages and can easily be read in an hour or two.

B.3.2 `xspec`

The `xspec` program is a powerful and fairly popular program used in the analysis of X-ray spectra. Although perhaps eclipsed by newer programs designed for Chandra and XMM data, `xspec` remains more than adequate for the analysis of spectra from RXTE, ROSAT, and ASCA. This guide will only provide a very small sample of what `xspec` can do. For more info, be sure to read the `xspec` user's guide (which is unfortunately very lengthy).

B.3.2.1 Creating a Response File

Before you can analyze the spectrum, `xspec` needs what is known as a response (`.rsp`) file. This file describes the response of the detectors as a function of energy. You can roughly think of it as being analogous to a flat/dark/bias in optical astronomy.

To create the response file, we use a perl script called `pcarsp`. Type `pcarsp` to run the script, then give it the name of your spectrum (it will have a `.pha` extension). `pcarsp` asks for the name of the file containing attitude information. If you are confident that the source was in the center of the field you can enter `none`, otherwise point it towards your filter (`.xfl`) file (§ B.2.2.1 if you haven't made one).

Now we need to specify the anodes that the spectrum was extracted from. Assuming that you only used layer 1 data, enter `LR1` at the prompt. Now `pcarsp` asks whether the anodes were combined during extraction. Usually this is the case, so say yes. You are prompted next for which PCUs were used during the extraction.

Assuming you used only the first three, enter `0,1,2` at the prompt. `pcarsp` will ask again if they were combined during extraction, and you should say yes again. `pcarsp` will now create your response file, and we are ready to roll.

NOTE: In order to use `pcarsp`, you will need the `caldb` package installed. This provides pcarsp with the info it needs in order to generate the response matrices. To use the `caldb` package, put the following lines in your `.bashrc` file:

```
export CALDB=/nfs/hubble/marshall/caldb

source $CALDB/software/tools/caldbinit.sh
```

This assumes you are running bash. Source the `caldb.csh` file if you use C-shell. To make sure the caldb is properly running, type `caldbinfo` and choose the basic option. The program should report that everything is running smoothly.

B.3.2.2 Creating a 'Master' Spectrum

Before we actually load the data into `xspec`, we can save ourselves some time by associating all the files we'll need into one 'master' file. To do this, we use the `grppha` program, which groups pha files together. The format used is:

```
]$ grppha infile outfile
```

where `infile` is the name of our source spectrum, and `outfile` will be the name of the spectrum we'll load into `xspec`. I usually use something obvious like `spectrum.pha` for the outfile.

After running the program, `grppha` will display a list of all the keywords in the header of your pha file. The first thing we want to change is the background file, so

type:

```
GRPPHA[] chkey backfile layer1_bkg.pha
```

where `layer1_bkg.pha` is the name of your background spectrum that you extracted. If you used `rex` to extract your data, this step may already be done for you. Now we need to associate the response file with our spectrum:

```
GRPPHA[] chkey respfile response.rsp
```

where `response.rsp` is the name of our response file. Finally, I like to bin the spectrum so that each bin has at least 15 photons in it. You can change this value if you want, or leave it. To change the photon binning, enter:

```
GRPPHA[] group min 15
```

Now we are done. Type `exit` to save our spectrum and leave the program. Note that if you type `quit`, your changes will be discarded, so make sure you type `exit`. Now we should have a file called `spectrum.pha` which contains all the info we need to load it into `xspec`. You can also manually load in the background and response files in `xspec`, but if you are going to look at this spectrum more than once, you might as well save yourself some time and do it this way.

B.3.2.3 Loading and Plotting Your Data in Xspec

Now we are all set for analysis of our spectrum. To start `xspec`, simply type `xspec` at the prompt. It may or may not bring up a pgplot window that says 'XSPEC' in big letters. If not, then you should set your plot device to Xwindows. To do this, type `cpd /xw` at the xspec prompt, then move the pgplot window out of the way.

To read in your spectrum, type `data spectrum.pha`, where `spectrum.pha` is the name of the spectrum you want to look at. It should tell you some info about the spectrum, and should also give the names of the background and response files it is using.

Now let's take a look at the data. To do this, type `plot data` at the prompt. `xspec` will take your spectrum and plot it up in the pgplot window, as a function of channel vs. flux. It should be a bunch of little white crosses, with each cross representing a data point and its associated error bars. Not quite the same as an optical spectrum, eh?

Note that our spectrum is plotted as a function of channel. To change to energy, type `setplot energy`. Now if you replot the data, it should have energy (keV) along the x-axis. Let's switch over to logarithmic scaling. Type `plot ldata` to make the x- and y-axes both logarithmic.

You may notice that some of your data points have exceedingly large error bars. The spectral response of RXTE isn't so great below 2 keV and above 20 keV. To filter out these energies, use

```
XSPEC> ignore 1.-2.,20.-**
```

The decimal points after the numbers indicate that we are entering energy values, not channels, and the ** wildcard tells xspec that we wish to ignore data from 20 keV all the way to the end of the spectrum. Now if you replot your data, it should look much nicer.

B.3.2.4 Modeling Data

Now that we have our spectrum nicely plotted, let's try and fit it with a simple model. `xspec` has a VERY wide range of models for all sorts of X-ray emission, or you can write your own if you are really sadistic. Each of the 100+ models is explained in detail in the `xspec` manual. For now, we are going to use a very simple combination.

Let's assume that our object is a distant AGN. Most AGNs can be modeled with a power law spectrum, plus some kind of absorption. In our case, we will assume that we have 2 different absorption systems - galactic absorption from the Milky Way, and intrinsic absorption at the redshift of the object. To model this, we use the following command:

```
XSPEC> model phabs*zphabs(powerlaw)
```

This tells xspec that we want three different components for the model: `phabs` (photoelectric absorption), `zphabs` (redshifted photoelectric absorption), and `powerlaw` (duh). Also, the `zphabs` component will modify the `powerlaw` component in our model.

`xspec` will first ask for the value for the non-redshifted absorption. This should be set to whatever the $N_{\rm H}$ column density is towards that object. Let's say it's $1.9 \times 10^{20}{\rm cm}^{-2}$.

NOTE: `xspec` takes column densities in units of $10^{22}{\rm cm}^{-2}$. So for our example, we would put in a value of 0.019.

Next, `xspec` asks for the column density of the redshifted absorption. We have

no idea what this is, so just hit enter. Now you are prompted for the redshift of the absorption, so enter the redshift of your object. Now you are prompted for the photon index and normalization of the power law. We don't know these either, so just hit enter for both.

`xspec` will now show you all the parameters for your model, as well as chi-squared information (which at the moment is junk). For our model, we want to fix the value of the galactic column density, as well as the redshift of the absorbing system. So, type `freeze 1` and `freeze 3` to fix those values.

Now we are ready to fit our model to the data. To do this, simply type `fit`. `xspec` will run through a few iterations of fitting, and return with a result. If your model is really bad, `xspec` won't be able to fit properly, and will ask if you want to keep iterating. If this happens, you should probably say no and pick a different model.

The best-fit parameters are now displayed, as well as the chi-squared value for the fit. As always, your reduced chi-squared should be as close to 1 as possible. A reduced chi-squared much less than one indicates that your model is probably too complex, and you should think about removing some components. A reduced chi-squared much greater than one indicates that your model is not a good fit, and you should either add more components or perhaps change the model entirely.

Note the errors given next to each parameter value. These are NOT scientifically calculated errors, they are only estimates. To get an accurate error for a parameter, type `error x`, where `x` is the parameter number. `xspec` will give you the 90% con-

fidence range for that parameter. You can play around with the `error` command to get different types of error values if you want. Note that if your reduced chi-squared is greater than 2, `xspec` won't give you an error value.

To see how well your model fits, simply plot your data again, and the model will be displayed on top of it in the form of a solid line. Let's take a look at the residuals from our model. To do this, type:

```
XSPEC> plot ldata residuals
```

`xspec` will now create a log-log plot, with your data residuals shown in a small panel on the bottom.

Now let's see what the X-ray flux and luminosity are for our object. To do this, we use the flux and lumin commands. The format is:

```
XSPEC> flux 2 10
XSPEC> lumin 2 10 0.05
```

where we want to look at the 2–10 keV energy range, and 0.05 is the redshift of our object. Note that these numbers are based on your model, not your actual data. If your model is crap, then you are certain to get wacky values. Note that the luminosity is computed using H=50 km/s/Mpc and q=0. To change these, use:

```
XSPEC> cosmo H q
```

where `H` is Hubble's constant in km/s/Mpc and `q` is the cosmological deceleration parameter.

B.3.2.5 Shortcuts

As with some other programs, `xspec` allows you to shorten the names of commands as much as you like, as long as they don't conflict with other command names. In the above example, the commands could have been shortened to:

`plot data` $\longrightarrow$ `pl`

`plot ldata` $\longrightarrow$ `pl l`

`model phabs*zphabs(powerlaw)` $\longrightarrow$ `mo ph zph po`

`plot ldata residuals` $\longrightarrow$ `pl l re`

... and so on.

B.4 Miscellaneous

B.4.1 FAQs

B.4.1.1 Which background model is best for my data?

Assuming you are doing AGN analysis, with the counts < 40 per second, you will want to use the faint mode 'L7' model. And now that we have FTOOLS v5.2 installed, we can use the all-epoch files. This file should have the name:

`pca_bkgd_cmfaintl7_eMv20020201.mdl`

and is available from the PCA digest website.

B.4.1.2 Why does Rex say it can't find my ObsIDs?

First, make sure that you are pointing `rex` at your highest level data directory. This is usually the Proposer ID directory. Now make sure that directory has an FMI file in it. If not, copy one there from one of your ObsID directories and use recofmi to reconstruct it. If an FMI file already exists, you might want to try using `recofmi` anyway, just to make sure it has all the information it should.

B.4.1.3 Disk space is running low, what files can I delete?

If you have downloaded the full data products, you can delete the following subdirectories right off the bat: `ace, clock, eds, fds, gsace, ifog, ipsdu, pse, spsdu`. If you are certain that you won't be analyzing any HEXTE data, you can also delete the `hexte` subdirectory.

B.4.1.4 Where should I store all my data?

At present, PEGA doesn't have a standard location for the storage of RXTE data. If it's only one or two observations, you can put the files in your home directory. However, if you will be dealing with a lot of data, it can be stored in `/nfs/sync2/pega_data/xray`. From there, place the data in an appropriate object directory.

B.4.1.5 What's with this PLT> prompt I keep seeing, and how do I get rid of it?

PLT is the plotting routine used by most of the HEASARC programs. It's based on the pgplot routine, and has various commands you can use to make your plots look pretty. See the QDP/PLT page in the Resources section for more info. To get out of PLT, just type `quit`.

B.4.1.6 How can I tell if PCU1 is off for my data?

To examine this, use the `fplot` ftool. Run `fplot` followed by the name of your filter file. Enter `time` as the x-axis. For the y-axis, you can plot any of the following:

`PCU0_ON`

`PCU1_ON (etc.)`

`NUM_PCU_ON`

`ELV`

`OFFSET`

`TIME_SINCE_SAA`

`ELECTRON0`

If you plot `time` vs. `PCU1_ON`, a value of 1 will indicate that PCU1 is on, while 0 will indicate that PCU1 was turned off.

B.4.1.7 Ok, so it's turned off, now what?

Having PCU1 going off and on isn't a huge deal, except your count rates will change (since it is simply the count rate for however many PCUs are on). This can be fixed (see below). However, your readout noise (and thus error bars) will change over time. To exclude PCU1 from the extraction, do the following:

When creating the selection expression (either through `expression.txt` in Rex, or `select mkf` in xselect, or `maketime` if doing it manually), leave out the `PCU1_ON=1` term. This will allow data to be extracted when PCU1 is off.

If you are using Rex, edit the `aux/layer1.cols` file, and remove the lines which say `X1LSpecPcu1` and `X1RSpecPcu1`.

If you are using xselect, when you run the filter detector command, use `filter detector 01* 21*` instead.

If you are extracting your data manually, leave out the lines which end in '...Pcu1' from the `pcu012_layer1.col` file.

B.4.1.8 Is there any way to use PCU1 data anyway, even though it was turned off periodically?

The answer is yes, and now that we have FTOOLS v5.2 installed, it's easier than ever! You can use the tool `correctlc` to normalize the count rate to 1, 3, or however many PCUs you desire. All you need is the name of your light curve and the name of the filter file (see section 2.2.1 for info on how to create that). `correctlc` will also ask for the method used to correct the curve. Enter one to normalize to 1 PCU, full

to normalize to 5 PCUs, or choose user, and then specify which PCUs you want to use. Your new light curve will now be generated.

B.4.2 Resources

HEASARC website: `http://heasarc.gsfc.nasa.gov`

w3Browse: `http://heasarc.gsfc.nasa.gov/db-perl/W3Browse/w3browse.pl`

RXTE GOF: `http://heasarc.gsfc.nasa.gov/docs/xte/rxte.html`

RXTE ABCs: `http://heasarc.gsfc.nasa.gov/docs/xte/abc/contents.html`

RXTE Recipes: `http://heasarc.gsfc.nasa.gov/docs/xte/recipes/cook_book.html`

PCA Digest: `http://heasarc.gsfc.nasa.gov/docs/xte/pca_news.html`

QDP/PLT commands: `http://heasarc.gsfc.nasa.gov/docs/xte/`

`↪recipes/plotting.html`

xspec documentation: `http://heasarc.gsfc.nasa.gov/docs/xanadu/`

`↪xspec/manual/xspec.html`

xronos documentation: `http://heasarc.gsfc.nasa.gov/docs/xanadu/`

`↪xronos/manual/xronos.html`

– C –

X-ray Data

C.1 3C 390.3

Table C.1: 3C 390.3 Long Term X-ray Data

MJD[a]	exptime[b]	flux[c]	slope[d]	slope err[e]	counts[f]	count err[g]
51186.0284	976	2.545e-11	1.489	0.230	2.678	0.062
51189.1376	696	3.037e-11	1.573	0.162	3.015	0.091
51192.2832	1024	2.738e-11	1.986	0.355	2.954	0.064
51195.6700	752	2.662e-11	1.653	0.186	2.577	0.075
51198.6467	920	2.160e-11	2.135	0.461	2.419	0.068
51201.4588	1488	2.269e-11	1.420	0.144	2.285	0.056
51204.3856	1328	1.995e-11	1.874	0.376	2.111	0.056
51207.3574	1120	2.182e-11	1.625	0.243	2.217	0.057
51210.2836	1152	2.025e-11	1.372	0.208	2.085	0.059
51213.2840	1568	1.909e-11	1.931	0.394	1.984	0.040
51216.4938	848	1.671e-11	2.015	0.626	1.949	0.080
51219.4191	800	1.945e-11	1.531	0.276	2.010	0.071
51222.1574	1168	1.700e-11	1.599	0.191	1.669	0.062
51225.4199	1112	1.671e-11	1.358	0.224	1.703	0.059
51228.3390	704	1.506e-11	2.199	0.717	1.678	0.078
51231.2681	944	1.282e-11	1.734	0.637	1.523	0.070
51234.7359	480	1.722e-11	1.812	0.547	1.878	0.094
51237.7087	1016	2.093e-11	1.436	0.183	2.068	0.055
51240.5922	480	1.926e-11	1.706	0.337	1.885	0.088
51243.8613	1400	1.521e-11	1.918	0.518	1.705	0.047
51246.3242	976	1.446e-11	1.512	0.304	1.477	0.056
51249.3753	832	1.235e-11	1.219	0.281	1.390	0.082
51252.4145	504	1.151e-11	1.647	0.770	1.287	0.081
51255.2718	72	9.642e-12	1.250	1.606	1.081	0.154
51258.4093	656	1.510e-11	1.669	0.348	1.498	0.077
51261.7338	488	1.490e-11	1.008	0.633	1.700	0.094

Continued on Next Page...

Table C.1 – Continued

MJD[a]	**exptime**[b]	**flux**[c]	**slope**[d]	**slope err**[e]	**counts**[f]	**count err**[g]
51264.2855	1248	1.360e-11	2.191	0.626	1.483	0.058
51267.1401	1440	1.708e-11	1.753	0.337	1.797	0.051
51270.3263	936	1.656e-11	1.515	0.363	1.841	0.075
51273.4589	272	1.367e-11	3.174	1.408	1.673	0.140
51276.0426	856	1.886e-11	1.718	0.279	1.870	0.077
51279.4539	1056	1.309e-11	2.265	0.700	1.539	0.062
51282.2483	1248	1.231e-11	1.844	0.598	1.449	0.053
51285.0328	1168	1.363e-11	1.719	0.535	1.612	0.056
51290.7553	1248	1.585e-11	1.506	0.205	1.639	0.060
51291.0387	928	1.667e-11	1.478	0.231	1.692	0.075
51294.0327	784	1.776e-11	1.825	0.296	1.740	0.081
51297.3513	528	1.287e-11	1.034	0.307	1.485	0.094
51301.4793	1456	1.372e-11	1.797	0.452	1.549	0.053
51304.4568	520	1.619e-11	1.378	0.218	1.695	0.082
51306.1822	680	1.598e-11	1.651	0.266	1.606	0.061
51306.2488	680	1.503e-11	1.574	0.298	1.532	0.073
51309.0397	928	1.532e-11	1.734	0.477	1.734	0.064
51312.0493	1520	1.723e-11	2.058	0.459	1.972	0.053
51315.6172	744	2.058e-11	1.477	0.225	2.088	0.062
51318.9476	1136	2.528e-11	1.485	0.083	2.630	0.063
51321.4319	376	2.931e-11	1.884	0.282	2.735	0.089
51324.0150	632	2.599e-11	1.812	0.403	2.658	0.090
51327.2167	600	2.474e-11	1.965	0.503	2.873	0.094
51329.9415	1208	2.976e-11	1.679	0.127	2.943	0.071
51333.5224	1312	3.166e-11	1.632	0.111	3.120	0.064
51336.4699	768	2.495e-11	1.897	0.456	2.841	0.086
51339.9380	1008	2.633e-11	1.631	0.180	2.550	0.067
51342.7353	1008	2.294e-11	1.580	0.203	2.381	0.073
51346.2301	1048	2.126e-11	1.848	0.306	2.133	0.061
51348.4305	1032	2.493e-11	1.656	0.162	2.397	0.069
51351.3014	1616	2.623e-11	1.834	0.289	2.838	0.052
51354.5781	864	2.929e-11	1.968	0.368	3.143	0.078
51357.2777	336	2.752e-11	1.520	0.297	2.976	0.119
51360.9928	168	2.544e-11	1.851	0.358	2.645	0.193
51363.9231	1288	2.506e-11	1.901	0.347	2.728	0.060
51366.1978	272	3.054e-11	1.677	0.510	3.299	0.105
51369.8381	976	2.630e-11	1.951	0.380	2.793	0.068
51372.3826	1696	2.993e-11	1.620	0.121	2.981	0.050

Continued on Next Page...

Table C.1 – Continued

MJD[a]	**exptime**[b]	**flux**[c]	**slope**[d]	**slope err**[e]	**counts**[f]	**count err**[g]
51375.2526	992	3.337e-11	1.779	0.262	3.408	0.059
51378.0367	624	3.523e-11	1.658	0.225	3.490	0.074
51381.1658	1112	3.873e-11	1.706	0.107	3.864	0.070
51384.9580	656	3.922e-11	1.940	0.294	4.092	0.093
51387.9544	680	3.514e-11	1.965	0.357	3.828	0.076
51390.4879	864	3.810e-11	1.714	0.153	3.669	0.079
51393.6677	896	3.610e-11	1.539	0.101	3.605	0.083
51396.3374	1296	3.506e-11	1.727	0.096	3.474	0.060
51399.8448	1136	3.375e-11	1.935	0.295	3.662	0.077
51402.2603	1296	3.895e-11	1.923	0.249	4.185	0.077
51405.1133	1456	3.829e-11	1.851	0.236	4.092	0.054
51408.1626	568	3.371e-11	2.010	0.401	3.749	0.106
51411.1150	1152	3.992e-11	1.679	0.129	3.932	0.057
51414.8024	192	3.342e-11	1.897	0.569	3.591	0.210
51417.0142	1328	4.020e-11	1.798	0.225	4.147	0.058
51420.1407	768	3.697e-11	1.753	0.302	3.909	0.079
51423.3451	1312	4.122e-11	1.672	0.141	4.186	0.064
51425.7371	1216	4.122e-11	1.820	0.207	4.253	0.074
51429.6593	1280	3.533e-11	1.945	0.243	3.608	0.064
51432.6536	944	2.957e-11	1.961	0.369	3.230	0.065
51435.7738	1064	3.282e-11	1.567	0.143	3.270	0.069
51438.9055	1056	3.324e-11	1.761	0.240	3.435	0.070
51443.1595	912	3.704e-11	1.584	0.095	3.758	0.072
51447.2164	1392	3.425e-11	1.750	0.192	3.526	0.063
51450.2802	1296	3.047e-11	1.856	0.299	3.314	0.055
51453.1920	1264	3.587e-11	1.850	0.142	3.802	0.059
51456.0606	1264	4.391e-11	1.732	0.150	4.366	0.064
51459.1073	296	4.166e-11	1.530	0.183	4.256	0.144
51462.0320	312	4.000e-11	1.733	0.233	3.860	0.134
51465.6867	736	2.779e-11	1.832	0.369	3.058	0.072
51465.7534	736	2.684e-11	1.903	0.375	2.822	0.080
51468.6002	1056	2.511e-11	1.789	0.348	2.702	0.070
51471.5507	1760	2.996e-11	1.710	0.225	3.096	0.046
51474.5443	1024	3.471e-11	1.551	0.137	3.598	0.075
51477.6727	1280	3.688e-11	1.720	0.236	3.839	0.058
51480.8678	592	3.416e-11	1.890	0.250	3.478	0.074
51483.4521	1648	3.988e-11	1.676	0.080	3.873	0.050
51485.7209	864	4.001e-11	2.041	0.297	4.157	0.065

Continued on Next Page...

Table C.1 – Continued

MJD[a]	**exptime**[b]	**flux**[c]	**slope**[d]	**slope err**[e]	**counts**[f]	**count err**[g]
51489.4404	976	3.986e-11	1.827	0.186	3.995	0.060
51492.3707	976	4.359e-11	1.616	0.103	4.267	0.077
51495.9526	752	4.465e-11	1.762	0.161	4.355	0.074
51499.6084	1312	4.168e-11	1.830	0.151	4.084	0.059
51501.9382	944	4.177e-11	1.764	0.128	3.993	0.073
51504.6021	1248	4.466e-11	1.762	0.096	4.236	0.068
51507.1278	1456	4.188e-11	2.087	0.239	4.447	0.058
51510.5200	1344	4.708e-11	2.139	0.225	4.868	0.068
51513.6152	608	5.180e-11	1.870	0.125	4.852	0.096
51516.4717	440	4.695e-11	1.663	0.134	4.640	0.084
51519.8854	1000	4.748e-11	2.024	0.248	4.852	0.084
51522.4466	120	4.407e-11	2.054	0.380	4.317	0.198
51525.4623	1440	4.774e-11	1.764	0.085	4.675	0.059
51527.6008	896	4.482e-11	1.979	0.282	4.644	0.080
51531.9205	336	4.511e-11	1.526	0.189	4.423	0.123
51534.5625	1000	4.657e-11	1.703	0.097	4.617	0.083
51537.5608	1264	4.525e-11	1.899	0.241	4.669	0.069
51540.6883	1024	4.210e-11	1.805	0.256	4.398	0.083
51543.4812	864	3.777e-11	1.935	0.312	4.182	0.086
51546.3332	1136	4.116e-11	1.597	0.100	4.087	0.072
51552.4943	984	3.142e-11	2.133	0.339	3.489	0.071
51555.0502	624	3.305e-11	1.812	0.302	3.454	0.103
51561.6213	496	3.268e-11	1.650	0.216	3.228	0.082
51564.8882	1168	3.307e-11	1.549	0.155	3.332	0.064
51570.4331	48	4.175e-11	1.674	0.563	4.194	0.477
51573.6556	1744	4.290e-11	1.699	0.140	4.274	0.059
51576.6994	888	3.752e-11	1.797	0.290	3.960	0.076
51579.2943	896	4.017e-11	1.859	0.282	4.308	0.070
51582.4741	760	4.021e-11	1.639	0.171	3.956	0.081
51585.4809	400	3.715e-11	1.626	0.185	3.488	0.096
51588.2681	864	3.248e-11	1.764	0.258	3.411	0.075
51591.4558	1136	2.929e-11	1.723	0.324	3.244	0.057
51594.3038	1256	3.237e-11	1.858	0.195	3.149	0.072
51597.2310	968	2.932e-11	1.999	0.396	3.185	0.069
51600.1645	976	3.777e-11	1.637	0.141	3.653	0.079
51603.2819	1328	3.899e-11	1.607	0.110	3.788	0.068
51606.1991	400	3.730e-11	1.908	1.908	3.971	0.136
51609.5255	992	5.057e-11	1.862	0.238	5.340	0.074

Continued on Next Page...

Table C.1 – Continued

MJD[a]	exptime[b]	flux[c]	slope[d]	slope err[e]	counts[f]	count err[g]
51612.5825	1536	6.428e-11	1.817	0.085	6.244	0.060
51615.5544	1288	5.915e-11	1.729	0.080	5.655	0.069
51618.3404	584	5.937e-11	1.731	0.136	5.771	0.120
51618.4066	552	5.244e-11	1.981	0.294	5.675	0.116
51621.4679	1352	5.600e-11	1.829	0.158	5.569	0.063
51624.7512	1088	5.195e-11	1.850	0.214	5.454	0.073
51627.2343	312	4.764e-11	1.892	0.376	5.166	0.154
51627.3008	336	4.458e-11	2.039	0.427	4.998	0.141
51630.7661	1312	5.045e-11	1.788	0.109	4.815	0.093
51633.5148	1520	4.689e-11	1.901	0.203	4.806	0.063
51636.5260	144	4.423e-11	1.966	0.426	4.659	0.178
51639.2897	400	4.136e-11	1.824	0.266	4.214	0.130
51642.8676	1728	4.114e-11	1.630	0.066	4.062	0.053
51645.8495	1936	4.704e-11	1.683	0.090	4.720	0.048
51648.2440	1040	4.505e-11	1.736	0.153	4.524	0.067
51651.8320	1808	4.243e-11	1.830	0.203	4.396	0.054
51654.4252	1360	4.136e-11	1.663	0.130	4.133	0.059
51657.2772	1672	4.477e-11	1.747	0.111	4.456	0.056
51660.8686	1296	4.008e-11	1.790	0.239	4.234	0.060
51663.5846	1904	3.657e-11	1.845	0.215	4.008	0.056
51666.4909	1568	3.722e-11	1.805	0.207	3.866	0.055
51669.4814	1392	3.674e-11	1.614	0.115	3.581	0.063
51672.5375	480	3.808e-11	1.618	0.232	4.144	0.117
51675.5285	888	4.111e-11	1.801	0.185	4.103	0.081
51684.5041	1024	3.087e-11	1.801	0.329	3.639	0.081
51687.4884	960	3.352e-11	1.884	0.307	3.857	0.088
51690.1426	992	3.385e-11	1.762	0.323	3.994	0.100
51693.8337	1368	4.237e-11	1.648	0.090	4.591	0.067
51696.5531	1424	3.688e-11	1.737	0.237	4.234	0.086
51699.6311	720	3.704e-11	1.874	0.264	4.224	0.110
51702.7367	1552	3.709e-11	1.825	0.247	4.314	0.074
51705.6078	1200	3.849e-11	1.592	0.120	4.263	0.104
51708.0649	1072	3.823e-11	1.560	0.125	4.166	0.079
51711.7724	1640	3.590e-11	1.817	0.202	4.009	0.068
51714.3678	976	3.473e-11	1.885	0.277	4.002	0.085
51717.5430	1496	4.205e-11	1.550	0.091	4.713	0.076
51720.5450	1488	3.716e-11	1.657	0.177	4.155	0.071
51723.4584	1640	3.236e-11	1.802	0.244	3.646	0.063

Continued on Next Page...

Table C.1 – Continued

MJD[a]	**exptime**[b]	**flux**[c]	**slope**[d]	**slope err**[e]	**counts**[f]	**count err**[g]
51726.0939	1056	3.129e-11	1.908	0.338	3.675	0.080
51729.0255	1792	4.167e-11	1.653	0.103	4.549	0.074
51732.0152	1536	3.802e-11	1.874	0.233	4.212	0.066
51735.7743	1080	4.187e-11	1.628	0.149	4.648	0.085
51738.2527	1224	4.340e-11	1.884	0.244	5.051	0.080
51744.6935	1168	4.617e-11	1.642	0.108	5.054	0.089
51747.7294	1472	4.382e-11	1.885	0.218	5.031	0.075
51750.7307	1440	4.684e-11	1.705	0.133	5.119	0.075
51753.7170	1504	4.641e-11	1.672	0.086	4.980	0.072
51756.8979	720	4.415e-11	1.813	0.229	4.870	0.096
51759.5538	1752	4.255e-11	1.576	0.103	4.656	0.061
51762.4110	1296	3.415e-11	1.944	0.292	4.009	0.083
51765.4635	1776	3.606e-11	1.743	0.177	4.001	0.066
51768.5166	1776	3.929e-11	1.603	0.088	4.288	0.058
51771.3548	1288	4.332e-11	1.961	0.245	5.120	0.082
51774.9484	944	4.251e-11	1.628	0.129	4.684	0.098
51777.0695	1648	4.146e-11	1.696	0.085	4.394	0.072
51780.1815	840	2.987e-11	1.822	0.411	3.653	0.087
51783.9696	2096	2.828e-11	1.628	0.178	3.184	0.064
51786.2894	760	3.327e-11	1.480	0.119	3.734	0.096
51788.9332	1016	3.055e-11	1.558	0.206	3.414	0.088
51792.2553	1848	2.648e-11	1.644	0.210	2.894	0.066
51801.5288	1512	3.106e-11	1.549	0.160	3.447	0.067
51804.2668	1088	3.066e-11	1.613	0.245	3.616	0.113
51807.5062	1520	2.666e-11	1.739	0.308	3.101	0.074
51810.2390	976	2.883e-11	1.776	0.341	3.335	0.091
51813.5562	1408	3.420e-11	1.751	0.221	3.835	0.071
51816.5400	1728	3.202e-11	1.656	0.251	3.792	0.069
51819.4601	1616	3.582e-11	1.617	0.082	3.938	0.073
51822.1073	1904	3.634e-11	1.910	0.226	4.295	0.065
51825.8173	1208	4.047e-11	1.593	0.117	4.535	0.095
51828.7202	720	3.921e-11	1.607	0.155	4.306	0.110
51828.7863	680	3.682e-11	1.876	0.347	4.351	0.101
51831.7699	752	3.752e-11	1.673	0.198	4.195	0.087
51834.7684	1904	3.879e-11	1.634	0.139	4.297	0.065
51837.8368	2000	3.836e-11	1.613	0.157	4.342	0.063
51840.5371	1696	4.551e-11	1.603	0.092	4.961	0.072
51843.7958	1168	5.058e-11	1.721	0.084	5.587	0.085

Continued on Next Page...

Table C.1 – Continued

MJD[a]	**exptime**[b]	**flux**[c]	**slope**[d]	**slope err**[e]	**counts**[f]	**count err**[g]
51846.7013	1528	4.687e-11	1.870	0.217	5.327	0.080
51849.4963	864	3.978e-11	1.857	0.266	4.476	0.091
51849.5652	416	4.238e-11	1.813	0.270	4.414	0.128
51852.4760	1488	4.183e-11	1.653	0.114	4.606	0.067
51855.4468	1632	4.266e-11	1.746	0.174	4.801	0.073
51858.5006	1336	4.278e-11	1.891	0.243	4.943	0.071
51861.5587	1792	4.777e-11	1.616	0.076	5.232	0.067
51864.4709	1192	4.817e-11	1.596	0.080	5.402	0.080
51867.3965	1424	5.578e-11	1.858	0.183	6.353	0.074
51870.1125	1936	6.365e-11	1.798	0.116	6.786	0.065
51873.3033	1472	5.977e-11	1.701	0.090	6.472	0.074
51876.2817	1536	5.362e-11	1.818	0.183	6.182	0.075
51879.8389	1448	5.064e-11	1.640	0.099	5.482	0.067
51882.7536	1304	4.875e-11	1.539	0.025	5.333	0.072
51885.6127	1968	5.287e-11	1.705	0.061	5.594	0.069
51888.5826	1448	4.710e-11	1.741	0.159	5.150	0.068
51891.7923	1184	4.567e-11	1.717	0.145	5.118	0.076
51900.5198	1288	3.766e-11	1.528	0.075	4.106	0.075
51903.2956	1608	3.448e-11	1.673	0.211	3.940	0.068
51906.2077	1200	3.790e-11	1.864	0.244	4.313	0.079
51909.1243	1568	3.915e-11	1.820	0.193	4.364	0.066
51912.3862	1296	3.443e-11	1.785	0.270	4.012	0.081
51915.5055	1984	3.767e-11	1.807	0.210	4.413	0.060
51918.1457	1176	4.015e-11	1.805	0.177	4.392	0.085
51921.9861	1232	3.541e-11	1.625	0.134	3.876	0.090
51924.1128	1256	3.668e-11	1.670	0.145	4.011	0.075
51926.8277	968	3.967e-11	1.717	0.187	4.465	0.097
51930.2667	1440	3.662e-11	1.774	0.135	4.190	0.072
51933.5719	176	3.000e-11	1.019	0.168	3.663	0.191
51933.6380	144	3.382e-11	1.837	0.412	3.515	0.210
51936.4890	704	3.114e-11	1.730	0.242	3.309	0.093
51939.6771	536	2.781e-11	1.473	0.256	3.004	0.110
51939.7436	408	2.508e-11	1.503	0.396	2.959	0.118
51942.5239	1232	2.958e-11	1.663	0.215	3.292	0.075
51945.5079	1304	3.062e-11	1.578	0.163	3.371	0.072
51948.6402	560	3.019e-11	1.994	0.451	3.765	0.122
51951.5510	896	3.363e-11	1.694	0.226	3.841	0.089
51954.2468	1400	3.199e-11	1.613	0.140	3.473	0.068

Continued on Next Page...

Table C.1 – Continued

MJD[a]	**exptime**[b]	**flux**[c]	**slope**[d]	**slope err**[e]	**counts**[f]	**count err**[g]
51957.4452	1360	2.699e-11	1.734	0.200	3.069	0.060
51960.2178	1448	2.607e-11	1.716	0.297	3.108	0.075
51964.0003	1664	2.560e-11	1.710	0.199	2.892	0.054

[a] Modified Julian Date
[b] Exposure time (s)
[c] erg/s/cm^2
[d] Spectral photon index
[e] Error for spectral photon index
[f] Counts/sec/PCU
[g] Count rate error

Table C.2: 3C 390.3 Intermediate Sampling X-ray Data

MJD[a]	**exptime**[b]	**flux**[c]	**slope**[d]	**slope err**[e]	**counts**[f]	**count err**[g]
50220.6293	2144	2.334e-11	1.862	0.195	4.669	0.032
50221.6292	1888	2.096e-11	1.827	0.230	4.336	0.039
50222.3462	2752	2.072e-11	1.801	0.177	4.200	0.031
50223.4915	2168	1.834e-11	1.897	0.241	3.864	0.033
50224.5603	2128	1.906e-11	1.597	0.078	3.830	0.034
50226.8344	2144	1.807e-11	1.685	0.206	3.596	0.036
50227.5602	1776	1.630e-11	1.827	0.289	3.463	0.038
50228.8058	2448	1.682e-11	1.629	0.096	3.293	0.038
50229.6260	2608	1.716e-11	1.744	0.188	3.398	0.031
50230.6879	2512	1.483e-11	1.950	0.281	3.162	0.032
50231.8976	2080	1.665e-11	1.904	0.198	3.335	0.032
50232.8315	2320	1.530e-11	1.930	0.293	3.244	0.033
50233.8299	2232	1.668e-11	1.741	0.210	3.437	0.035
50234.7645	2464	1.645e-11	2.204	0.271	3.527	0.034
50235.6966	2560	1.754e-11	1.718	0.118	3.440	0.030
50236.4883	2704	1.566e-11	1.920	0.252	3.289	0.029
50237.4622	2320	1.434e-11	1.710	0.293	3.011	0.034
50238.2859	1648	1.378e-11	1.438	0.116	2.770	0.034
50239.4086	2784	1.238e-11	1.772	0.283	2.608	0.029
50240.8207	1920	1.147e-11	1.942	0.378	2.522	0.032
50241.6946	2432	1.165e-11	1.789	0.271	2.375	0.030
50242.8184	2952	1.187e-11	1.676	0.167	2.316	0.026
50243.5488	2896	1.043e-11	1.750	0.343	2.183	0.028
50244.5402	1200	1.033e-11	1.680	0.414	2.161	0.040
50244.6087	1368	9.772e-12	1.758	0.410	2.144	0.038
50245.5476	1352	9.328e-12	2.032	0.579	2.101	0.036
50246.6887	1576	1.126e-11	1.593	0.294	2.316	0.036
50249.0784	944	1.130e-11	1.770	0.411	2.287	0.054
50249.1400	1392	1.025e-11	1.624	0.387	2.196	0.039
50249.9605	1264	1.036e-11	1.701	0.320	2.063	0.045
50250.0714	1664	9.930e-12	2.289	0.476	2.188	0.035
50251.0099	2544	1.076e-11	1.528	0.119	2.161	0.028
50251.8805	1696	9.620e-12	1.639	0.349	2.010	0.031
50251.9381	1424	9.831e-12	1.555	0.199	2.072	0.037
50252.9356	1712	9.886e-12	1.750	0.303	2.029	0.033
50253.0058	1120	9.694e-12	1.675	0.443	2.126	0.032

Continued on Next Page...

Table C.2 – Continued

MJD[a]	**exptime**[b]	**flux**[c]	**slope**[d]	**slope err**[e]	**counts**[f]	**count err**[g]
50253.9405	768	8.201e-12	2.104	0.791	1.894	0.045
50254.0009	1840	9.636e-12	1.613	0.359	2.082	0.035
50254.8714	1056	9.590e-12	1.966	0.560	2.065	0.043
50254.9311	2256	9.994e-12	1.747	0.336	2.070	0.030
50256.1387	2816	8.689e-12	2.040	0.416	1.944	0.026
50257.0671	3088	9.330e-12	1.861	0.302	1.962	0.025
50258.0680	3136	8.914e-12	1.738	0.326	1.867	0.027
50258.9999	3120	9.685e-12	1.611	0.184	1.948	0.026
50259.9999	3168	9.016e-12	1.625	0.349	1.933	0.027
50260.9978	3200	8.991e-12	1.816	0.296	1.866	0.026
50261.8549	3152	9.655e-12	1.673	0.268	1.998	0.025
50261.9928	1888	9.931e-12	1.738	0.309	2.052	0.032
50267.9264	2352	1.090e-11	1.808	0.292	2.282	0.027
50263.4436	1880	8.874e-12	1.707	0.358	1.887	0.033
50265.0045	2368	9.591e-12	1.792	0.395	2.074	0.030
50265.7859	3056	1.025e-11	1.546	0.141	2.047	0.025
50266.8594	2992	1.029e-11	1.661	0.328	2.127	0.025
50269.2519	1616	1.085e-11	1.282	0.237	2.217	0.072
50271.5970	1680	1.228e-11	1.441	0.153	2.438	0.042
50273.5958	2400	1.202e-11	1.684	0.265	2.484	0.030
50275.5283	2224	1.265e-11	1.523	0.157	2.537	0.028
50276.9327	1792	1.272e-11	1.712	0.301	2.646	0.032

[a] Modified Julian Date
[b] Exposure time (s)
[c] erg/s/cm^2
[d] Spectral photon index
[e] Error for spectral photon index
[f] Counts/sec/PCU
[g] Count rate error

C.2 Akn 120

Table C.3: Akn 120 Long Term X-ray Data

MJD[a]	exptime[b]	flux[c]	slope[d]	slope err[e]	counts[f]	count err[g]
50868.0902	928	4.118e-11	1.994	0.279	4.223	0.068
50871.2233	896	4.982e-11	2.084	0.252	5.091	0.081
50874.4351	904	4.184e-11	2.140	0.273	4.399	0.085
50877.1507	832	4.587e-11	2.161	0.284	4.583	0.095
50880.4264	344	4.417e-11	1.913	0.321	4.464	0.090
50883.1538	1032	5.568e-11	2.077	0.219	5.596	0.082
50886.1803	704	4.544e-11	1.996	0.299	4.728	0.081
50889.1806	800	3.603e-11	2.579	0.373	3.822	0.076
50892.2458	880	4.763e-11	1.864	0.142	4.633	0.084
50898.0222	608	3.796e-11	1.819	0.177	3.581	0.081
50901.1784	1024	3.417e-11	2.126	0.315	3.729	0.073
50904.2472	1664	4.423e-11	1.921	0.131	4.220	0.058
50907.2355	824	3.159e-11	2.250	0.386	3.440	0.070
50910.0953	920	4.735e-11	2.029	0.142	4.242	0.079
50913.2339	1096	2.766e-11	2.111	0.325	2.780	0.064
50916.2482	1280	2.901e-11	1.860	0.286	2.974	0.060
50919.0438	880	3.433e-11	1.875	0.163	3.242	0.079
50922.0969	1000	3.028e-11	1.773	0.191	3.012	0.072
50925.0338	744	3.682e-11	1.772	0.127	3.538	0.077
50928.0308	792	3.623e-11	1.996	0.308	3.739	0.056
50931.2318	744	2.949e-11	2.426	0.433	3.210	0.084
51026.2067	896	3.023e-11	1.682	0.199	2.908	0.060
51029.3419	440	2.470e-11	2.285	0.595	2.635	0.103
51032.2008	344	2.533e-11	2.016	0.471	2.608	0.104
51035.3446	608	2.915e-11	1.766	0.206	2.843	0.099
51038.4096	136	2.293e-11	1.223	0.428	2.706	0.146
51041.2004	112	3.241e-11	2.388	0.694	3.446	0.251
51044.2700	224	2.829e-11	1.792	0.320	2.751	0.146
51047.2088	768	3.366e-11	2.183	0.374	3.461	0.086
51050.1980	216	3.490e-11	1.770	0.266	3.337	0.175
51053.2025	888	3.449e-11	2.159	0.329	3.736	0.071
51056.1870	1048	2.375e-11	1.927	0.366	2.530	0.061
51062.0597	856	3.030e-11	2.111	0.377	3.227	0.083
51065.3891	752	4.140e-11	2.180	0.309	4.354	0.078

Continued on Next Page...

Table C.3 – Continued

MJD[a]	**exptime**[b]	**flux**[c]	**slope**[d]	**slope err**[e]	**counts**[f]	**count err**[g]
51068.2100	768	3.356e-11	2.199	0.380	3.473	0.100
51071.1817	704	3.708e-11	2.142	0.327	3.729	0.068
51074.1800	416	3.938e-11	1.890	0.152	3.770	0.090
51077.0771	688	3.218e-11	1.792	0.174	3.033	0.078
51080.2102	152	2.794e-11	1.743	0.450	2.638	0.199
51086.2114	576	2.939e-11	2.184	0.449	2.996	0.093
51092.4090	864	2.935e-11	1.913	0.350	3.031	0.070
51095.4029	944	2.909e-11	2.209	0.335	2.799	0.065
51098.3153	896	2.212e-11	1.989	0.449	2.341	0.080
51100.9968	304	3.179e-11	2.139	0.582	3.557	0.128
51107.3995	920	3.074e-11	1.824	0.195	2.954	0.069
51110.1841	624	3.014e-11	2.269	0.484	3.204	0.075
51113.3847	576	2.224e-11	2.402	0.572	2.443	0.084
51116.3882	880	2.936e-11	1.807	0.153	2.762	0.069
51119.3892	864	2.178e-11	2.167	0.487	2.354	0.067
51122.3901	720	2.625e-11	1.693	0.294	2.640	0.095
51125.3892	864	3.978e-11	1.901	0.198	3.824	0.055
51128.3891	848	3.186e-11	2.114	0.357	3.244	0.068
51131.3880	848	3.740e-11	1.802	0.201	3.703	0.080
51134.3887	800	3.654e-11	1.944	0.324	3.861	0.078
51137.3834	824	3.682e-11	1.895	0.107	3.417	0.073
51140.3888	856	3.075e-11	2.196	0.378	3.124	0.065
51143.6005	96	2.767e-11	2.300	1.029	3.376	0.178
51149.4008	784	3.673e-11	2.196	0.346	3.820	0.071
51152.4008	656	4.445e-11	2.062	0.296	4.510	0.095
51155.3114	1152	3.680e-11	2.161	0.285	3.689	0.067
51158.3933	880	3.433e-11	2.270	0.346	3.646	0.065
51161.2394	872	4.350e-11	1.985	0.261	4.354	0.076
51167.3695	824	3.347e-11	2.390	0.368	3.510	0.085
51170.4441	888	3.412e-11	2.037	0.274	3.420	0.069
51173.3864	880	4.294e-11	2.277	0.285	4.584	0.093
51176.3844	1088	3.647e-11	2.513	0.293	4.013	0.071
51179.3831	1168	4.203e-11	2.058	0.245	4.141	0.068
51182.3126	880	3.429e-11	2.115	0.337	3.745	0.075
51185.2407	944	3.451e-11	2.032	0.252	3.344	0.073
51188.1691	832	2.933e-11	1.946	0.289	2.830	0.064
51191.2947	800	3.154e-11	1.951	0.315	3.222	0.079
51194.1917	80	3.392e-11	2.702	0.834	3.780	0.179

Continued on Next Page...

Table C.3 – Continued

MJD[a]	exptime[b]	flux[c]	slope[d]	slope err[e]	counts[f]	count err[g]
51197.3900	288	3.117e-11	1.670	0.359	3.228	0.142
51200.1679	872	3.612e-11	2.049	0.287	3.639	0.082
51203.3876	768	3.995e-11	1.886	0.260	3.885	0.087
51206.3162	640	3.731e-11	1.999	0.247	3.561	0.092
51209.3150	864	3.295e-11	1.993	0.269	3.336	0.070
51212.2389	928	3.757e-11	2.025	0.294	3.730	0.066
51215.4184	784	4.216e-11	2.049	0.269	4.158	0.085
51218.3619	928	4.482e-11	2.129	0.270	4.730	0.074
51221.3749	912	4.147e-11	1.854	0.258	4.213	0.070
51224.2283	1520	3.291e-11	1.943	0.263	3.424	0.056
51227.2791	856	3.597e-11	2.169	0.331	3.910	0.078
51230.3706	1368	3.780e-11	2.109	0.251	3.825	0.069
51233.2268	888	3.811e-11	1.883	0.208	3.674	0.080
51236.2192	888	3.711e-11	1.876	0.234	3.739	0.081
51239.2241	888	3.111e-11	2.079	0.354	3.163	0.087
51242.2989	384	3.091e-11	1.727	0.203	2.949	0.091
51245.4079	808	2.467e-11	2.096	0.462	2.783	0.083
51248.3358	888	3.191e-11	1.873	0.234	3.118	0.079
51251.3377	216	2.872e-11	2.238	0.572	3.070	0.084
51254.2906	128	3.131e-11	1.793	0.450	3.048	0.229
51257.2874	432	3.644e-11	1.944	0.196	3.307	0.080
51260.2184	624	3.498e-11	2.074	0.285	3.467	0.092
51263.1953	936	3.878e-11	1.978	0.295	4.009	0.084
51266.4851	736	4.304e-11	2.177	0.322	4.617	0.084
51269.2586	1272	3.877e-11	2.050	0.251	3.867	0.068
51272.3219	656	4.482e-11	1.899	0.153	4.186	0.093
51275.3328	936	3.787e-11	1.973	0.268	3.901	0.094
51278.3182	936	4.102e-11	2.260	0.286	4.490	0.076
51425.0716	944	3.606e-11	2.280	0.308	3.960	0.065
51428.0569	376	5.563e-11	1.948	0.135	5.185	0.107
51430.9990	256	4.447e-11	2.225	0.467	4.806	0.113
51431.0059	736	4.622e-11	2.089	0.293	4.949	0.074
51434.0621	904	4.223e-11	2.126	0.286	4.459	0.089
51437.2645	720	4.699e-11	1.946	0.200	4.728	0.086
51443.1245	608	4.977e-11	2.036	0.282	5.110	0.091
51446.0538	720	4.613e-11	2.021	0.263	4.705	0.094
51449.1138	368	4.741e-11	1.862	0.199	4.469	0.120
51452.0459	704	3.398e-11	1.622	0.114	3.451	0.074

Continued on Next Page...

Table C.3 – Continued

MJD[a]	**exptime**[b]	**flux**[c]	**slope**[d]	**slope err**[e]	**counts**[f]	**count err**[g]
51455.0436	656	4.190e-11	2.152	0.331	4.432	0.097
51458.0395	672	3.328e-11	2.153	0.400	3.563	0.087
51461.0246	200	4.199e-11	1.870	0.318	4.014	0.186
51464.0336	816	3.394e-11	2.066	0.365	3.586	0.068
51467.0173	176	3.010e-11	1.533	0.391	3.107	0.176
51470.0189	928	3.849e-11	2.038	0.303	4.025	0.089
51476.0149	720	3.386e-11	2.158	0.375	3.559	0.073
51479.2568	872	2.159e-11	1.905	0.474	2.499	0.077
51482.1810	424	2.383e-11	1.760	0.337	2.421	0.097
51485.0501	824	2.787e-11	2.127	0.411	3.016	0.070
51488.6629	752	2.567e-11	1.913	0.184	2.502	0.086
51491.5170	864	2.294e-11	1.832	0.428	2.552	0.066
51494.0581	224	2.693e-11	2.118	0.494	2.592	0.135
51497.0522	352	2.099e-11	1.736	0.371	2.095	0.119
51500.6443	784	1.606e-11	1.653	0.393	1.668	0.067
51503.0441	224	1.776e-11	2.651	1.047	2.163	0.137
51506.0392	240	2.223e-11	2.278	0.811	2.576	0.149
51509.1017	336	2.389e-11	1.567	0.285	2.358	0.130
51512.0281	688	2.188e-11	1.832	0.435	2.294	0.079
51515.0877	312	2.942e-11	1.956	0.294	2.815	0.098
51518.0169	464	2.151e-11	1.508	0.277	2.095	0.096
51521.2064	816	2.845e-11	2.075	0.402	3.282	0.071
51524.0709	832	3.293e-11	2.009	0.309	3.383	0.079
51527.0670	656	2.882e-11	2.167	0.423	3.298	0.083
51530.2346	984	2.379e-11	2.612	0.426	2.782	0.074
51533.3077	1008	2.461e-11	1.764	0.211	2.427	0.067
51536.7098	824	2.721e-11	1.801	0.162	2.697	0.088
51539.0229	1072	2.346e-11	1.720	0.193	2.322	0.070
51542.1495	752	2.434e-11	1.662	0.158	2.333	0.081
51545.2155	736	2.695e-11	1.760	0.217	2.630	0.076
51547.9650	64	2.681e-11	1.503	0.696	2.775	0.195
51550.8895	256	3.044e-11	2.043	0.610	3.399	0.097
51554.1978	816	2.449e-11	2.023	0.286	2.456	0.077
51557.2573	1128	2.733e-11	1.823	0.262	2.814	0.054
51560.0444	800	2.693e-11	1.954	0.415	2.887	0.076
51566.2363	1528	3.113e-11	1.884	0.189	3.165	0.046
51569.0481	936	3.430e-11	2.112	0.334	3.669	0.080
51572.1144	640	2.768e-11	2.036	0.431	2.937	0.075

Continued on Next Page...

Table C.3 – Continued

MJD[a]	**exptime**[b]	**flux**[c]	**slope**[d]	**slope err**[e]	**counts**[f]	**count err**[g]
51575.2415	640	2.639e-11	1.997	0.359	2.795	0.075
51578.2070	712	2.808e-11	1.917	0.409	3.020	0.078
51581.0296	752	3.340e-11	2.313	0.383	3.614	0.076
51584.2121	752	4.221e-11	2.068	0.321	4.457	0.104
51586.9482	256	3.337e-11	2.417	0.649	3.731	0.165
51590.1281	736	3.143e-11	1.907	0.354	3.342	0.076
51596.3030	800	3.226e-11	1.708	0.146	3.151	0.077
51599.9643	832	2.823e-11	1.896	0.330	2.898	0.066
51602.1713	1168	3.401e-11	1.845	0.211	3.356	0.065
51605.2378	880	3.523e-11	2.063	0.340	3.738	0.062
51608.2322	752	4.151e-11	1.984	0.266	4.070	0.086
51611.1682	224	3.629e-11	1.666	0.291	3.600	0.110
51617.0177	800	2.722e-11	1.994	0.351	2.780	0.068
51620.3197	320	3.224e-11	2.181	0.499	3.450	0.108
51623.3153	960	3.854e-11	2.108	0.313	3.995	0.064
51626.1693	992	4.164e-11	1.905	1.905	3.993	0.071
51629.0357	912	3.938e-11	1.968	0.161	3.818	0.066
51632.1092	896	3.869e-11	1.629	0.110	3.949	0.072
51635.2398	864	3.561e-11	2.214	0.354	3.716	0.089
51638.2861	824	3.843e-11	2.188	0.261	3.914	0.095
51644.0716	1280	2.535e-11	1.836	0.251	2.600	0.050
51650.2681	480	3.608e-11	2.031	0.311	3.675	0.111
51653.2970	760	3.232e-11	2.232	0.389	3.334	0.081
51656.1117	784	3.466e-11	1.857	0.137	3.259	0.072
51659.0969	1008	5.116e-11	2.139	0.214	5.031	0.084
51662.0731	816	4.719e-11	2.093	0.227	4.580	0.067

[a] Modified Julian Date
[b] Exposure time (s)
[c] erg/s/cm^2
[d] Spectral photon index
[e] Error for spectral photon index
[f] Counts/sec/PCU
[g] Count rate error

Table C.4: Akn 120 Short Term X-ray Data

time[a]	**counts**[b]	**error**[c]
0	7.309	0.112
2000	7.161	0.205
4000	7.404	0.233
6000	7.647	0.111
8000	7.677	0.270
10000	7.636	0.292
12000	7.595	0.110
14000	7.993	0.542
16000	7.250	0.133
18000	7.410	0.110
20000	7.326	0.341
22000	7.243	0.341
24000	7.160	0.341
26000	7.076	0.341
28000	6.993	0.341
30000	6.910	0.341
32000	6.827	0.323
34000	6.674	0.120
36000	6.766	0.169
38000	6.659	0.212
40000	6.765	0.120
42000	6.948	0.211
44000	7.131	0.174
46000	6.571	0.123
48000	6.753	0.194
50000	6.934	0.150
52000	6.895	0.135
54000	7.187	0.192
56000	7.478	0.137
58000	7.448	0.142
60000	7.453	0.187
62000	7.458	0.187
64000	7.464	0.187
66000	7.469	0.187
68000	7.474	0.187
70000	7.480	0.187

Continued on Next Page...

Table C.4 – Continued

time[a]	**counts**[b]	**error**[c]
72000	7.485	0.187
74000	7.490	0.187
76000	7.495	0.187
78000	7.501	0.187
80000	7.506	0.187
82000	7.511	0.187
84000	7.517	0.187
86000	7.522	0.123
88000	7.673	0.160
90000	7.769	0.201
92000	7.864	0.122
94000	8.127	0.186
96000	7.998	0.223
98000	7.869	0.123
100000	7.731	0.227
102000	7.720	0.148
104000	7.808	0.107
106000	7.933	0.336
108000	7.523	0.139
110000	7.463	0.107
112000	7.410	0.171
114000	7.358	0.134
116000	7.422	0.114
118000	7.355	0.359
120000	7.288	0.122
122000	7.372	0.176
124000	7.278	0.309
126000	7.185	0.309
128000	7.091	0.309
130000	6.997	0.253
132000	7.059	0.114
134000	6.911	0.224
136000	6.763	0.193
138000	6.928	0.120
140000	7.056	0.205
142000	7.184	0.166
144000	7.211	0.121
146000	7.155	0.181

Continued on Next Page...

Table C.4 – Continued

time[a]	**counts**[b]	**error**[c]
148000	7.100	0.181
150000	7.044	0.181
152000	6.989	0.181
154000	6.933	0.181
156000	6.878	0.181
158000	6.822	0.181
160000	6.767	0.181
162000	6.711	0.181
164000	6.656	0.181
166000	6.600	0.181
168000	6.545	0.181
170000	6.489	0.181
172000	6.434	0.134
174000	6.577	0.132
176000	6.661	0.187
178000	6.745	0.133
180000	6.583	0.144
182000	6.672	0.208
184000	6.686	0.104
186000	6.571	0.164
188000	6.476	0.171
190000	6.804	0.105
192000	7.203	0.198
194000	7.525	0.171
196000	7.955	0.107
198000	8.179	0.458
200000	8.554	0.172
202000	8.533	0.109
204000	8.749	0.507
206000	8.137	0.151
208000	8.197	0.179
210000	7.769	0.220
212000	7.342	0.129
214000	7.076	0.262
216000	7.098	0.284
218000	7.121	0.110
220000	7.182	0.583
222000	6.903	0.387

Continued on Next Page. . .

Table C.4 – Continued

time[a]	**counts**[b]	**error**[c]
224000	7.135	0.113
226000	7.032	0.263
228000	6.929	0.237
230000	7.025	0.108
232000	6.997	0.265
234000	6.969	0.242
236000	6.784	0.108
238000	7.474	0.354
240000	7.069	0.175
242000	7.048	0.184

[a] Time since start of observation (MJD=51163.20)
[b] Counts/sec/PCU
[c] Count rate error

C.3 3C 120

Table C.5: 3C 120 Long Term X-ray Data

MJD[a]	exptime[b]	flux[c]	slope[d]	slope err[e]	counts[f]	count err[g]
50812.0596	912	3.605e-11	2.120	0.309	3.895	0.112
50818.3412	920	2.262e-11	1.678	0.364	2.435	0.106
50825.2271	592	2.746e-11	2.241	0.463	3.194	0.142
50830.4711	312	3.373e-11	1.802	0.442	3.882	0.228
50837.5430	368	6.065e-11	1.690	0.162	5.629	0.242
50844.4734	256	4.171e-11	2.088	0.417	4.457	0.130
50851.2965	896	4.712e-11	1.864	0.151	4.669	0.137
50858.1418	808	5.233e-11	1.758	0.176	5.518	0.121
50865.4374	896	4.581e-11	2.062	0.256	5.076	0.108
50871.2357	864	5.865e-11	1.745	0.129	5.799	0.102
50878.4955	176	3.865e-11	2.127	0.609	4.846	0.277
50885.4279	472	5.735e-11	1.777	0.188	5.798	0.170
50892.4291	184	6.648e-11	2.179	0.436	7.116	0.263
50899.1045	1184	3.994e-11	1.709	0.093	3.965	0.101
50907.2236	848	4.358e-11	1.779	0.275	4.690	0.145
50914.1006	856	4.010e-11	1.897	0.285	4.409	0.119
50925.0445	600	4.365e-11	1.635	0.238	4.723	0.123
50933.5242	856	4.298e-11	1.959	0.292	4.684	0.123
50997.9085	928	5.539e-11	1.980	0.221	5.694	0.106
51005.0706	624	5.563e-11	2.283	0.280	6.235	0.168
51011.9099	816	5.326e-11	1.769	0.173	5.393	0.131
51018.8658	160	5.999e-11	1.578	0.174	6.541	0.217
51026.1943	48	3.683e-11	1.024	0.286	4.905	0.482
51034.8607	904	4.784e-11	1.706	0.097	4.684	0.126
51039.9191	304	5.010e-11	1.787	0.188	4.872	0.215
51047.2002	392	4.563e-11	1.716	0.159	4.731	0.170
51069.1824	1000	5.961e-11	1.679	0.088	5.927	0.114
51077.0647	1056	5.460e-11	1.969	0.214	5.976	0.110
51085.5975	920	5.143e-11	1.764	0.134	5.099	0.118
51091.9991	208	4.759e-11	2.281	0.515	5.256	0.187
51098.3331	888	5.555e-11	1.850	0.203	5.656	0.112
51113.3923	800	5.998e-11	1.789	0.158	6.146	0.117
51109.9918	96	4.410e-11	2.331	0.761	6.019	0.492
51119.3774	784	6.641e-11	2.127	0.216	6.883	0.138

Continued on Next Page...

Table C.5 – Continued

MJD[a]	exptime[b]	flux[c]	slope[d]	slope err[e]	counts[f]	count err[g]
51125.3766	920	6.560e-11	1.705	0.116	6.625	0.112
51134.3763	856	5.268e-11	1.948	0.236	5.819	0.119
51140.9301	432	5.308e-11	1.884	0.281	5.524	0.141
51148.5957	256	5.988e-11	1.664	0.289	6.030	0.226
51155.3293	1056	6.373e-11	1.788	0.136	6.504	0.119
51161.2547	960	5.631e-11	1.777	0.144	5.649	0.122
51170.4580	864	5.817e-11	1.968	0.225	6.195	0.116
51177.4299	824	5.457e-11	2.021	0.230	5.931	0.126
51185.2277	856	5.291e-11	1.727	0.110	4.972	0.110
51193.7189	896	5.177e-11	1.840	0.162	5.265	0.111
51197.5165	288	3.959e-11	2.103	0.463	4.559	0.179
51201.6367	616	5.054e-11	1.855	0.264	5.394	0.164
51204.3557	824	5.045e-11	1.976	0.240	5.506	0.115
51209.2966	944	6.110e-11	1.684	0.018	6.168	0.108
51212.2258	944	6.187e-11	1.816	0.099	5.900	0.123
51215.4321	856	5.423e-11	1.892	0.237	5.862	0.137
51218.3531	856	5.715e-11	1.874	0.196	5.940	0.176
51221.3617	984	4.668e-11	1.781	0.185	4.834	0.111
51225.3702	1008	4.363e-11	1.525	0.112	4.496	0.106
51228.8117	672	4.152e-11	1.705	0.176	4.297	0.139
51233.2143	904	2.692e-11	2.002	0.386	3.015	0.106
51236.2071	808	3.514e-11	1.860	0.305	3.889	0.119
51239.2114	920	3.797e-11	1.930	0.271	4.051	0.105
51242.2895	856	3.359e-11	1.967	0.320	3.966	0.106
51245.4199	888	4.955e-11	1.808	0.089	4.890	0.131
51249.3354	776	5.630e-11	1.908	0.198	5.821	0.136
51253.3540	576	5.064e-11	1.772	0.151	5.068	0.164
51256.4038	416	4.848e-11	1.926	0.359	5.067	0.156
51260.2068	976	5.384e-11	1.768	0.085	5.389	0.108
51267.1933	920	5.733e-11	1.934	0.219	5.785	0.124
51270.3476	672	5.574e-11	2.049	0.270	5.868	0.129
51274.3874	152	5.652e-11	1.754	0.219	5.358	0.374
51277.4505	984	4.350e-11	2.032	0.257	4.868	0.115
51281.2719	880	5.074e-11	1.882	0.159	4.953	0.126
51284.6435	384	4.523e-11	1.576	0.178	4.569	0.200
51288.5349	568	5.921e-11	1.883	0.160	5.699	0.141
51291.5319	496	4.943e-11	2.109	0.318	5.606	0.150
51295.3880	512	6.231e-11	2.056	0.209	6.063	0.162

Continued on Next Page...

Table C.5 – Continued

MJD[a]	exptime[b]	flux[c]	slope[d]	slope err[e]	counts[f]	count err[g]
51356.2017	424	6.237e-11	1.808	0.203	6.447	0.159
51359.2670	184	6.806e-11	1.911	0.214	6.598	0.306
51363.1312	792	5.944e-11	1.990	0.239	6.239	0.133
51366.4680	960	6.350e-11	1.810	0.117	6.430	0.098
51369.8633	976	5.904e-11	1.978	0.200	6.609	0.118
51373.7881	896	6.928e-11	1.806	0.151	7.062	0.127
51380.7109	848	6.267e-11	2.047	0.215	6.530	0.135
51383.7079	944	5.916e-11	2.010	0.206	6.728	0.115
51388.6942	1000	4.311e-11	1.933	0.262	4.848	0.112
51391.7006	928	3.929e-11	1.831	0.284	4.341	0.108
51395.1641	928	4.089e-11	1.514	0.106	4.205	0.117
51398.0984	1112	4.061e-11	1.698	0.212	4.126	0.100
51401.3050	480	3.912e-11	1.631	0.227	4.150	0.140
51405.0896	600	4.588e-11	1.860	0.236	4.646	0.135
51408.9604	304	4.211e-11	2.327	0.463	4.805	0.210
51412.2212	392	4.365e-11	1.608	0.107	4.337	0.229
51415.8844	224	4.330e-11	1.855	0.405	4.675	0.175
51419.2083	128	4.902e-11	2.024	0.506	5.382	0.456
51422.8540	384	3.893e-11	1.615	0.205	4.176	0.166
51425.0615	400	4.659e-11	1.735	0.171	4.832	0.151
51428.0667	944	4.558e-11	1.886	0.235	4.982	0.121
51432.7288	1584	4.950e-11	1.707	0.125	4.995	0.096
51436.6580	704	5.021e-11	1.641	0.173	5.333	0.159
51443.1141	808	6.007e-11	1.719	0.099	5.927	0.111
51447.1863	272	5.329e-11	1.814	0.308	5.606	0.221
51452.0384	216	4.912e-11	2.042	0.412	5.427	0.307
51455.0350	432	4.907e-11	2.177	0.346	5.386	0.167
51458.0307	456	5.982e-11	1.936	0.179	5.903	0.174
51461.0333	752	4.473e-11	1.910	0.296	4.747	0.166
51464.0222	352	5.130e-11	2.125	0.378	5.641	0.225
51468.0831	160	5.061e-11	2.360	0.582	6.012	0.287
51471.5911	824	5.700e-11	1.774	0.100	5.520	0.113
51479.2692	888	5.035e-11	1.765	0.128	4.882	0.111
51482.1907	888	6.197e-11	1.802	0.111	5.843	0.115
51485.0387	752	6.101e-11	1.798	0.115	5.755	0.136
51488.6507	952	4.926e-11	1.915	0.235	5.585	0.089
51491.5044	920	6.016e-11	1.762	0.193	6.294	0.119
51496.0532	80	5.915e-11	2.144	0.456	6.751	0.387

Continued on Next Page...

Table C.5 – Continued

MJD[a]	**exptime**[b]	**flux**[c]	**slope**[d]	**slope err**[e]	**counts**[f]	**count err**[g]
51500.6308	1048	4.419e-11	1.593	0.093	4.628	0.118
51503.0393	40	2.723e-11	2.392	1.311	3.228	0.207
51506.0338	48	3.464e-11	1.021	0.365	3.975	0.395
51513.1600	32	5.593e-11	1.466	0.546	5.789	1.043
51521.1914	888	5.786e-11	1.781	0.128	5.965	0.132
51524.0560	888	5.753e-11	2.125	0.235	5.811	0.098
51527.1302	880	5.258e-11	1.836	0.128	5.212	0.130
51530.2503	992	4.828e-11	1.926	0.246	5.316	0.148
51533.2930	848	5.217e-11	1.779	0.162	5.222	0.122
51538.0926	1120	5.304e-11	1.614	0.106	5.465	0.112
51541.6379	704	5.404e-11	2.254	0.267	6.161	0.123
51545.2042	712	5.917e-11	1.808	0.137	5.928	0.142
51551.8169	200	7.138e-11	1.656	0.157	7.480	0.234
51555.9479	144	4.833e-11	1.619	0.242	4.907	0.237
51558.8720	288	5.089e-11	1.816	0.278	5.172	0.244
51563.1800	944	4.952e-11	1.782	0.155	4.955	0.114

[a] Modified Julian Date
[b] Exposure time (s)
[c] erg/s/cm^2
[d] Spectral photon index
[e] Error for spectral photon index
[f] Counts/sec/PCU
[g] Count rate error

Table C.6: 3C 120 Intermediate Sampling X-ray Data

MJD[a]	**exptime**[b]	**flux**[c]	**slope**[d]	**slope err**[e]	**counts**[f]	**count err**[g]
52450.0841	896	4.857e-11	1.547	0.103	5.947	0.196
52452.1356	688	4.789e-11	1.654	0.166	5.266	0.146
52454.1131	744	4.750e-11	1.761	0.149	5.098	0.123
52455.3076	360	4.321e-11	1.670	0.199	4.869	0.230
52457.5610	152	3.696e-11	2.364	0.685	4.571	0.300
52459.1237	456	3.846e-11	1.898	0.295	4.422	0.232
52461.0317	520	4.879e-11	1.559	0.119	5.640	0.152
52463.0335	496	5.242e-11	1.927	0.204	5.624	0.151
52464.4077	32	5.244e-11	2.211	0.843	7.044	0.407
52466.1138	608	4.281e-11	1.977	0.349	5.290	0.162
52467.9105	912	4.207e-11	1.714	0.222	4.978	0.117
52469.0792	584	3.954e-11	1.889	0.315	4.473	0.146
52471.1229	120	4.063e-11	2.048	0.684	5.621	0.282
52472.8525	928	4.790e-11	1.800	0.228	5.501	0.128
52475.0773	208	5.583e-11	1.565	0.180	6.571	0.376
52476.8778	896	5.161e-11	1.627	0.105	5.720	0.123
52478.9660	944	5.198e-11	1.769	0.162	5.828	0.127
52479.7738	880	5.645e-11	1.607	0.110	6.189	0.150
52481.8210	864	6.969e-11	1.624	0.086	7.816	0.154
52483.7280	864	6.686e-11	1.613	0.074	7.455	0.129
52485.8466	768	6.020e-11	1.917	0.241	6.933	0.123
52486.9035	840	6.135e-11	1.631	0.097	6.664	0.139
52488.8087	776	6.018e-11	1.715	0.104	6.682	0.144
52490.5770	912	5.414e-11	1.650	0.086	6.091	0.123
52494.1532	408	4.315e-11	1.747	0.369	5.336	0.183
52495.9408	688	4.443e-11	1.505	0.106	4.988	0.161
52498.0383	576	5.099e-11	1.560	0.118	5.637	0.197
52500.1536	576	4.735e-11	1.733	0.171	5.198	0.141
52506.8241	160	5.526e-11	1.576	0.204	7.469	0.464
52508.4679	752	6.973e-11	1.751	0.069	7.332	0.148
52509.9662	440	5.825e-11	1.727	0.190	6.639	0.186
52511.6983	752	6.725e-11	1.616	0.083	7.402	0.154
52513.6759	784	6.682e-11	1.723	0.178	7.267	0.168
52514.9070	456	5.435e-11	1.851	0.204	6.331	0.145
52516.6398	896	4.858e-11	1.561	0.096	5.488	0.136
52518.5505	608	4.399e-11	1.793	0.217	4.768	0.151

Continued on Next Page...

Table C.6 – Continued

MJD[a]	**exptime**[b]	**flux**[c]	**slope**[d]	**slope err**[e]	**counts**[f]	**count err**[g]
52520.5233	992	4.967e-11	1.783	0.114	4.995	0.160
52523.8950	736	4.390e-11	1.752	0.294	5.133	0.149
52525.9386	704	5.721e-11	1.527	0.109	6.613	0.185
52527.6422	944	5.455e-11	1.689	0.126	5.793	0.122
52528.7003	960	7.413e-11	1.579	0.042	8.086	0.120
52530.8172	528	5.178e-11	1.663	0.146	5.447	0.163
52532.6524	1088	5.897e-11	1.674	0.119	6.529	0.136
52535.2056	816	4.715e-11	1.814	0.270	6.657	0.278
52536.1934	752	5.587e-11	1.638	0.113	6.215	0.237
52537.5931	912	5.498e-11	1.671	0.125	6.052	0.133
52539.5558	928	5.387e-11	1.583	0.052	5.984	0.119
52541.0975	432	4.454e-11	1.756	0.324	5.020	0.172
52543.0738	568	5.094e-11	1.785	0.192	5.478	0.143
52544.9760	1016	3.930e-11	1.812	0.292	4.576	0.133
52546.7564	920	4.886e-11	1.624	0.118	5.269	0.134
52548.4605	896	4.148e-11	1.688	0.244	4.945	0.140
52550.1258	352	4.490e-11	1.728	0.204	5.050	0.245
52551.8936	392	3.761e-11	1.855	0.402	4.493	0.165
52557.1083	240	4.535e-11	1.742	0.197	5.033	0.294
52558.7383	464	4.162e-11	1.639	0.147	4.782	0.159
52560.8521	480	4.352e-11	1.582	0.117	5.015	0.166
52565.9270	248	5.697e-11	1.798	0.209	6.208	0.368
52567.6281	784	6.187e-11	1.669	0.099	6.595	0.125
52571.6740	752	6.565e-11	1.732	0.081	7.239	0.146
52574.6359	944	6.303e-11	1.529	0.008	6.947	0.125
52576.7887	264	6.558e-11	1.769	0.227	7.518	0.212
52578.3020	984	6.325e-11	1.740	0.194	7.215	0.140
52579.5528	840	5.490e-11	1.625	0.087	6.136	0.130
52581.3413	864	5.591e-11	1.807	0.208	6.264	0.154
52583.3822	992	6.644e-11	1.697	0.068	7.240	0.113
52585.4290	816	6.576e-11	1.700	0.106	7.117	0.140
52586.6239	904	6.821e-11	1.562	0.069	7.691	0.149
52588.5950	872	7.101e-11	1.611	0.083	7.858	0.121
52590.2943	944	6.919e-11	1.707	0.092	7.547	0.124
52592.2690	880	6.250e-11	1.821	0.182	7.099	0.115
52593.3953	1056	5.513e-11	1.727	0.101	5.811	0.112
52595.3710	880	5.059e-11	1.754	0.179	5.745	0.138
52596.7702	832	5.882e-11	1.735	0.179	6.416	0.115

Continued on Next Page...

Table C.6 – Continued

MJD[a]	**exptime**[b]	**flux**[c]	**slope**[d]	**slope err**[e]	**counts**[f]	**count err**[g]
52598.8012	264	6.522e-11	1.825	0.254	7.311	0.269
52601.1555	592	9.524e-11	1.676	0.083	9.820	0.182
52604.8632	472	7.821e-11	1.822	0.225	9.060	0.206
52607.6859	520	6.649e-11	1.893	0.243	7.722	0.146
52609.7304	744	7.341e-11	1.656	0.075	8.058	0.160
52611.7024	424	5.798e-11	1.920	0.318	6.594	0.211
52613.5381	496	5.650e-11	1.945	0.302	6.729	0.182
52614.8010	320	6.269e-11	1.534	0.068	6.888	0.227
52616.6370	448	5.745e-11	1.637	0.144	6.422	0.231
52618.3676	896	5.792e-11	1.581	0.019	6.363	0.139
52620.0165	704	5.263e-11	1.708	0.119	5.634	0.146
52627.4517	848	5.085e-11	1.747	0.203	5.827	0.138
52628.3662	1328	4.507e-11	1.647	0.109	4.906	0.115
52630.3398	1200	6.708e-11	1.703	0.076	7.244	0.094
52632.5254	752	5.587e-11	1.773	0.133	6.423	0.149
52634.2201	800	5.194e-11	1.714	0.116	5.690	0.128
52635.4157	880	4.553e-11	1.622	0.176	6.134	0.396
52636.9388	496	5.034e-11	1.914	0.273	5.821	0.160
52639.1522	896	5.606e-11	1.896	0.207	6.206	0.150
52641.5893	896	5.600e-11	1.636	0.106	6.164	0.131
52642.8619	344	4.791e-11	1.942	0.399	6.002	0.258
52644.2265	912	5.291e-11	1.729	0.090	5.915	0.126
52646.4013	984	4.968e-11	1.631	0.131	5.198	0.119
52648.3107	920	5.238e-11	1.560	0.089	5.749	0.131
52650.0763	944	6.069e-11	1.895	0.181	6.733	0.136
52651.4184	464	5.683e-11	1.704	0.116	6.289	0.236
52653.6460	584	6.022e-11	1.632	0.118	6.506	0.149
52655.5496	560	6.098e-11	1.707	0.186	6.986	0.131
52656.8168	656	5.229e-11	1.923	0.279	5.905	0.159
52658.5087	536	5.520e-11	1.683	0.109	6.086	0.204
52660.6892	544	4.506e-11	1.601	0.159	5.059	0.155
52662.0814	688	4.383e-11	1.684	0.287	5.246	0.155
52663.5807	824	4.196e-11	1.827	0.231	4.862	0.149
52667.5246	536	5.566e-11	1.942	0.276	6.319	0.173
52669.2532	864	5.127e-11	1.659	0.095	5.636	0.196
52670.7579	80	4.885e-11	1.701	0.426	5.496	0.660
52672.6641	568	4.729e-11	1.707	0.199	5.428	0.155
52674.4549	608	5.297e-11	1.602	0.115	5.698	0.142

Continued on Next Page...

Table C.6 – Continued

MJD[a]	exptime[b]	flux[c]	slope[d]	slope err[e]	counts[f]	count err[g]
52676.5450	976	5.033e-11	1.602	0.084	5.675	0.131
52677.4166	592	5.192e-11	1.604	0.129	5.757	0.144
52679.1153	800	5.890e-11	1.714	0.126	6.447	0.138
52681.1542	912	5.207e-11	1.735	0.156	5.883	0.130
52683.3342	1104	3.799e-11	1.842	0.216	4.189	0.118
52685.0309	864	4.461e-11	1.508	0.101	4.865	0.138
52687.4211	624	5.541e-11	1.884	0.177	6.310	0.185
52688.7725	792	5.695e-11	1.847	0.126	5.884	0.143
52690.2399	832	5.976e-11	1.583	0.083	6.578	0.127
52692.1411	1120	5.867e-11	1.717	0.109	6.566	0.124
52693.3262	1352	4.820e-11	1.761	0.164	5.538	0.105
52695.4973	936	4.827e-11	1.771	0.206	5.428	0.125
52697.0728	960	6.639e-11	1.620	0.102	7.399	0.131
52699.1139	1264	5.502e-11	1.893	0.197	6.179	0.116
52701.0187	816	5.497e-11	1.620	0.112	6.041	0.147
52705.4405	1040	6.106e-11	1.698	0.087	6.418	0.118
52709.4459	480	5.965e-11	1.755	0.133	6.328	0.187
52711.4180	504	5.053e-11	1.842	0.261	5.899	0.150
52712.4729	472	4.120e-11	1.833	0.339	5.061	0.178
52714.4451	488	5.228e-11	1.601	0.135	5.750	0.145
52716.4851	288	5.157e-11	1.505	0.174	5.406	0.245
52718.2510	560	5.577e-11	2.033	0.292	6.625	0.120
52719.4459	824	5.851e-11	1.648	0.085	6.386	0.139
52721.2776	504	6.617e-11	1.863	0.181	7.193	0.184
52723.4566	424	5.737e-11	1.982	0.305	6.802	0.191
52725.1797	1056	6.567e-11	1.672	0.074	7.221	0.127
52727.0848	928	6.891e-11	1.717	0.111	7.529	0.152
52728.4538	184	6.335e-11	1.976	0.279	7.029	0.240
52730.4247	40	4.794e-11	1.948	0.670	6.363	0.742
52732.3973	216	3.791e-11	2.307	0.566	5.105	0.169
52734.1232	960	5.034e-11	1.686	0.169	5.934	0.113
52735.8212	880	6.407e-11	1.879	0.214	7.534	0.130
52737.7933	624	5.632e-11	1.615	0.108	6.360	0.172
52739.1908	1000	5.850e-11	1.621	0.122	6.586	0.132
52741.0236	1120	4.444e-11	1.725	0.218	5.182	0.124
52742.9951	1152	5.380e-11	1.667	0.119	6.053	0.126
52744.3914	704	5.079e-11	1.680	0.190	5.895	0.147
52746.4879	904	7.200e-11	1.626	0.066	7.640	0.156

Continued on Next Page...

Table C.6 – Continued

MJD[a]	**exptime**[b]	**flux**[c]	**slope**[d]	**slope err**[e]	**counts**[f]	**count err**[g]
52747.9256	944	6.797e-11	1.690	0.070	7.353	0.124
52749.8266	992	6.949e-11	1.643	0.066	7.749	0.144
52751.4240	768	6.589e-11	1.752	0.069	6.982	0.136
52753.3148	320	6.385e-11	1.893	0.273	7.598	0.309
52754.3792	472	5.759e-11	1.965	0.275	6.318	0.178
52756.2770	984	6.342e-11	1.895	1.895	7.275	0.200

[a] Modified Julian Date
[b] Exposure time (s)
[c] erg/s/cm^2
[d] Spectral photon index
[e] Error for spectral photon index
[f] Counts/sec/PCU
[g] Count rate error

Table C.7: 3C 120 Short Term X-ray Data

time[a]	**counts**[b]	**err**[c]
0	5.114	0.2025
1000	5.3995	0.2156
2000	5.3235	0.2889
3000	5.2475	0.2889
4000	5.1715	0.1923
5000	5.066	0.1784
6000	5.2495	0.1772
7000	5.172	0.2902
8000	4.995	0.4859
9000	4.81955	0.3898
10000	5.2225	0.1877
11000	5.0935	0.1787
12000	5.084	0.1766
13000	5.0015	0.8009
14000	5.0155	0.8389
15000	5.0295	0.2497
16000	5.1275	0.1912
17000	5.108	0.1784
18000	4.97875	0.2055
19000	5.007	0.3798
20000	5.035	0.3798
21000	5.064	0.3798
22000	5.092	0.3798
23000	5.12	0.3798
24000	5.148	0.3798
25000	5.177	0.3798
26000	5.204	0.3798
27000	5.233	0.3798
28000	5.261	0.3798
29000	5.289	0.3798
30000	5.318	0.3798
31000	5.346	0.3798
32000	5.374	0.3798
33000	5.4025	0.3194
34000	5.358	0.1904
35000	5.352	0.3819

Continued on Next Page...

Table C.7 – Continued

time[a]	**counts**[b]	**err**[c]
36000	5.388	0.4629
37000	5.423	0.4629
38000	5.458	0.4629
39000	5.4945	0.2616
40000	5.7615	0.1887
41000	5.5335	0.8278
42000	5.56	0.8824
43000	5.587	0.8824
44000	5.614	0.8824
45000	5.641	0.8824
46000	5.667	0.8824
47000	5.694	0.8824
48000	5.721	0.8824
49000	5.748	0.8824
50000	5.774	0.8824
51000	5.801	0.8824
52000	5.828	0.8824
53000	5.855	0.8824
54000	5.881	0.8824
55000	5.908	0.3057
56000	5.823	0.1863
57000	5.849	0.1834
58000	5.9345	0.2499
59000	5.864	0.3879
60000	5.7935	0.3879
61000	5.723	0.2967
62000	5.758	0.186
63000	5.811	0.1834
64000	5.884	0.3754
65000	5.88	0.473
66000	5.876	0.473
67000	5.872	0.2878
68000	5.7105	0.1833
69000	5.9045	0.1881
70000	5.884	0.8524
71000	5.864	0.8524
72000	5.843	0.8524
73000	5.823	0.8524

Continued on Next Page...

Table C.7 – Continued

time[a]	**counts**[b]	**err**[c]
74000	5.803	0.8524
75000	5.782	0.8524
76000	5.762	0.8524
77000	5.741	0.8524
78000	5.721	0.8524
79000	5.701	0.8524
80000	5.68	0.8524
81000	5.66	0.8524
82000	5.639	0.8524
83000	5.619	0.8314
84000	5.6405	0.1824
85000	5.777	0.1844
86000	5.5595	0.1782
87000	5.6355	0.3054
88000	5.7115	0.3054
89000	5.7875	0.2483
90000	5.714	0.1842
91000	5.5655	0.1783
92000	5.653	0.2159
93000	5.68	0.2963
94000	5.71	0.2963
95000	5.748	0.2029
96000	5.5605	0.1856
97000	5.6825	0.1792
98000	5.5205	0.2891
99000	5.5985	0.5227
100000	5.6765	0.4355
101000	5.782	0.1917
102000	5.6155	0.1872
103000	5.614	0.1872
104000	5.602	0.5841
105000	5.59	0.5841
106000	5.578	0.5841
107000	5.567	0.5841
108000	5.555	0.5841
109000	5.543	0.5841
110000	5.531	0.5841
111000	5.519	0.5841

Continued on Next Page...

Table C.7 – Continued

time[a]	**counts**[b]	**err**[c]
112000	5.507	0.5841
113000	5.495	0.5841
114000	5.484	0.5841
115000	5.472	0.5841
116000	5.46	0.5841
117000	5.448	0.5841
118000	5.436	0.5841
119000	5.424	0.5841
120000	5.412	0.5841
121000	5.401	0.5841
122000	5.389	0.5841
123000	5.377	0.5841
124000	5.365	0.5533
125000	5.5465	0.1845
126000	5.3855	0.339
127000	5.47	0.3985
128000	5.55	0.3985
129000	5.63	0.2096
130000	5.5295	0.1825
131000	5.7005	0.1819
132000	5.7435	0.546
133000	5.775	0.7883
134000	5.806	0.7883
135000	5.837	0.7883
136000	5.868	0.7883
137000	5.899	0.7883
138000	5.931	0.7883
139000	5.962	0.7883
140000	5.993	0.5686
141000	5.8615	0.1859
142000	5.6915	0.1843
143000	5.7575	0.1929
144000	5.65	0.5583
145000	5.55	0.5583
146000	5.447	0.5239
147000	5.6895	0.1852
148000	5.831	0.1845
149000	5.871	0.239

Continued on Next Page. . .

Table C.7 – Continued

time[a]	**counts**[b]	**err**[c]
150000	5.7817	0.5396
151000	5.692	0.5396
152000	5.6005	0.4838
153000	5.686	0.182
154000	5.643	0.1822
155000	5.545	0.3383
156000	5.647	0.5727
157000	5.75	0.5727
158000	5.853	0.4621
159000	5.6685	0.1959
160000	5.685	0.2764
161000	5.702	0.2764
162000	5.719	0.2764
163000	5.736	0.2764
164000	5.753	0.2764
165000	5.769	0.2764
166000	5.786	0.2764
167000	5.803	0.2764
168000	5.82	0.2764
169000	5.8365	0.195
170000	5.828	0.1831
171000	5.864	0.179
172000	5.7935	0.3108
173000	5.9628	0.5152
174000	6.132	0.4109
175000	5.8495	0.1851
176000	5.998	0.1834
177000	5.935	0.356
178000	6.081	0.5745
179000	6.23	0.5745
180000	6.3765	0.4509
181000	6.195	0.1913
182000	6.1425	0.1837
183000	6.166	0.2161
184000	6.247	0.308
185000	6.329	0.308
186000	6.4125	0.2195
187000	6.038	0.1924

Continued on Next Page. . .

Table C.7 – Continued

time[a]	**counts**[b]	**err**[c]
188000	6.1265	0.1837
189000	6.373	0.2867
190000	6.1868	0.5411
191000	6.0005	0.459
192000	6.2115	0.1931
193000	6.094	0.1929
194000	6.0255	0.1852
195000	6.011	0.3393
196000	5.997	0.3393
197000	5.982	0.3393
198000	5.968	0.3393
199000	5.954	0.3393
200000	5.939	0.3393
201000	5.925	0.3393
202000	5.911	0.3393
203000	5.896	0.3393
204000	5.882	0.3393
205000	5.867	0.3393
206000	5.853	0.3393
207000	5.839	0.3393
208000	5.824	0.3393
209000	5.81	0.3393
210000	5.796	0.3393
211000	5.781	0.3393
212000	5.767	0.3393
213000	5.752	0.3393
214000	5.738	0.2843
215000	5.825	0.182
216000	5.957	0.1851
217000	5.999	0.3027
218000	6.012	0.3656
219000	6.026	0.3656
220000	6.039	0.3656
221000	6.053	0.3656
222000	6.066	0.3656
223000	6.08	0.3656
224000	6.093	0.3656
225000	6.107	0.3656

Continued on Next Page. . .

Table C.7 – Continued

time[a]	**counts**[b]	**err**[c]
226000	6.12	0.205
227000	6.0785	0.1854
228000	6.128	0.1869
229000	6.4705	0.386
230000	6.323	0.4357
231000	6.1745	0.4357
232000	6.022	0.2021
233000	6.0755	0.1849
234000	6.1475	0.1949
235000	6.3788	0.2773
236000	6.34	0.2773
237000	6.3	0.2773
238000	6.263	0.1972
239000	6.046	0.1828
240000	6.3395	0.2362
241000	6.2411	0.304
242000	6.143	0.304
243000	6.044	0.304
244000	5.946	0.1914
245000	5.9965	0.1806
246000	6.0505	0.3399
247000	6.036	0.4194
248000	6.021	0.4194
249000	6.007	0.4194
250000	5.992	0.4194
251000	5.978	0.4194
252000	5.963	0.4194
253000	5.949	0.4194
254000	5.934	0.2457
255000	5.9455	0.1829
256000	5.881	0.1804
257000	5.887	0.2176
258000	5.934	0.2957
259000	5.978	0.2957
260000	6.0245	0.3007
261000	5.8915	0.1818
262000	5.843	0.1809
263000	5.862	0.2988

Continued on Next Page...

Table C.7 – Continued

time[a]	**counts**[b]	**err**[c]
264000	5.805	0.3505
265000	5.748	0.3505
266000	5.691	0.3505
267000	5.634	0.1832
268000	5.7955	0.182
269000	5.7915	0.7276
270000	5.8785	0.773
271000	5.9655	0.2611
272000	5.905	0.2032
273000	5.9685	0.1816
274000	6.009	0.2141
275000	6.03	0.3007
276000	6.06	0.3007
277000	6.0835	0.2112
278000	5.8945	0.1994
279000	5.9435	0.1815
280000	6.268	0.3952
281000	6.1198	0.6752
282000	5.9715	0.5474
283000	5.8725	0.1865
284000	5.662	0.1939
285000	5.9795	0.5103
286000	5.955	0.5899
287000	5.931	0.5899
288000	5.906	0.5899
289000	5.882	0.5899
290000	5.857	0.5899
291000	5.833	0.5899
292000	5.809	0.5899
293000	5.784	0.5899
294000	5.76	0.5899
295000	5.735	0.5899
296000	5.711	0.5899
297000	5.686	0.5899
298000	5.662	0.5899
299000	5.638	0.5899
300000	5.613	0.5899
301000	5.589	0.5899

Continued on Next Page. . .

Table C.7 – Continued

time[a]	**counts**[b]	**err**[c]
302000	5.564	0.5899
303000	5.54	0.5899
304000	5.515	0.5899
305000	5.491	0.296
306000	5.5725	0.1835
307000	5.7075	0.1827
308000	5.73	0.2493
309000	5.72	0.3467
310000	5.71	0.3467
311000	5.694	0.241
312000	5.628	0.1857
313000	5.6765	0.1833
314000	5.66	0.2468
315000	5.58	0.341
316000	5.5	0.341
317000	5.435	0.2353
318000	5.625	0.1844
319000	5.824	0.1836
320000	5.6825	0.3759
321000	5.664	0.5202
322000	5.646	0.5202
323000	5.627	0.5202
324000	5.609	0.5202
325000	5.59	0.5202
326000	5.572	0.5202
327000	5.553	0.5202
328000	5.535	0.5202
329000	5.516	0.5202
330000	5.498	0.5202
331000	5.479	0.5202
332000	5.461	0.5202
333000	5.442	0.5202
334000	5.424	0.5202
335000	5.405	0.5202
336000	5.387	0.5202
337000	5.368	0.5202
338000	5.35	0.5202
339000	5.331	0.3596

Continued on Next Page...

Table C.7 – Continued

time[a]	**counts**[b]	**err**[c]
340000	5.5665	0.1821
341000	5.4445	0.1782
342000	5.4525	0.1791
343000	5.434	0.4416
344000	5.415	0.4416
345000	5.396	0.4416
346000	5.377	0.4416
347000	5.358	0.4416
348000	5.339	0.4416
349000	5.32	0.4416
350000	5.301	0.4416
351000	5.2825	0.4037
352000	5.3495	0.1822
353000	5.311	0.1775
354000	5.264	0.2968
355000	5.3075	0.5437
356000	5.351	0.4556
357000	5.445	0.2114
358000	5.2125	0.1811
359000	5.3235	0.179
360000	5.7555	0.7391
361000	5.479	0.7836
362000	5.2025	0.2605
363000	5.337	0.2044
364000	5.2215	0.1811
365000	5.408	0.2601
366000	5.34	0.3309
367000	5.28	0.3309
368000	5.2255	0.2046
369000	5.153	0.1909
370000	5.0365	0.2892
371000	5.044	0.8709
372000	5.051	0.8709
373000	5.058	0.8709
374000	5.065	0.8709
375000	5.072	0.8709
376000	5.079	0.8709
377000	5.086	0.8709

Continued on Next Page. . .

Table C.7 – Continued

time[a]	**counts**[b]	**err**[c]
378000	5.094	0.8709
379000	5.101	0.8709
380000	5.108	0.8709
381000	5.115	0.8709
382000	5.122	0.8709
383000	5.129	0.8709
384000	5.136	0.8709
385000	5.143	0.8709
386000	5.15	0.8709
387000	5.157	0.8709
388000	5.164	0.8709
389000	5.171	0.8709
390000	5.179	0.8215
391000	5.1435	0.1802
392000	5.088	0.1811
393000	5.12	0.1998
394000	5.16	0.3728
395000	5.2	0.3728
396000	5.241	0.3154
397000	5.257	0.1834
398000	5.145	0.1827
399000	5.239	0.1933
400000	5.2	0.3599
401000	5.18	0.3599
402000	5.154	0.3037
403000	5.18	0.1819
404000	5.2215	0.1819
405000	5.1755	0.2382
406000	5.22	0.3785
407000	5.26	0.3785
408000	5.3085	0.2941
409000	5.086	0.1907
410000	5.116	0.2677
411000	5.146	0.2677
412000	5.176	0.2677
413000	5.206	0.2677
414000	5.236	0.2677
415000	5.265	0.2677

Continued on Next Page...

Table C.7 – Continued

time[a]	**counts**[b]	**err**[c]
416000	5.295	0.2677
417000	5.325	0.2677
418000	5.355	0.2677
419000	5.385	0.2677
420000	5.415	0.2677
421000	5.445	0.2677
422000	5.475	0.2677
423000	5.505	0.2677
424000	5.535	0.2677
425000	5.5645	0.188
426000	5.4535	0.1802
427000	5.588	0.1779
428000	5.651	0.3259
429000	5.6008	0.5168
430000	5.5505	0.4011
431000	5.752	0.1848
432000	5.821	0.1824
433000	5.7405	0.1808
434000	5.82	0.3215
435000	5.9	0.3215
436000	6.0175	0.2659
437000	5.7895	0.1872
438000	5.839	0.1823
439000	6.015	0.2196
440000	6.04	0.3735
441000	6.07	0.3735
442000	6.1035	0.2334
443000	5.7805	0.1874
444000	5.8735	0.1825
445000	5.75	0.2961
446000	5.738	0.4374
447000	5.726	0.4374
448000	5.714	0.4374
449000	5.702	0.4374
450000	5.69	0.4374
451000	5.678	0.4374
452000	5.666	0.4374
453000	5.654	0.4374

Continued on Next Page. . .

Table C.7 – Continued

time[a]	**counts**[b]	**err**[c]
454000	5.642	0.4374
455000	5.63	0.4374
456000	5.618	0.4374
457000	5.606	0.4374
458000	5.594	0.4374
459000	5.582	0.4374
460000	5.57	0.4374
461000	5.558	0.4374
462000	5.546	0.4374
463000	5.534	0.4374
464000	5.522	0.4374
465000	5.51	0.4374
466000	5.498	0.4374
467000	5.486	0.4374
468000	5.474	0.4374
469000	5.462	0.4374
470000	5.45	0.4374
471000	5.4495	0.322
472000	5.2275	0.1812
473000	5.41	0.643
474000	5.404	0.8285
475000	5.399	0.8285
476000	5.393	0.8285
477000	5.387	0.8285
478000	5.382	0.8285
479000	5.376	0.8285
480000	5.371	0.8285
481000	5.365	0.8285
482000	5.359	0.8285
483000	5.354	0.8285
484000	5.348	0.8285
485000	5.342	0.8285
486000	5.337	0.8285
487000	5.331	0.5225
488000	5.356	0.1852
489000	5.272	0.1808
490000	5.388	0.1923
491000	5.4	0.5173

Continued on Next Page...

Table C.7 – Continued

time[a]	**counts**[b]	**err**[c]
492000	5.42	0.5173
493000	5.442	0.4802
494000	5.2645	0.1806
495000	4.91505	0.6324
496000	4.94	0.6627
497000	4.965	0.6627
498000	4.99	0.6627
499000	5.015	0.6627
500000	5.04	0.6627
501000	5.065	0.6627
502000	5.09	0.6627
503000	5.114	0.6627
504000	5.139	0.6627
505000	5.164	0.6627
506000	5.189	0.6627
507000	5.214	0.6627
508000	5.239	0.6627
509000	5.264	0.6627
510000	5.289	0.6627
511000	5.314	0.6627
512000	5.339	0.6627
513000	5.364	0.6627
514000	5.389	0.6627
515000	5.414	0.6627
516000	5.4385	0.198
517000	5.276	0.1782
518000	5.235	0.1785
519000	5.386	0.3155
520000	5.4838	0.5335
521000	5.5815	0.4302
522000	5.408	0.1914
523000	5.2535	0.1776
524000	5.2625	0.1816
525000	5.991	1.103
526000	5.7163	1.1849
527000	5.4415	0.4329
528000	5.1555	0.1908
529000	4.88875	0.3715

Continued on Next Page...

Table C.7 – Continued

time[a]	**counts**[b]	**err**[c]
530000	4.87776	0.418
531000	4.86677	0.418
532000	4.85578	0.418
533000	4.84479	0.418
534000	4.8338	0.418
535000	4.82281	0.418
536000	4.81182	0.418
537000	4.80083	0.418
538000	4.78984	0.418
539000	4.77885	0.418
540000	4.76786	0.418
541000	4.75687	0.418
542000	4.74588	0.418
543000	4.73489	0.418
544000	4.7239	0.418
545000	4.71291	0.418
546000	4.70192	0.418
547000	4.69093	0.418
548000	4.67994	0.418
549000	4.66895	0.418
550000	4.65796	0.418
551000	4.64697	0.418
552000	4.63598	0.418
553000	4.62499	0.418
554000	4.614	0.418
555000	4.60301	0.418
556000	4.59202	0.418
557000	4.58103	0.418
558000	4.57004	0.418
559000	4.55905	0.418
560000	4.54806	0.418
561000	4.53707	0.418
562000	4.53685	0.1915
563000	4.51355	0.1766
564000	4.1792	0.3133
565000	4.25	0.3799
566000	4.34	0.3799
567000	4.4181	0.2149

Continued on Next Page. . .

Table C.7 – Continued

time[a]	**counts**[b]	**err**[c]
568000	4.6005	0.179
569000	4.427	0.1767
570000	4.7465	0.2652
571000	4.7	0.3293
572000	4.66	0.329
573000	4.63525	0.1953
574000	4.6068	0.1781
575000	4.90305	0.1776
576000	4.68235	0.3778
577000	4.75	0.43
578000	4.82	0.43
579000	4.88355	0.1901
580000	4.76065	0.1772
581000	4.9282	0.1859
582000	4.9481	0.2715
583000	4.96	0.2715
584000	4.98	0.2715
585000	5.008	0.198
586000	4.984	0.6605
587000	4.961	0.6605
588000	4.937	0.6605
589000	4.913	0.6605
590000	4.889	0.6605
591000	4.866	0.6605
592000	4.842	0.6605
593000	4.818	0.6605
594000	4.794	0.6605
595000	4.7707	0.6301
596000	5.076	0.1788
597000	5.1005	0.1755
598000	4.94645	0.1825
599000	5.02	0.3077
600000	5.1	0.3077
601000	5.1975	0.2478
602000	4.99365	0.179
603000	5.224	0.1765
604000	5.1645	0.227
605000	5.22	0.3055

Continued on Next Page. . .

Table C.7 – Continued

time[a]	**counts**[b]	**err**[c]
606000	5.29	0.3055
607000	5.35	0.2044
608000	4.903	0.178
609000	5.083	0.1777
610000	5.2025	0.3195
611000	5.0328	0.6159
612000	4.86315	0.5265
613000	5.1755	0.2266
614000	4.9907	0.1782
615000	5.2185	0.1849
616000	5.2369	0.7251
617000	5.2553	0.7251
618000	5.2737	0.7251
619000	5.2921	0.7251
620000	5.3105	0.7251
621000	5.3289	0.7251
622000	5.3473	0.7251
623000	5.3657	0.7251
624000	5.3841	0.7251
625000	5.4025	0.7251
626000	5.4209	0.7251
627000	5.4393	0.7251
628000	5.4577	0.7251
629000	5.4761	0.7251
630000	5.4945	0.7251
631000	5.5129	0.7251
632000	5.5313	0.7251
633000	5.5497	0.7251
634000	5.5681	0.7251
635000	5.5865	0.7251
636000	5.6049	0.7251
637000	5.6233	0.7251
638000	5.6417	0.7251
639000	5.6601	0.7251
640000	5.6785	0.7251
641000	5.6969	0.7251
642000	5.7153	0.7251
643000	5.7337	0.7251

Continued on Next Page...

Table C.7 – Continued

time[a]	**counts**[b]	**err**[c]
644000	5.7521	0.7251
645000	5.7705	0.7251
646000	5.8085	0.729
647000	6.02	0.184
648000	6.029	0.1858
649000	6.081	0.2294
650000	6.11	0.3824
651000	6.14	0.3824
652000	6.162	0.306
653000	6.1605	0.1887
654000	6.3025	0.1882
655000	6.4135	0.2226
656000	6.44	0.3307
657000	6.48	0.3307
658000	6.5195	0.2445
659000	6.441	0.1863
660000	6.4705	0.1878
661000	6.612	0.2568
662000	6.65	0.3499
663000	6.69	0.3499
664000	6.7235	0.2378
665000	6.6405	0.1851
666000	6.6665	0.1873
667000	6.5745	0.4014
668000	6.574	0.4582
669000	6.574	0.4582
670000	6.574	0.4582
671000	6.574	0.4582
672000	6.574	0.4582
673000	6.574	0.4582
674000	6.574	0.4582
675000	6.574	0.4582
676000	6.574	0.2209
677000	6.746	0.1842
678000	7.0055	0.2567
679000	6.97	0.3214
680000	6.95	0.3214
681000	6.9235	0.1934

Continued on Next Page...

Table C.7 – Continued

time[a]	**counts**[b]	**err**[c]
682000	6.9515	0.1879
683000	6.821	0.1867
684000	7.2415	0.3781
685000	6.9868	0.5448
686000	6.732	0.3923
687000	6.9735	0.1902
688000	6.672	0.1871
689000	6.992	0.196
690000	6.99	0.3337
691000	6.99	0.3337
692000	6.99	0.2701
693000	6.6745	0.1889
694000	6.5715	1.479
695000	6.6338	1.504
696000	6.6962	1.504
697000	6.7586	1.504
698000	6.821	0.2776
699000	6.595	0.1883
700000	6.6455	0.1891
701000	6.985	0.3291
702000	6.863	0.5848
703000	6.741	0.4834
704000	6.984	0.2706
705000	6.7745	0.2578
706000	6.7718	0.3671
707000	6.7691	0.3671
708000	6.7664	0.3671
709000	6.7637	0.3671
710000	6.761	0.3671
711000	6.7583	0.3671
712000	6.7556	0.3671
713000	6.7529	0.3671
714000	6.7502	0.3671
715000	6.7475	0.3671
716000	6.7448	0.3671
717000	6.7421	0.3671
718000	6.7394	0.3671
719000	6.7367	0.3671

Continued on Next Page...

Table C.7 – Continued

time[a]	**counts**[b]	**err**[c]
720000	6.734	0.3671
721000	6.7313	0.3671
722000	6.7286	0.3671
723000	6.7259	0.3671
724000	6.7232	0.3671
725000	6.7205	0.3671
726000	6.7178	0.3671
727000	6.7151	0.3671
728000	6.7124	0.3671
729000	6.7097	0.3671
730000	6.707	0.3671
731000	6.7043	0.3671
732000	6.7016	0.3671
733000	6.7015	0.2613
734000	6.6505	0.1992
735000	6.62	0.7881
736000	6.6	0.7881
737000	6.583	0.7625
738000	6.5725	0.192
739000	6.5035	0.1887
740000	6.5695	0.1939
741000	6.56	0.37
742000	6.55	0.37
743000	6.5495	0.3152
744000	6.6405	0.1896
745000	6.5575	0.1868
746000	6.5695	0.2053
747000	6.59	0.3676
748000	6.61	0.3676
749000	6.628	0.3049
750000	6.5935	0.1861
751000	6.6745	0.185
752000	6.549	0.2553
753000	6.545	0.4827
754000	6.542	0.4827
755000	6.538	0.4827
756000	6.534	0.4827
757000	6.53	0.4827

Continued on Next Page. . .

Table C.7 – Continued

time[a]	**counts**[b]	**err**[c]
758000	6.527	0.4827
759000	6.523	0.4827
760000	6.519	0.4097
761000	6.455	0.1989
762000	6.501	0.184
763000	6.5655	0.1983
764000	6.6	0.3099
765000	6.64	0.3099
766000	6.6905	0.2381
767000	6.6495	0.1849
768000	6.6175	0.1855
769000	6.7695	0.2547
770000	6.74	0.3233
771000	6.71	0.3233
772000	6.688	0.1992
773000	6.654	0.1853
774000	6.498	0.1875
775000	6.6545	0.3655
776000	6.854	0.5486
777000	7.0535	0.4091
778000	6.7565	0.1947
779000	6.655	0.1852
780000	7.0275	0.197
781000	7.17	0.4584
782000	7.34	0.4584
783000	7.4785	0.4139
784000	6.5565	0.1944
785000	6.4755	0.2419

[a] Time since start of observation (MJD=52622.40)
[b] Counts/sec/PCU
[c] Count rate error

C.4 Mkn 509

Table C.8: Mkn 509 Long Term X-ray Data

MJD[a]	exptime[b]	counts[c]	count err[d]
52726.3465	672	5.611	0.068
52729.2379	1168	6.023	0.056
52732.0588	1472	5.863	0.046
52735.0206	2224	6.680	0.036
52737.9185	1648	4.946	0.041
52741.1371	1264	5.844	0.040
52744.1631	1208	5.515	0.052
52747.0519	1336	5.499	0.039
52750.1399	2000	5.506	0.036
52753.4931	912	6.528	0.052
52756.1382	1776	5.274	0.038
52759.0979	1696	5.276	0.042
52762.8467	1680	5.334	0.039
52765.0164	1776	5.957	0.041
52769.0304	1360	5.548	0.049
52770.9999	1088	6.035	0.043
52774.4721	592	5.829	0.060
52777.9705	1504	5.859	0.042
52780.9962	1496	6.597	0.044
52783.3060	304	6.543	0.097
52786.7173	1200	5.045	0.042
52790.0018	1128	5.384	0.047
52792.4265	912	6.147	0.071
52796.6981	1656	5.438	0.035
52798.9427	1632	5.846	0.042
52801.2383	1504	5.359	0.042
52804.3934	1008	5.644	0.061
52807.9650	1240	5.179	0.051
52810.4405	1728	5.479	0.040
52813.6643	2096	5.909	0.038
52816.4913	2064	5.343	0.040
52819.4498	1696	5.946	0.044
52822.4067	1552	5.434	0.041
52825.9089	1360	5.576	0.040

Continued on Next Page...

Table C.8 – Continued

MJD[a]	**exptime**[b]	**counts**[c]	**count err**[d]
52828.8656	1504	5.646	0.044
52831.8221	1592	5.822	0.047
52834.0641	736	5.681	0.060
52837.8013	1344	6.470	0.045
52840.8941	1144	5.839	0.046
52843.6460	1776	6.126	0.044
52846.8038	896	6.010	0.049
52849.2353	1488	6.265	0.044
52853.7240	560	5.599	0.083
52855.6908	1440	5.317	0.044
52858.4422	1744	5.061	0.039
52862.3152	1392	4.773	0.041
52864.3535	1728	5.210	0.036
52867.8549	848	5.931	0.067
52870.8790	784	6.890	0.066
52873.8356	1024	5.897	0.054
52876.8595	944	6.678	0.052
52882.2447	1664	4.855	0.041
52885.9984	432	4.713	0.079
52888.8875	976	4.179	0.057
52891.0385	1872	5.037	0.038
52894.1426	1696	5.945	0.039
52897.6860	1464	5.778	0.042
52900.4517	1936	5.312	0.036
52903.3925	1304	4.375	0.046
52906.4427	1456	4.905	0.043
52909.2477	1904	4.482	0.037
52912.3421	1904	5.024	0.036
52915.1582	1728	5.987	0.038
52918.6558	1872	6.527	0.047
52921.5363	1392	5.542	0.041
52924.0941	1456	5.955	0.049
52927.5952	1488	5.448	0.045
52930.6856	1104	4.542	0.042
52933.5039	1488	5.386	0.039
52936.0730	1216	4.929	0.049
52939.1595	1536	4.339	0.041
52942.6381	728	4.110	0.060

Continued on Next Page...

Table C.8 – Continued

MJD[a]	**exptime**[b]	**counts**[c]	**count err**[d]
52945.2033	1408	3.633	0.042
52948.3618	1232	4.395	0.043
52952.3702	1136	7.552	0.051
52954.8484	976	6.495	0.057
52957.2239	1728	6.639	0.045
52960.1063	1840	7.295	0.048
52963.3958	1928	6.243	0.037
52966.9998	1648	7.279	0.047
52969.0375	1856	7.095	0.042
52972.0644	1328	6.574	0.048
52976.1363	1760	5.934	0.040
52981.1386	1584	6.314	0.042
52984.2108	936	6.590	0.058
52987.9530	1760	7.875	0.043
52990.4587	416	7.687	0.090
52993.0938	1424	6.398	0.043
52996.0472	1424	5.617	0.040
53000.1882	1520	6.135	0.042
53002.9366	1312	6.452	0.048
53005.8898	1120	7.397	0.058
53064.7899	1936	5.938	0.040
53064.7899	1936	5.938	0.040
53067.7432	1744	6.286	0.040
53070.7639	1856	4.978	0.036
53073.9306	1664	5.799	0.039
53076.8251	688	5.438	0.052
53079.0521	1584	5.322	0.036
53082.2718	1088	6.452	0.054
53085.1570	1560	5.351	0.037
53088.5124	368	6.150	0.073
53091.3995	624	6.258	0.082
53094.0841	1288	5.747	0.046
53097.0397	1776	6.609	0.041
53099.9781	1064	6.029	0.114
53102.5466	1152	6.858	0.053
53109.9754	1312	5.772	0.043
53112.9295	1248	6.118	0.045
53115.8054	1224	4.849	0.049

Continued on Next Page...

Table C.8 – Continued

MJD[a]	**exptime**[b]	**counts**[c]	**count err**[d]
53119.0305	1808	4.548	0.039
53121.9859	1520	5.886	0.046
53124.6642	1936	5.163	0.037
53127.6368	1760	5.131	0.047
53130.9746	1272	5.207	0.044
53133.5196	1416	6.196	0.041
53136.0992	1216	5.252	0.043
53139.9624	864	4.764	0.055
53142.7787	1528	4.424	0.037
53145.7301	1648	5.241	0.040
53148.0379	888	4.642	0.055
53151.6459	2208	4.022	0.035
53154.9212	664	4.013	0.060
53157.3503	1200	4.623	0.043
53160.7082	1888	5.234	0.037
53163.7374	2048	5.069	0.038
53166.8741	1728	5.847	0.044
53169.6313	1760	5.350	0.041
53173.4948	1824	5.423	0.040
53175.8056	1728	5.227	0.039
53178.5645	1312	5.022	0.045
53181.5031	2224	5.090	0.036
53184.7919	1400	4.637	0.040
53187.8809	1496	5.170	0.041
53190.1857	288	5.405	0.105
53193.9858	1024	4.582	0.049
53196.6627	1520	4.818	0.043
53199.6814	1408	4.481	0.046
53202.6326	1568	4.499	0.036
53205.8532	640	4.827	0.075
53208.3435	1872	5.321	0.035
53214.6672	1568	5.335	0.042
53217.6178	1088	4.439	0.048
53220.3519	1904	4.696	0.039
53223.2356	1280	7.231	0.057
53226.2548	1392	4.920	0.041
53229.7516	1472	6.435	0.046
53232.2254	1248	6.366	0.051

Continued on Next Page...

Table C.8 – Continued

MJD[a]	**exptime**[b]	**counts**[c]	**count err**[d]
53238.5988	1064	6.488	0.056
53242.0276	384	6.686	0.086
53244.9117	944	5.927	0.053
53247.2046	1616	6.235	0.047
53250.7444	1336	6.834	0.048
53253.5062	1440	6.219	0.048
53256.3879	1424	6.458	0.051
53259.2008	1504	6.139	0.042
53262.2195	1168	5.870	0.050
53265.3768	1536	6.530	0.043
53268.3277	1392	6.507	0.045
53271.2060	1632	5.907	0.039
53274.1559	1600	5.795	0.046
53277.1745	1712	4.942	0.040
53280.4071	1344	6.071	0.042
53283.4785	2040	5.486	0.036
53286.9083	240	4.110	0.123
53289.3790	1144	4.307	0.042
53292.4003	1512	4.654	0.036
53295.8896	1344	4.457	0.049
53298.3002	1768	4.800	0.040
53301.7296	1344	5.221	0.046
53304.4055	1808	6.572	0.038
53307.3702	1696	6.207	0.042
53310.4374	1096	5.734	0.059
53313.3389	1840	5.988	0.046
53316.2879	2032	6.530	0.038
53319.3163	1552	5.361	0.038
53322.2534	1944	7.711	0.040
53325.9822	1392	6.057	0.050
53328.4886	2176	4.541	0.035
53331.1147	1760	5.383	0.041
53334.4611	1552	5.762	0.041
53337.6800	608	4.764	0.054
53340.3578	1536	4.288	0.043
53343.3063	1552	6.257	0.043
53346.3922	1464	4.692	0.047
53352.1522	1528	6.180	0.043

Continued on Next Page...

Table C.8 – Continued

MJD[a]	exptime[b]	counts[c]	count err[d]
53355.3022	824	4.997	0.069
53358.9114	1952	6.935	0.042
53361.6876	1184	7.172	0.045
53364.7464	848	5.945	0.060
53367.8936	1552	8.071	0.047
53370.8434	1360	6.782	0.045
53432.3087	960	4.933	0.056
53433.2243	1320	6.602	0.047
53439.2566	1264	4.928	0.051
53442.5416	64	5.223	0.116
53445.2207	1336	4.993	0.046
53448.4392	592	5.076	0.055
53454.2696	1416	4.574	0.042
53457.0711	896	5.307	0.061
53460.2318	1944	5.789	0.044
53463.4336	1120	4.713	0.047
53466.7835	1952	4.027	0.038
53469.7315	1824	4.275	0.039
53472.6100	1584	4.602	0.039
53475.5587	1344	4.642	0.042
53478.2042	720	4.903	0.054
53481.0854	1552	6.085	0.043
53484.1012	1280	4.923	0.045
53487.5777	912	5.646	0.052
53490.2669	608	5.745	0.069
53493.0807	1416	6.278	0.054
53496.1635	1120	6.021	0.049
53499.1792	1104	5.582	0.043
53502.1984	544	5.745	0.067
53505.7296	1872	6.025	0.042
53508.0193	1104	5.172	0.051
53511.8193	1464	6.131	0.046
53514.5018	1808	5.311	0.041
53517.3195	800	4.216	0.055
53520.0974	864	5.058	0.056
53523.0882	1808	5.440	0.041
53526.4289	1456	4.645	0.037
53529.6577	1728	5.304	0.039

Continued on Next Page...

Table C.8 – Continued

MJD[a]	**exptime**[b]	**counts**[c]	**count err**[d]
53532.4604	1648	6.454	0.043
53535.4977	1552	5.790	0.061
53538.4435	1248	6.624	0.070
53541.9123	1000	6.612	0.050
53547.0304	1088	5.971	0.049
53549.9776	1240	6.631	0.048
53553.7691	1392	5.835	0.042
53556.7291	1680	5.694	0.046
53559.8670	1144	5.099	0.047
53562.8130	1104	4.913	0.051
53565.7749	1648	3.529	0.039
53568.3833	1248	4.851	0.046
53571.3980	1600	4.419	0.048
53574.3436	1632	3.384	0.040
53577.5565	1880	4.079	0.032
53580.5909	848	5.032	0.049
53583.1875	944	4.897	0.044
53586.8143	1328	4.356	0.045
53592.8438	1232	4.168	0.049
53595.8586	1200	3.994	0.045
53597.9581	800	3.722	0.063
53601.9555	912	3.049	0.051
53604.8363	1520	3.680	0.039
53607.4541	1888	3.894	0.033
53610.2003	1616	3.501	0.037
53616.5732	1184	3.722	0.046
53623.2377	1552	3.626	0.039
53626.4694	1264	3.498	0.038
53629.1988	1696	3.680	0.035
53632.6907	1184	3.179	0.040
53635.2284	1800	3.139	0.032
53640.1614	1120	4.202	0.048
53650.3234	1120	5.083	0.048
53653.5863	1288	5.422	0.049
53659.6827	1072	4.547	0.048
53662.5591	1056	4.276	0.047
53665.1815	1504	5.520	0.041
53668.0600	1376	5.582	0.053

Continued on Next Page...

Table C.8 – Continued

MJD[a]	**exptime**[b]	**counts**[c]	**count err**[d]
53671.0723	1504	3.827	0.036
53674.0866	1760	4.129	0.032
53677.1019	1760	4.885	0.038
53680.1159	1984	5.383	0.036
53683.1311	2016	4.491	0.038
53686.3406	1984	4.632	0.035
53689.0247	1584	4.290	0.039
53692.3766	1416	6.664	0.045
53695.2493	1688	4.194	0.039
53698.3392	1976	4.596	0.031
53701.2104	1080	3.881	0.047
53704.3102	1136	3.641	0.045
53707.5831	1120	4.001	0.048
53710.4594	1128	4.283	0.050
53713.2680	1320	3.954	0.043
53716.6923	1632	3.981	0.043
53719.8853	1520	3.875	0.039
53722.2026	1776	3.787	0.039
53725.9128	1584	3.224	0.038
53731.0875	1440	2.638	0.041
53734.3139	1872	2.755	0.037
53736.3397	1784	3.372	0.032
53795.1043	1424	5.312	0.040
53797.2026	992	4.946	0.045
53800.4211	704	4.961	0.060
53803.9539	1536	5.147	0.042
53806.9682	1456	5.206	0.038
53809.9662	1648	4.138	0.040
53812.0641	1160	5.033	0.051
53815.0952	1008	5.286	0.050
53818.6134	1600	5.230	0.041
53821.1718	2112	5.589	0.034
53824.7076	1632	4.397	0.035
53827.7895	2016	4.728	0.035
53830.5978	1424	4.190	0.040
53833.2410	688	4.444	0.053
53836.1200	1264	4.166	0.041
53839.0653	1440	4.312	0.041

Continued on Next Page...

Table C.8 – Continued

MJD[a]	**exptime**[b]	**counts**[c]	**count err**[d]
53842.2133	928	5.032	0.045
53845.0919	1488	3.983	0.044
53848.4103	416	5.148	0.093
53851.0513	1200	5.678	0.051
53854.2654	848	5.431	0.063
53857.8657	1344	4.993	0.045
53860.0856	944	5.352	0.058
53863.1724	1328	4.893	0.041
53866.8415	1200	4.984	0.044
53869.6438	1952	5.695	0.042
53871.6060	2016	5.401	0.038
53875.5335	1696	6.145	0.048
53878.6160	1968	6.702	0.039
53881.6302	2064	6.388	0.043
53884.5064	1728	5.594	0.041
53887.9947	992	5.539	0.065
53888.0024	128	5.370	0.131
53890.9415	1472	4.039	0.040
53894.0215	1168	5.180	0.048
53896.8999	1728	4.626	0.034
53899.7033	1240	4.710	0.042
53903.0597	1104	4.556	0.041
53905.6629	1720	4.766	0.037
53911.4332	1904	5.392	0.038
53917.4567	1536	4.897	0.041
53923.4825	1664	4.873	0.040
53929.6552	1136	4.999	0.049
53935.8732	1120	4.362	0.045
53941.7613	1160	4.135	0.044
53945.8257	1424	4.875	0.045

[a] Modified Julian Date
[b] Exposure time (s)
[f] Counts/sec/PCU
[g] Count rate error

– D –

Optical Data

D.1 Mkn 509

Table D.1: Mkn 509 Optical Data

MJD[a]	obj–chkA[b]	mkn509[c]	flux[d]
52935	-1.21	12.69	24.59
52935	-1.22	12.68	24.91
52939	-1.22	12.68	24.98
52939	-1.22	12.68	24.90
52942	-1.21	12.69	24.63
52942	-1.24	12.66	25.33
52948	-1.27	12.63	26.06
52948	-1.28	12.62	26.35
52951	-1.28	12.62	26.43
52951	-1.28	12.62	26.36
52954	-1.29	12.61	26.66
52954	-1.29	12.61	26.66
52957	-1.31	12.59	26.96
52957	-1.31	12.59	27.00
52961	-1.31	12.59	27.11
52961	-1.31	12.59	27.12
52964	-1.30	12.60	26.86
52964	-1.32	12.58	27.36
52968	-1.33	12.57	27.54
52968	-1.32	12.58	27.28
53125	-1.22	12.68	24.88
53130	-1.22	12.68	24.95
53134	-1.23	12.67	25.15
53142	-1.20	12.70	24.55
53153	-1.17	12.73	23.87
53157	-1.19	12.71	24.24

Continued on Next Page...

Table D.1 – Continued

MJD[a]	**obj–chkA**[b]	**mkn509**[c]	**flux**[d]
53174	-1.17	12.73	23.84
53180	-1.18	12.72	24.08
53188	-1.18	12.72	24.11
53194	-1.20	12.70	24.41
53197	-1.22	12.68	24.90
53206	-1.26	12.64	25.76
53223	-1.27	12.63	26.05
53224	-1.27	12.63	26.13
53240	-1.26	12.64	25.95
53243	-1.26	12.64	25.86
53248	-1.26	12.64	25.96
53250	-1.26	12.64	25.77
53251	-1.25	12.65	25.51
53254	-1.23	12.67	25.26
53262	-1.23	12.67	25.07
53265	-1.21	12.69	24.60
53268	-1.22	12.68	25.02
53278	-1.21	12.69	24.78
53281	-1.23	12.67	25.08
53289	-1.19	12.71	24.30
53296	-1.21	12.69	24.77
53298	-1.22	12.68	24.90
53307	-1.25	12.65	25.65
53311	-1.24	12.66	25.48
53324	-1.23	12.67	25.03
53329	-1.22	12.68	25.02
53560	-1.06	12.84	21.48
53563	-1.04	12.86	21.17
53570	-1.00	12.90	20.43
53575	-0.95	12.95	19.41
53578	-0.96	12.94	19.56
53581	-0.93	12.97	19.09
53584	-0.90	13.00	18.60
53587	-0.93	12.97	19.10
53588	-0.91	12.99	18.65
53591	-0.94	12.96	19.25
53599	-0.92	12.98	18.88
53608	-0.91	12.99	18.75

Continued on Next Page...

Table D.1 – Continued

MJD[a]	**obj–chkA**[b]	**mkn509**[c]	**flux**[d]
53618	-0.93	12.97	18.99
53626	-0.93	12.97	19.06
53633	-0.96	12.94	19.58
53640	-0.98	12.92	19.98
53644	-1.01	12.89	20.53
53654	-1.00	12.90	20.37
53661	-1.01	12.89	20.48
53668	-1.04	12.86	21.10
53676	-1.01	12.89	20.48
53682	-0.98	12.92	19.93
53704	-0.94	12.96	19.26
53946	-1.08	12.82	21.80
53951	-1.05	12.85	21.21
53960	-1.07	12.83	21.67
53963	-1.06	12.84	21.58
53968	-1.03	12.87	20.95
53970	-0.99	12.91	20.15
53974	-1.01	12.89	20.61

[a] Modified Julian Date
[b] Object – Check star A
[c] Object R magnitude
[d] Object flux (mJy)